Norwegian University of Life Sciences
Faculty of Veterinary Medicine and Biosciences
Department of Chemistry, Biotechnology and Food Science

Master Thesis 2015
60 credits

Characterization of Immune Cells in Human Non-Small Cell Lung Cancer

Branislava Stankovic

Contents

1 Acknowledgements

The work presented in this master thesis was done in the Tumor immunology group, at the Department of Pathology of Rikshospitalet, which is part of Oslo University Hospital (OUS). The work was done from August 2014 to August 2015 under direct supervision of Alexandre Corthay while internal supervision was assigned to Tor Erling Lea.

I would like to thank my supervisor Alexandre Corthay for giving me the opportunity to work on this project, and for great advice and guidance. I am especially grateful for the critical feedback I got during the lab work and writing process.

I would like to thank Heidi Anine Korsmo for introducing me to this project and for the help with biobank procedures. I would like to thank Heidi for starting this project and establishing some of the protocols which allowed me to build up on her work and expand this project. I am grateful to Elisabeth Muller for advices I got on the practical issues in the lab and comments during the writing process. My thanks go to Kahsai Beraki for wise advice, and to Inger Øynebråten for critical feedback on my work and writing.

My gratitude goes to Ingjerd Solvoll, for collaborating with us and for coordinating biopsy sampling. I would like to thank the surgical team at Department for Thoracic surgery in Ullevål hospital for accepting me to the operating theatre. Henrik Aamot deserves a special thanks for teaching me the techniques for tissue sampling and for introducing me to basic protocols in operating theatre. My appreciation goes to Yan Zhang for teaching me basic principles of flow cytometry, to Ania Bujko and Lisa Gruber for teaching me deeper understanding of flow cytometry and for help in times when the machine was not working.

2 Abstract

Lung cancer is the fourth most prevalent cancer in Norway, holding first place in mortality rate. Non-Small Cell Lung Cancer (NSCLC) is the most frequent type, representing about 85% of all lung cancer patients. Presently, the TNM staging, which is based on tumor size and localization, is used for diagnosis and prognosis in NSCLC. However, previous reports suggest that the analysis of tumor-infiltrating immune cells may represent a more accurate prognostic tool. The aim of this project was to perform comprehensive analysis of tumor-infiltrating immune cells in NSCLC using flow cytometry, as a first step to understanding the relationship between tumor-infiltrating immune cells and clinicopathological parameters. We used 10 colour flow cytometry to investigate immune cells in tumors, distant lung tissue, lymph node and peripheral blood, from 67 patients with primary NSCLC. The following populations of tumor-infiltrating immune cells were identified: $CD4^+$ T cells, $CD8^+$ T cells, each with memory and naive phenotypes; $CD19^+$ B cells, with naive, memory, germinal center and plasma cell subsets; $CD14^+$ macrophages, $CD123^+$ plasmacytoid dendritic cells (pDCs), $CD11c^+CD1c^+$ dendritic cells (DCs), and $CD11c^+CD141^+$ DCs, $CD3^+CD56^+$ natural killer T cells (NKT), $CD56^+$ natural killer (NK) cells, with $CD16^+$ and $CD16^-$ subset, and four granulocyte population: eosinophils, basophils, neutrophils and mast cells. Statistical analysis revealed increased percentage of leukocytes within tumors compared to distant lung tissue. In the leukocyte population $CD19^+$ B cells showed increase in tumor compared to the distant lung ($p= 0.0001$). This suggests that tumor microenvironment of NSCLC recruits immune cells and has different immunological structure compared to lung tissue.

3 Introduction

3.1 Lung cancer

Lung cancer is the most common cause of cancer related death both worldwide and in Norway, attributing to one in five cancer related deaths. Lung cancer incidence is passed only by breast and prostate cancers. In 2012 there were 1.8 million new cases of lung cancer and 1.6 million lung cancer related deaths worldwide [4]. This illustrates the poor survival rates in lung cancer patients. In the period from 2002 to 2004 the five year relative survival was 16.1 % and in the period from 2005 to 2011 survival rates increased to 18.4%. The overall survival rates have been increasing during the years possibly because of the advancement in therapy, however this increase is very small [5]. The relation between incidence and mortality rates in lung cancer illustrates the poor prognosis for lung cancer patients, and a need for better diagnosis and treatment options.

Despite the general public being aware of the risks of smoking, cigarette smoke remains the most common cause of lung cancer. Cigarette smoke contains 20 different types of carcinogens and it is known that there is a dosage related relationship between the number of cigarettes smoked and risk of developing lung cancer. However there are risk factors that do not include smoking. 10-20% of patients that develop lung cancer have no previous smoking history. Risk factors that do not include cigarettes are immunodeficiency, long term exposure to asbestos, radon, and plutonium and even genetic predisposition. There are individuals who have a family history of lung cancer that gives a predisposition to develop lung cancer [6].

3.1.1 Classification of lung cancer

Lung cancer can be classified based on its histological appearance and disease progression.

3.1.1.1 Histological classification of lung cancer

Based on its histological features lung cancer is classified into two types: small-cell lung cancer (SCLC) and non-small cell lung cancer. SCLC is diagnosed in about 15% of all lung cancer patients while NSCLC is diagnosed in 85%.

SCLC arises from neuro-endocrine cells, called the Kulchitsky cells, of the lung [7]. This is an aggressive and fast growing type of cancer with a high mortality rate. It metastasize early, and even though this type of tumor has a good response to the

radiotherapy, the response is short lasting and most patients die from metastasis. SCLC occurs almost exclusively in smokers [8, 9].

NSCLC is relatively less aggressive and has a slower growth rate than SCLC, and thereby correlates with slightly better prognosis. NSCLC arises from epithelial cells in the lungs. Since there are different types of epithelial cells in the airways, NSCLC includes different subtypes of tumors, like adenocarcinoma, squamous cell carcinoma, carcinoid carcinoma, adenosquamous carcinoma, large cell carcinomas and undifferentiated carcinomas. The most predominant NSCLC are adenocarcinoma (about 50%) and squamous cell carcinoma (about 40%) [10].

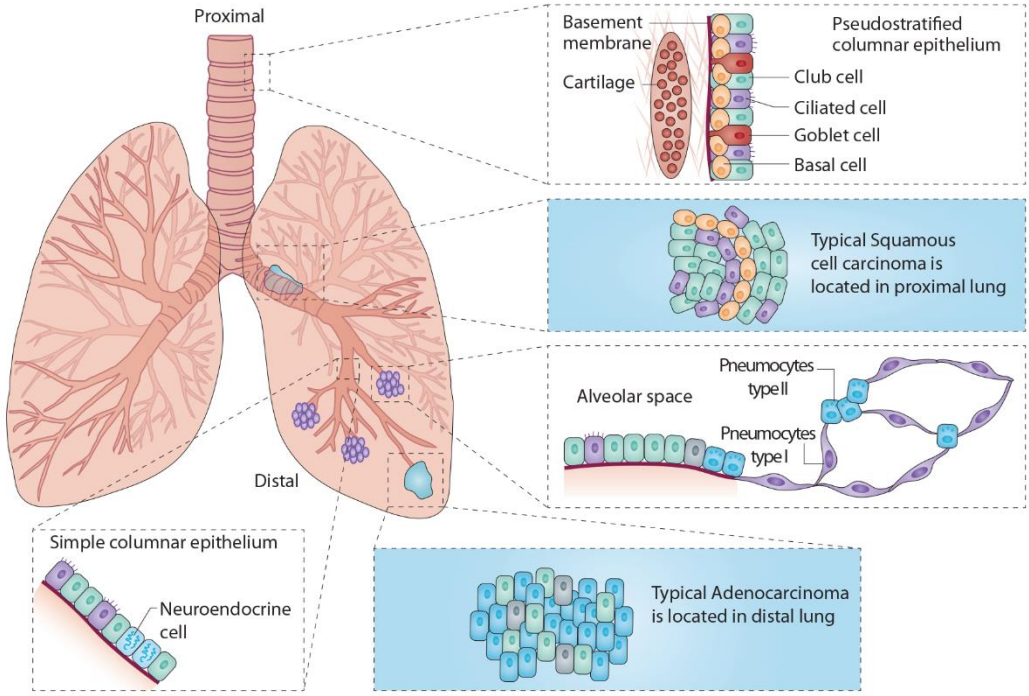

Figure 1. Anatomy of proximal and distal lung cells. Figure shows different types of epithelial cells in proximal and distal lung parts and typical location of squamous cell carcinoma and adenocarcinoma. Figure modified from [10]

Adenocarcinomas arise from type II pneumocytes that are typically found in the alveoli, hence the tumor is often localized at the periphery of the lung [7]. On the other side squamous cell carcinoma arise from bronchial epithelial cells that are located in the large airways, and because of this, squamous cell carcinoma is often located in central parts of the lung (Fig.1) [11].

In recent years incidence rates of adenocarcinoma have risen, while incidence rates of squamous cell carcinoma have fallen. This can be attributed to mass production of filtered cigarettes. The filter on the cigarettes has a dual effect on cancer epidemiology;

it prevents bigger tobacco particles from entering lung, but it lowers nicotine content in filtered cigarettes compare to rolled cigarettes. This causes smokers to inhale more deeply and more frequently, consequently the peripheral epithelial cells are more exposed to carcinogens of cigarette smoke, and hence the increase of adenocarcinoma over the squamous cell carcinoma [12, 13].

3.1.1.2 Classification based on disease progression

Tumor classification based on disease progression is called staging. Staging is a process that describes severity of the disease based on size and extent of primary cancer. Cancer stage is an important parameter for the patience since survival prognosis and treatment options are based on the stage of the disease [14]. Cancer staging of solid cancers uses tumor, node, and metastasis (TNM) system to calculate the final stage of the tumor. TNM staging system is based on the size of the primary tumor (T), metastasis to regional lymph node (N) and presence of distal metastasis (M). Numbers are added to the letters to describe disease progression in detail, and combination of different T, N and M stages puts the disease into one of four finals stages of cancer (table 1)

Table 1. TNM staging for solid cancers (table modified from [15])

		Tumor(T)	Lymph node(N)	Metastasis(M)
Stage 0		Tis (in situ)	N0 (no lymph node involvement)	M0 (no metastasis)
Stage I	IA	T1a, b(≤3cm)	N0	M0
	IB	T2a (3cm≤5cm)	N0	M0
Stage II	IIA	T1a, b	N1 (ipsilatheral hilar lymph nodes)	M0
		T2a	N1	M0
		T2b (5cm≤7cm)	N0	M0
	IIB	T2b	N1	M0
		T3 (>7cm/ invading chest wall etc.)	N0	M0
Stage III	IIIA	T1, T2	N2 (ipsilatheral mediastinal and/or subcardinallymph nodes)	M0
		T3	N1, N2	M0
		T4 (severalipsilateral tumors or invading mediastinum)	N0, N1	M0
	IIIB	T4	N2	M1a, b*
		Any T	N3 (contralateral or supraclavicular lymph nodes)	M0
Stage IV		Any T	Any N	M1a, b

*M1a: Plural or pericardial effusion or separate tumors in the cotralateral lung. M1b: Distant metastasis

The T part of staging system represents tumor size and invasion to the neighboring tissues. If the tumor is under 2cm in diameter the stage is set to T1a, for tumors from 2-3 cm the stage is set to T1b. Tumors with diameter between 3-5 cm have stage T2a and tumors with diameter over 7 cm have stage T3. If the tumor invades the pleura, chest wall, diaphragm, or pericardium it will automatically be set to stage T3 regardless of size. If tumor invades mediastinum it will be set to stage T4. The N part of the staging process depends on metastasis to Lymph node. N0 stage marks no lymph node involvement, N1 marks metastasis to ipsilateral hilar lymph node, and N2 marks metastasis to ipsilateral mediastinal and subcarinal lymph nodes. The M part of staging is based on metastasis. If there is no metastasis of tumor them stage is set to M0, if tumor has metastasized to contralateral lobe stage is set to M1a and if tumor has metastasized to distant parts of the body the stage is set to M1b [16].

3.2 Cancer immunoediting and immunosurveillance

Cancer arises from normal cells that have acquired a series of mutations in oncogenes or tumor suppressor genes. These mutations allow uncontrolled cell replication, and invasion into the neighboring tissues [17]. Mutated cells express tumor-associated antigens and danger signals which may potentially activate the immune system. The concept that the immune system fights cancer was first proposed by Paul Ehrlich in 1909 and later Burnet and Thomas introduced concept of immunosurveillance proposing that in long lived animals there must be a system that prevents cancer development [18]. In 2001 Shankaran *et al* confirmed that lymphocytes protect against cancer development in mice. In their studies on mice insensitive to IFN-γ (by knocking out IFN-γ receptor or by knocking out IFN-γ transcription factor STAT1) they induced sarcomas in both knockout mice and wilt-type mice. The key observation was that IFN-γ insensitive mice were more susceptible to tumor development [19]. Shankaran *et al* further showed that $RAG^{-/-}$ mice develop tumors at the same rate as $STAT1^{-/-}$ mice and continued their work by crossing $RAG^{-/-}$ with $STAT1^{-/-}$ mice and challenging them with sarcomas. This research showed that immune system in fact does protect against tumor and that multiple immunological mechanisms are involved in immunesurveillance. Multiple other studies supported the idea of immunosurveillance. Perforin knock out mice show reduced ability to resist transplanted tumors as well as spontaneous tumors, showing that cytotoxic cells like $CD8^+$ CTL and NK cells are critical for immunosurveillance of spontaneous tumors [20-22].

Even though the concept of immunosurveillance was evident, it posed another question: how does a mutated cell evade this immunosurveillance to become a cancer? Answer to that question came from studies in mice, where Shankaran *et al* noticed that when immunocompetent mice were challenged with tumors from $RAG^{-/-}$ mice, the immunocompetent mice rejected most of the tumors. However when 20 tumors from immunocompetent mice were transplanted into wild type mice they reported that 8 out of

20 tumors actually continued growing. This led to the conclusion that tumors developing in an immunodeficient host are more immunogenic than tumors developing in presence of intact immune system [19]. This suggests that immune system does not only surveil the tumor but also alters the immunogenicity of the tumor. Shankaran *et al* suggested that the term immunoediting, and not immunosurveillance, would better describe the complex interactions between tumor cells and the immune system.

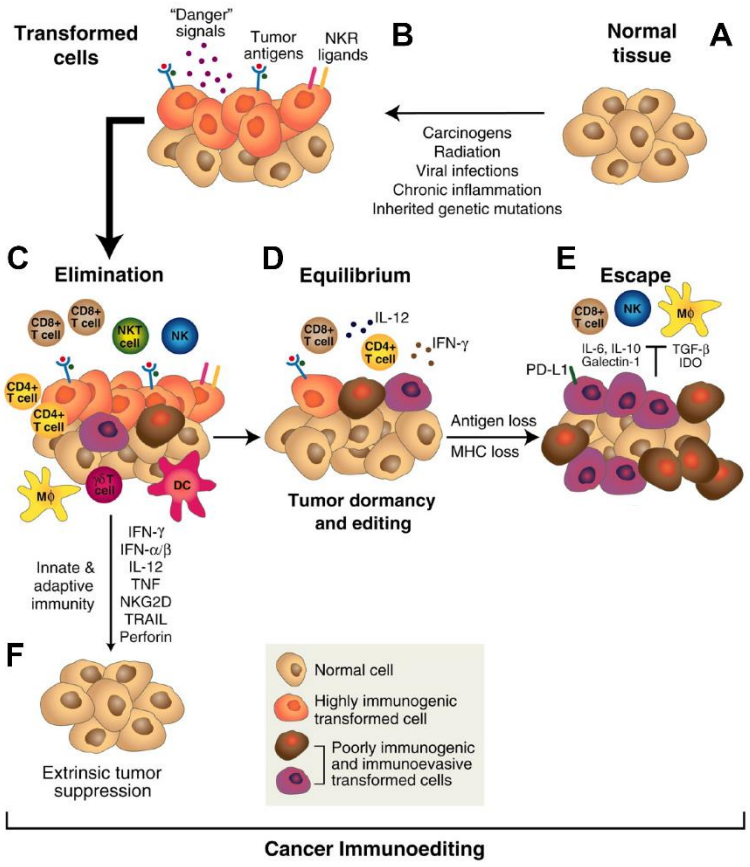

Figure 2. Three E's of immunoediting. A. Normal tissue exposed to carcinogens will develop mutations. **B.** Mutated cells express danger signals and tumor antigens. **C.** Complete elimination of mutated cells leads to **F.** tumor suppression. Incomplete elimination of mutated cells will lead to the next stage of immunoediting called equilibrium. **D.** Equilibrium stage, the immune system cannot eliminate mutated cells but it prevents development of cancer. During equilibrium stage the mutated cells undergo selection under pressure of immune system and become immunoevasive. **E.** Escape of cancer from immune cells and development of cancer. Figure modified from [23].

Immunoediting has 3 stages, also called the three E's of immunoediting (Figure 2). The stages are elimination, equilibrium and escape. Elimination can be seen as an equivalent of the original concept of immunosurveillance. In the elimination stage, the immune system detects and eradicates tumor cells, and if eradication is complete, then the immunoediting process will stop here. However, if any cancer cell variants survive elimination phase, they will enter into the equilibrium phase. In equilibrium phase, the

immune system can contain but not eradicate cancer cells, and during this equilibrium some of cancer cell variants are eradicated while new ones also appear. If these new cancer cells carry mutations that will help them evade immune attacks, they will be selected for survival. Eventually these mutated cells will manage to escape immune system, proliferate uncontrollably, and invade surrounding tissues, at which point the tumor can be detected clinically [24].

3.3 Cancer microenvironment

As mentioned above, cancer arise from normal cells that acquire mutations, however cancer is not only a mass of mutated, malignant cells, but a complex “organ” that contains many non-cancerous cells. Interactions between malignant and non-cancerous cells create the tumor microenvironment (TME). In the TME, cancer cells from tumor islets are interspersed with tumor vasculature and lymphatics and surrounded by fibroblast, adipocytes, pericytes and immune cells. This section will describe function of healthy, non-immune cells in the TME, and the next section will describe in detail the immune cells in the TME.

Fibroblasts are the most abundant population of healthy cells in TME. In normal tissues fibroblasts synthetize collagen and extracellular matrix (ECM), and have a role in would healing. In TME fibroblasts synthetize ECM [25] and produce cytokines that promote angiogenesis and cancer cell survival [26]. Myofibroblasts are specialized type of fibroblasts that respond to the loss of homeostasis in tissues by producing actin, which stiffen the ECM and promote tumor invasion in neighboring tissue [25]. Even though fibroblasts are themselves not cancerous cells they have a tumor promoting role in TME.

Other types of cells in the tumor stroma include pericytes and adipocytes. Pericytes, or perivascular cells, give structural support to blood vessels in the tumor. Studies on pericytes in human cancer suggest that pericytes have dual effect. They support blood vessels allowing cancer cells access to oxygen and nutrients, but pericytes also inhibit metastasis. Decrease of pericytes in the TME caused suppression of primary tumor, but it also causes hypoxia and MET receptor expression [27]. Activated MET receptor will trigger angiogenesis and tumor growth. Studies on human colon cancer show that low infiltration of pericytes in the tumors combined with MET expression correlates with poor prognosis and a higher degree of metastasis [28]. While pericytes inhibit metastasis, adipocytes have the opposite effect. Intra-abdominal tumors usually metastasize to the omentum, a large organ made primarily of adipocytes. Neiman *et al* showed that adipocytes attract tumor cells through the secretion of cytokines like IL-8 and aid the invasion and metastasis of cancer cells, and also serve as an energy source to these cells [29].

The tumor microenvironment is heterogeneous mix of both cancer cells and various non-cancerous cells that have different influences on cancer development. The influence

of non-cancerous cells depends on many different parameters like cell type, cancer type and cytokines produced in tumor microenvironment.

3.4 Tumor infiltrating immune cells

Tumor infiltrating immune cells are part of the body's immune response against malignancy and have important roles in tumor destruction. Leukocytes represent a huge population of non-cancerous cells in the cancer microenvironment. All leukocytes come from common pluripotent hematopoietic stem cell (HSC) in the bone marrow which can develop in two directions: it can differentiate into common lymphoid progenitor (CLP)or into common myeloid progenitor cell (CMP). CLP stems T cells, B cells, NK cells, and CMP stems monocytes, dendritic cells and granulocytes.

3.4.1.1 T cells

T cells play a role in both cellular and humoral immunity and they can be distinguished from other leukocytes by the presence of a T cell receptor (TCR). TCR is a specific marker for T cells and together with CD3 it creates the TCR-CD3 complex. This complex has an important role in the differentiation and function of T cells [30]. T cells are the only cells which express this complex, which makes it a perfect candidate for discrimination of T cells from other leukocytes. Further discrimination between T cell subsets is done based on expression of CD45 isotype, CCR7, and most importantly CD4 and CD8 molecules.

Differentiation of naive T cells into memory is followed by change in surface molecules like CD45 and CCR7. CD45 is transmembrane protein tyrosine phosphatase that and it plays a role in the activation of leukocytes. In human T cells this protein has two isoforms that are used to identify memory from naive T cells [31]. Memory T cells express low molecular weight isoform CD45RO and naive T cells express CD45RA isoform [32]. CCR7 is a chemokine receptor, found on naive cells, that enables them to migrate to lymph nodes. Once T cells encounter antigen they will change CD45 isoform from RA to RO, and become central memory. Upon further stimulation these cells will lose expression of CCR7 and become effector memory [33].

T cells that express CD4 molecule are called $CD4^+$ T cells. Naive $CD4^+$ T cell receives its first activating signal through binding of the TCR and CD4 to different parts of the major histocompatibility complex (MHC) class II and the peptide presented in it's groove. MHC class II is present only on professional antigen presenting cells (APCs). The second activation signal comes from interaction between CD80/CD86 (B7-1/B7-2) expressed on APCs and CD28, on $CD4^+$ cells [34]. This leads to expression of CD40

ligand (CD40L) on T cell and activation of $CD4^+$ T cells [35]. Once activated, $CD4^+$ T cells regulate both cell-mediated [36] and humoral immunity [37]. Activated CD4 T cells are able to induce antitumor immunity. CD4 T cells are divided into five subtypes: Th1, Th2, Tfh, Th17 and Treg.

T cells that express CD8 costimulatory molecule are called $CD8^+$ T cells and they surveille the intracellular environment. The TCR on $CD8^+$ T cells binds to peptide presented in MHC class I molecules, which are found on all nucleated cells in the body. If the detected peptide in MHC class I groove is foreign or mutated, $CD8^+$ T cells will induce apoptosis of the cell. After antigen-specific activation, $CD8^+$ T cells release granules with perforin and granzyme. Perforin make pores in the target cell's membrane, and granzymes enter the cell and activate caspase 8, an enzyme that starts apoptotic process [38-40].

T cells that do not express either CD4 or CD8 molecule, called double negative T cells, are observed in mice and humans. In mice, they seem to inhibit $CD8^+$ T cells which carry TCR of the same specificity. In humans these cells seem to aid tumor rejection through cytotoxic activity and IFN-γ production, and aid Th1 T cell and M1 macrophage activation. Another population of T cells that does not express either CD4 or CD8, and is found in tumor microenvironment is natural killer T cells (NKT cells). Their name is based on the observation that they express αβ-TCR but also express NK cells markers not present on T cells. NKT cells are a bridge between the innate and the adaptive immune system. Upon activation they have quick response like cells of innate immune system and at the same time they produce cytokines typical for Th1, Th2, and Th17. In tumor immunity NKT cells can have protective role, but also immune-inhibitory role and this is because of presence of different types of NKT cells in tumor.

Antitumor immunity is led by Th1 and Th2 $CD4^+$ T cells. Th1 cells are polarized towards this phenotype as a response to IL-12 and IFN- γ, and expression of the transcription factor T-bet. They regulate cell mediated immunity through secretion of IL-2, IFN-γ and TNF-α. The increased IL-2 and IFN-γ activate $CD8^+$ T cells to kill tumor cells [41]. However Th1 antitumor response can kill tumor cells without assistance of CD8 T. IFN- γ from Th1 cells recruit and activate macrophages that produce superoxide and nitric oxide and can cause destruction of tumor cells [42-44]. Production of IFN- γ causes increased production of IL-12 by DC and this further polarizes $CD4^+$ T cell towards Th1 so that the Th1 antitumor response has a self-sustaining mechanism [45]. Humoral antitumor immunity is led by Th2 cells that develops as a result of exposure of $CD4^+$ T cells to IL-4. Th2 cells are controlled by transcription factor GATA-3. These cells recruit eosinophils to the tumor site [42]. It has been observed that eosinophils can kill tumor cells with granzyme and TNF-α [46]. Th2 also secrete IL-4, IL-5, IL-6, and IL-13 which activate B cells and stimulate them to produce antibodies [47].

3.4.1.2 B cells

B cells arise in the bone marrow, and leave it as immature naive B cells that express IgM and IgD and are negative for CD27. Once B cells are activated by binding of BCR to its specific antigen, they travel to secondary lymphoid organs where they proliferate, create germinal center B cells and downregulate surface Ig and upregulate CD38 [48]. In the germinal centers, B cells undergo affinity maturation. Some of the mature B cells will differentiate into memory B cells and some will differentiate into plasma cells. Memory B cells can either continue to express IgM or they can undergo class switching and express IgG, IgA or IgE, nevertheless both types of memory B cells express CD27. Plasma cells are characterize by the production of antibodies and loss of almost all surface molecules except for CD19 and CD38 [32].

The role of B cells in tumor immunology has been overlooked because it has long been thought that NK and T cells are the major cells which mediate tumor eradication. However, B cells have multiple functions in tumor immunity: a) they act as professional APCs, presenting antigens to $CD4^+$ T cells b) they produce antitumor antibodies and mediate humoral immunity against the tumor [49]. There is evidence that B cells can also produce cytokines and enhance Th1 and Th2 anti-tumor response, but this is still subject of the debate.

In the tumor microenvironment B cells produce antibodies against tumor antigens and cause destruction of tumor cells through the complement reaction. Qiao Li *et al* used murine models to show tumor rejection aided by antitumor antibodies [50]. Another study in human NSCLC patients showed that antitumor antibodies were produced by plasma cells in the tumor [49]. The antitumor antibodies can mark tumor cells for destruction by DCs, NK cells and macrophages [51]. In tumor microenvironment B cells are mainly found in tertiary lymphoid structures (TLS). TLS are transient lymphoid structures found in sites of inflammation, infections and in tumors. TLS are histologically similar to lymph nodes - as they have separate B and T cell areas, specialized dendritic cells (DCs) and high endothelial venules [49, 52, 53].

3.4.1.3 Macrophages

Macrophages originate from the bone marrow, from the common myeloid progenitor cells, and circulate in the blood as monocytes. Once they are recruited to tissues they become macrophages. Their role in immunity is to phagocytose pathogens and dying cells and to present antigens to $CD4^+$ T cells in the context of MHC class I and II molecules. Macrophages are activated by T cells and depending on the cytokine that activates them, they can take on two different phenotypes – M1 and M2 [54]. M1 macrophages are activated by IFN-γ secreted by Th1 cells. This type of macrophages produces IL-12 and nitric oxide that kill microorganisms. The second type of

macrophages, M2 macrophages, are activated by IL-4 which is produced by Th2 cell [55, 56]. The M2 macrophages support angiogenesis and wound healing, release growth factors, and have an anti-inflammatory function.

In tumor immunology it is a widely excepted view that M1 type macrophages coordinate antitumor immunity and inhibit cancer growth while M2-like macrophages have pro-tumor effect [57]. This can explain the controversial findings in studies of macrophages in tumors. Studies in lung, gastric and urogenital cancer show poor survival in patients with high infiltration of macrophages, while studies in colorectal cancer show better survival in patients with high infiltration of macrophages [58]. This duality can further be explained by capacity of macrophages to switch from M1 to M2 type and back depending on the microenvironment [59].

3.4.1.4 Myeloid dendritic cells

Dendritic cells (DCs) are professional APCs that reside in peripheral tissues and sites of infection looking for foreign antigens. Once they encounter foreign entities, they phagocytose the antigen and present it to T cells in the context of MHC class I and class II molecules. Presentation of antigen through MHC class II to $CD4^+$ T cells is the classical way to present exogenous antigen. Presentation of extracellular antigen on MHC class I by APCs is called cross-presentation, and it primes cytotoxic T cells [60]. Myeloid DCs express MHC class I and class II (HLA-DR) and typical myeloid antigens CD11b, CD11c, CD13 and CD33. They typically lack CD3, CD19, CD56 and CD14. Myeloid DC can be divided into two well defined fractions: the $CD1c^+$ mDCs and the $CD141^+$ mDCs [61]. The $CD1c^+$ mDCs are the major population of human DCs and they present tumor antigen to Th1 cells activating antitumor Th1 response [62]. The $CD141^+$ mDCs represent 1% of blood mononuclear cells and also have a role in presenting tumor antigen to Th1 and mediating antitumor response. The $CD141^+$ DCs have high potential in presenting antigens from necrotic cells from tumor [63].

3.4.1.5 Plasmacytoid DCs

Plasmacytoid dendritic cells (pDCs) arise from the lymphoid progenitor cells in bone marrow and they lack myeloid antigens like CD11c, CD11b, CD13 and CD33. pDCs express CD123, CD303 and CD304, which distinguishes them from myeloid DCs. These cells home to an inflamed microenvironment, where they secrete IFN-α, IFN-β and IL-12. The tumor microenvironment attracts pDCs as a result of general inflammation and CXCL12 production [64]. Once in the tumor, the pDCs will activate NK cells, reduce angiogenesis, keep activated T cells alive, and prime $CD8^+$ T cells [65-68].

Even though pDCs have antitumor functions some studies have showed that infiltration of pDCs correlate with poorer survival in patients with ovarian cancer [69] and breast cancer [70]. This could be due to the downregulation of IFN-α from pDCs by the tumor cell. Tumor cells produce TGF-β and PGE2 and downregulate IFN-α production in pDCs while upregulating IL-8 secretion which helps proliferation of cancer cells [71]. The pDCs also suffer downregulation of TLR9 by tumor [68].

3.4.1.6 NK cells

Natural killer (NK) cells belong to the innate arm of the immune system. They are differentiated from other leukocytes by the CD56 receptor. $CD56^+$ NK cells can be divided into two subsets. One subset is naturally more cytotoxic and expresses Ig-like NK receptor and Fcγ receptor III (CD16). These cells are CD56 positive but dim. The other subset of NK cells lacks CD16 receptor, and it is CD56 bright. This subset has higher ability to produce cytokines, but it is not very cytotoxic [72, 73].

NK cells can detect and kill tumor cells without the need for prior sensitization by antigen. The recognition of some tumor cells is based on missing-self model and stress-induced self ligands. Many tumors downregulate MHC class I receptors to avoid detection by CD8 T cells. NK cells detect “missing self”, or missing MHC class I, this activates NK cells to kill tumor cells [74]. In addition NK cells have activation signals that recognize stress molecules on tumor cells, which helps NK cells to discriminate between healthy cells that do not express MHC molecules (like erythrocytes) and sick and stressed tumor cells. Studies of NK cells in tumor environment have shown that NK cells have an important role in the prevention of metastasis. In lung cancer challenged mice whit inhibited cytotoxic activity of CD8 T cells, NK cells take over cytotoxic regulation and decrease the number of metastasis [73, 75].

3.4.1.7 Granulocytes

Granulocytes are a population of lymphocytes characterized by the presence of granules in their cytoplasm. There are four types of granulocytes: neutrophils, eosinophils, basophils and mast cells. Neutrophils are phagocytic cells that are the first line of defense in an acute inflammatory response. They phagocytose particles coated with antibodies or proteins of the complement system and form pus at the site of inflammation. In order to reach the site of inflammation neutrophils need to migrate from the blood stream to the tissues and this migration has two stages. The first stage is a process of slowing down their speed in the blood stream by low level adhesion to endothelial cells. This process is mediated by the CD15 molecule on the surface of neutrophils. The second stage is strong adhesion to endothelial cells, mediated by CD11b

[76]. The influence of neutrophils on tumor growth and metastasis is controversial. Evidence suggests that neutrophils promote tumor growth through the secretion of hepatocyte growth factor (HGF), a cytokine promoting angiogenesis and cell proliferation [77]. In contrast there are evidence showing that in early stages of lung cancer neutrophils promote T cell response [78].

Eosinophils are responsible for the immune response to parasitic infections and their migration from blood to tissues is mediated by CD11b and CD49d (also found on basophils and mast cells). These cells contain granules with cationic proteins that in the tumor microenvironment can be released to kill cancer cells [46].

Basophils and mast cells are granulocytes that have histamine in their granules. Both basophils and mast cells have high affinity IgE receptor (FcεR) that binds Immunoglobulin E. Crosslinking of IgE antibodies and antigen on surface of these cells causes degranulation and allergic reactions. In the tumor microenvironment these cells have been reported to help angiogenesis, tissue remodeling and inflammation [79].

3.4.2 Clinical implications of tumor infiltrating immune cells

Tumor infiltrating immune cells are considered to play important role in tumor immunosurveillance. Tumor infiltrating immune cells can be used as a factor in survival prediction and also in therapeutic purposes. Today the survival prognosis of the NSCLC patient is based on TNM staging, however this method has proven to be somewhat unreliable. Some of the patients with seemingly localized disease shown shorter survival than patients with more widespread disease. Welsh *et al* demonstrated that the presence of macrophages in tumor isles is a more accurate prognostic factor than cancer stage [80]. They demonstrated, in NSCLC, that stage IIIA patients with high macrophage count in tumor islands had better survival rates than patients with stage IA with low infiltration of macrophages [80]. Ohri *et al* builds up on this findings by showing that presence of M2 polarized macrophages in tumor is associated with poor survival [81] while M1 macrophages are associated with extended survival [82]. These findings prove that not only the numbers, but also the phenotype of immune cells has clinical implications. NK cells and DC cells [83] as well as $CD3^+$ and $CD4^+$ T cells in tumor stroma are associated with better prognosis [84]. On the other side $CD20^+$ cells in both tumor stroma and isles are indicators of prolonged survival [85]. $CD8^+$ T cells in stroma correlate with improved survival [85] and $CD8^+$ cells in tumor isles correlate with poorer survival [84]. Showing that the location of tumor infiltrating lymphocytes also has an impact on survival.

Cancer patients have three main treatment options: surgical tumor resection, chemotherapy and radiotherapy. Surgery is offered to patients with more localized tumors (stages I to III in NSCLC) and adjuvant postoperative chemotherapy is given to prevent disease recurrence. However, the adjuvant therapy is only beneficial for 4 % of the patients [86]. Patients with non-operable, more widespread, tumors are given

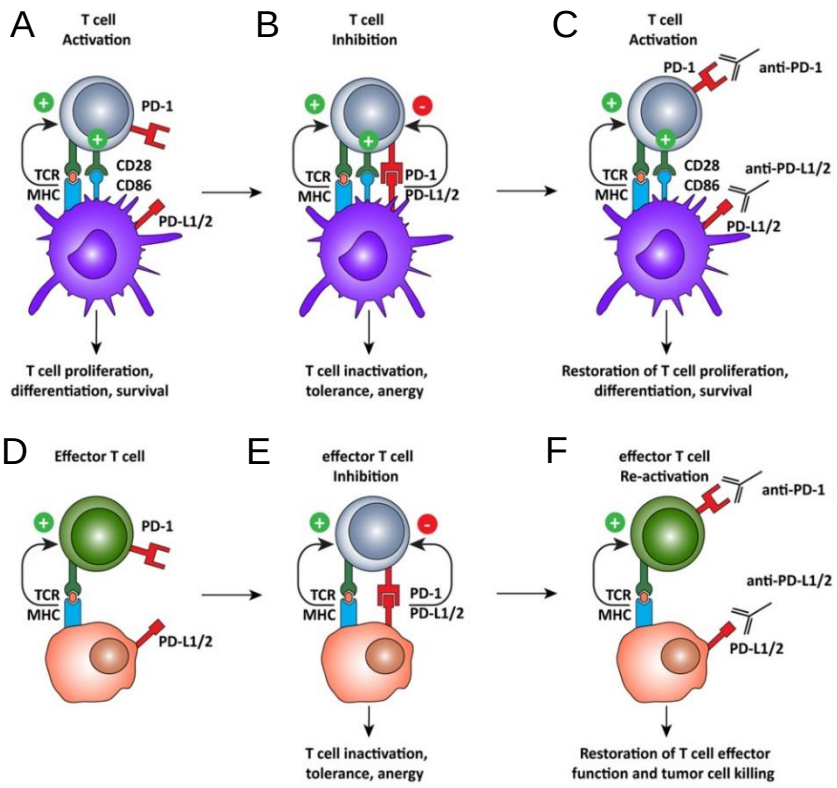

Figure 3. PD-1 blocade releases the breaks on immune system and promotes tumor distruction. Checkpoint inhibitors PD-1 based therapy has two levels and the first level starts with APC cells. **A.** APC cell presents tumor antigen to T cells, activating it. Activated T cells in the tissue upregulate PD-1 expression to avoid autoimmunity and collateral tissue damage. **B.** PD-1 binds to PD-1L/PD-2L sending a supressing signalt to the T cell. **C.** However if this pathway is blocked by monoclonal antibodies, this will allow T cell activation. The second level of PD-1 based therapy is based in tumor microenvironment. **D.** The T cells recognize tumor antigen presented by tumor cell in MHC class I, **E.** however T cells are incativated by PD-1L expressed by tumor cells. This causes anergy and tolerance. **F.** If PD-1 pathway is blocked in tumor microenvironment T cells will undertake effector function and kill tumor cells. Figure modified from [3].

chemotherapy and radiotherapy as an option to prolong life and with low hopes of tumor eradication. Recently another therapeutic option started to demonstrate very promising results for cancer patients – immunotherapy. Immunotherapy is a new and fast developing treatment therapy that harnesses the body's own immune system to fight cancer. This strategy includes many different approaches including anti-tumor antibodies, cancer vaccines, adaptive immunotherapy and checkpoint inhibitors. For adaptive immunotherapy tumor-infiltrating lymphocytes (TILs) are isolated from the patient and expended *in vitro*. This approach makes an assumption that most of the TILs are tumor specific. After the TILs have been expended in vitro, the TILs are returned to the patients to battle the cancer.

Adaptive immunotherapy is still in the experimental stage of the development, but antibodies against checkpoint inhibitors are on their way into the clinics. Two major targets are CTLA-4 and PD-1. CTLA-4 is a co-inhibitory molecule that competitively binds to CD28 on APCs and puts a break on the immune response. PD-1 or programed cell

death protein is another co-inhibitory molecule that binds to PD-1L or PD-2L (ligands for PD-1) and also dampens down immune response. In the healthy individuals co-inhibitory molecules reduce the chance of autoimmunity [87]. In the cancer microenvironment the PD-1/PD-L pathway causes inhibition of Th1 and Th2 antitumor response and leads to cancer cell escape from cytotoxic lymphocytes [88]. Given that PD-L1, is upregulated in many cancers including lung, ovary and colon carcinoma [89, 90], and that it is main pathway in immune system evasion, PD-1 pathway has been the focus of antitumor immunotherapy.

Antibodies against both CTLA-4 and PD-1 have been tested in different tumors. Anti CTLA-4 treatment showed response in melanoma patients. Inhibition of PD-1/PD-L pathway with anti PD-1 antibodies (nivolumab and lambrolizumab) is novel cancer treatment that showed objective response in one out of four patients with NSCLC, renal carcinoma and melanoma [91].

3.5 Aim of the project

Most of the studies of immune cells in NSCLC immune cells were done based on immunocytochemistry and, to the best of our knowledge, none of the studies indicated complete characterization of the TILs in NSCLC. We set out to do comprehensive study of immune cells in NSCLC with flow cytometry.

The main goals of the project was to establish appropriate flow cytometry strategies so that we can perform such a comprehensive characterization of the different immune cells in NSCLC.

Two additional goals were to: Examine the PD-1 expression on T cells and to perform statistical analysis of TILs in NSCLC in order to better understand the relationship between TILs and clinicopathological parameters.

4 Materials and Methods

4.1 Patients and biopsies

Biopsies were obtained from patients diagnosed with primary non-small cell lung cancer (NSCLC) stages IA to IIIB. Out of the 67 patients included in the study 29 are male and 38 are female. 34 patients were diagnosed with adenocarcinoma, 26 with squamous cell carcinoma, 3 with carcinoid carcinoma, 2 with large cell carcinoma, 1 with adenosquamous carcinoma and 1 with undifferentiated carcinoma. According to the smoking history patients were divided into three categories: 7 patients were non-smokers (never smoked), 29 patients were previous smokers at the time of the diagnosis and 31 patients were smoking at the time of the diagnosis. All of the patients were operated at Rikshospitalet and Ullevål hospitals (both part of Oslo University Hospital OUS - Oslo Universitetet sykehus) in the period from August 2013 to May 2015. All the patients included in the study have signed informed consent form, agreeing to participate in the study. The study has been approved by the Regional Ethical Committee (ref: S-05307).

4.2 Tissue sampling

Samples were taken from four different anatomical locations: blood, lymph node, tumor, and non-tumorous lung tissue. From here on these four entities will be called “tissues”. In most patients the lung tissue was inflamed, probably due to the presence of the tumor. Because of this inflammation we decided to use the term “distant lung” and not “normal lung” to refer to lung tissue.

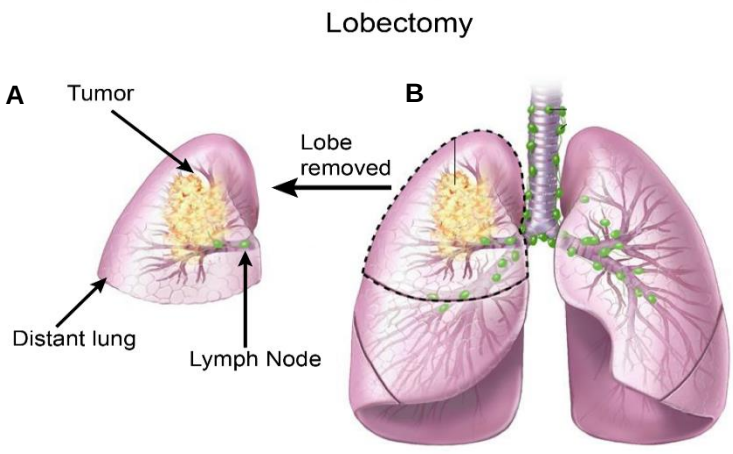

Figure 4. Lobectomy
A. Location of tissue sampled from removed lobe. **B.** Lobectomy of right superior lobe. Figure modified from [1]

Blood was sampled from the central venous catheter after the patient was sedated, and before the surgeons made the first incision. Blood samples were collected in 9 ml tubes containing EDTA and kept at room temperature until further processing in the lab. Tumor, lung tissue and, lymph node were sampled after the lobectomy. Lobectomy is a surgical procedure where a lobe of diseased lung is removed. The removed lobe contains tumor tissue, normal lung tissue, bronchial tissue and lymph nodes adjacent to the lobar bronchus (Figure 3).

The tumor was sampled by cutting out a slice of tissue 2-3mm tick. The slice of tumor was sampled through the central mass of the tumor, and the slice stretched from one end of tumor to another, in order to include all layers of tumor. Tumor tissue was cut at the site of minimal invasion to the pleura to avoid destruction of diagnostic parameters. Distant lung biopsies were sampled from part of the lobe that was furthest away from the tumor. Lymph nodes were procured from the lobar bronchus. Tumor, distant lung and lymph node were transported in transportation media (DMEM + 0.25 µg/ml Amphotericin Sigma) on ice.

4.3 Protocols for cell isolation and staining

All tissues were handled under sterile conditions throughout the analysis. In the operating theatre we used surgical gloves when handling the samples, and in the lab, all of the steps of cell isolation were done in sterile environment (under ventilated hood).

4.3.1 Protocol for isolation of peripheral blood mononuclear cells (PBMCs) from blood

Reagents:

- Lymphoprep; Axis shield
- PBS; Gibco, Life Technologies
- Trypan blue; Life Technologies

Procedure:

1. Density gradient Lymphoprep (Axis shield) was used to isolate PBMCs from the blood samples of patient. 9 ml blood samples were diluted in 30 ml room temperature PBS. Diluted blood was carefully placed on top of 10 ml of Lymphoprep in the 50 ml falcon tube and the tube was centrifuged for 20 min at 800 g at 4^{o}C. (Fig. 2**)**

2. After centrifugation the PBMCs formed a distinct band at the interface of plasma layer and Lymphoprep (Fig. 2). The band of PBMCs was removed from the tube

with a Pasteur pipette and placed in a sterile 50 ml Falcon tube. The tube was filed with PBS up to 50 ml and centrifuged for 10 min at 250 g at 4°C to remove remaining Lymphoprep.

3. Following the centrifugation, the supernatant is discarded and the pellet is resuspended in 50 ml of PBS. Centrifugation was repeated two more times to remove any residual Lymphoprep from the PBMCs.

4. Following the last centrifugation the pellet was diluted in 1ml of PBS and the cells were stained with Trypan blue. Trypan blue stains apoptotic, necrotic and dead cells by crossing the cell membrane.

5. Stained cells were counted manually using KOVA Glasstic counting chambers.

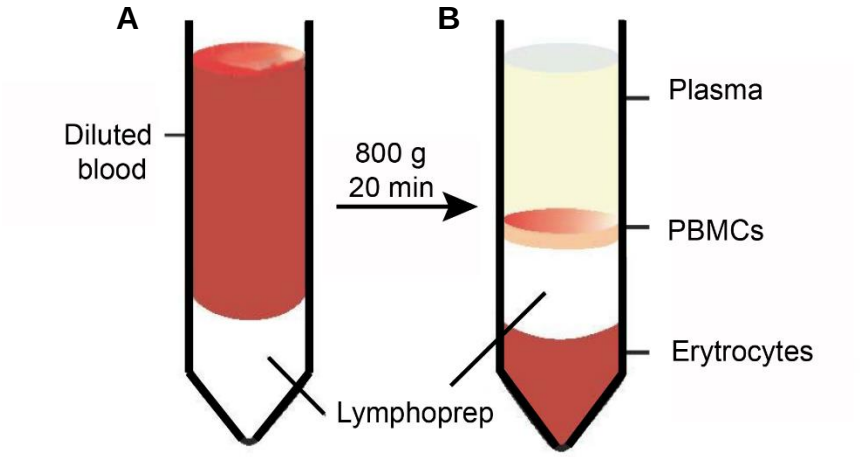

Figure 5. Isolation of PBMCs from the blood of NSCLC patients. A. Diluted blood placed on top of density gradient Lymphoprep before centrifugation. B. Layers created after centrifugation. PBMCs create a band on top of Lymphoprep. Figure modified from: [2]

4.3.2 Protocol for cell isolation from tumor, distant lung and lymph node

Reagents:

- Digestion media: DMEM + 0.25 µg/ml collagenase A (Roche) + 500 units/ml DNase (Roche)
- Termination media: DMEM + 10%FBS Sigma
- Trypan blue: Life technologies
- KOVA Glasstic counting chambers

Procedure

1. The tumor and distant lung samples were squeezed with sterile tweezers and washed in the transport media to reduce blood contamination. Bronchial tissue, large blood vessels, and obvious necrosis were removed from the samples. The

samples were then minced with scissors in 6 well plates. The lymph node was also minced with scissors in 6 well plates.

2. The minced tissue was suspended in 5ml digestion media each and incubated with a stirring magnet at 37^{o}C and 5%CO_2 for 1h. After 30 min of incubation the samples were taken out of the incubator and pipetted up and down, under sterile conditions, to increase the dissociation of the tissue and help the digestion process.

3. The digestion process was stopped by adding 25 ml termination media to the samples to inhibit the enzyme reaction and the samples were then filtrated through 100 µm mesh to isolate single cells.

4. The single cell suspension was centrifuged at 410g at 4^{o}C for 6 minutes. The supernatant was discarded and the pellet was diluted in 20ml termination media and centrifuged at 410g at 4^{o}C for 6 min.
5. Following centrifugation the pellet was resuspended in 1 ml of termination buffer and cells were stained with Trypan blue and counted manually using KOVA Glasstic counting chambers.

4.3.3 Protocol for immunostaining for flow cytometry analysis

The immunostaining was done in 96 well plates in final volume of 50 µl in order to reduce amount of antibodies used for staining to half of volume suggested in the datasheet.

Reagents:

- IgG from mouse serum (Sigma)
- Flow media: cold (+4^{o}C) PBS + 10% Fetal bovine serum
- Propidium Iodide (BioRad)

Procedure:

1. A minimum of one million cells isolated from each sample (tumor, distant lung, blood and lymph node) was added to appropriate wells in 96 well plate and centrifuged at 410g at 4^{o}C for 6 minutes.

2. The pellet with single cells was resuspended in 25 µl of 12.5 µg/ml IgG from mouse serum (diluted in PBS) to inhibit unspecific binding. The cells were incubated on ice for 20 min.

3. After the incubation with IgG from mouse serum, the samples were stained with antibody mixes. Six different antibody mixes were used to stain immune cells in four tissues. The volume of each mix was corrected with flow media to 25 µl. The

antibody mixes (25 µl per million cells) were added to appropriate samples and incubated on ice in dark for 20 minutes.

4. 150 µl flow medium was added to each well. The samples were centrifuged at 420 g at 4°C for 6 minutes. The supernatant was discarded and the pellet was resuspended in 150 µl Flow buffer. This step was repeated one more time.

5. The samples were centrifuged one last time at 410g at 4°C for 6 minutes. The supernatant was discarded and the pellet is resuspended in 200µl of Flow buffer.

6. Right before running the samples in the flow cytometer they were filtrated through 100 µl mesh (to avoid clogging the machine) and transferred to FACS tubes. 3 µl of propidium iodide was added to the FASC tube with samples, the tube was vortexed and run in the BD LSRFortessa for analysis.

Antibody mixes for assessing the immune cells in tumor environment

Table 2. Antibody mix used to assess APC cells in NSCLC patients.

Specificity	Fluorophore	Clone	Volume	Manufacturer
CD11c	A488	3.9	2.5 µl	Biolegend
CD14	APC/Cy7	HCD14	2.5 µl	Biolegend
HLA-DR	PE/Cy7	L243	2.5 µl	Biolegend
CD141	APC	AD5-14H12	2.5 µl	Biolegend
CD1c	PE	L161	2.5 µl	Biolegend
CD123	BV605	6H6	2.5 µl	Biolegend
CD19	A700	HIB19	1 µl	Biolegend
CD45	Pacific Blue	HI30	2.5 µl	Biolegend

Table 3. Antibody mix used to assess B cells in NSCLC patients.

Specificity	Fluorophore	Clone	Volume	Manufacturer
CD14	APC/Cy7	HCD14	2.5 µl	Biolegend
CD38	APC	HB-7	2.5 µl	Biolegend
CD19	PE/Cy7	HIB19	2.5 µl	Biolegend
CD27	PE	O323	2.5 µl	Biolegend
IgD	A488	IA6-2	2.5 µl	Biolegend
CD3	A700	UCHT1	1 µl	Biolegend
IgM	BV605	MHM-88	2.5 µl	Biolegend
CD45	Pacific Blue	HI30	2.5 µl	Biolegend

Table 4. Antibody mix used to assess granulocyte populations in NSCLC patients

Specificity	Fluorophore	Clone	Volume	Manufacturer
CD45	Pacific Blue	HI30	2.5 µl	Biolegend
HLA DR	BV605	I243	2.5 µl	Biolegend
CD19	A700	HIB19	1 µl	Biolegend
CD3	A700	UCHT1	1 µl	Biolegend
CD14	APC/Cy7	HCD14	2.5 µl	Biolegend
CD15	A488	W6D3	2.5 µl	Biolegend
CD11b	BV510	ICRF44	2.5 µl	Biolegend
CD49d	PE	9F10	2.5 µl	Biolegend
CD117	PE/Cy7	104D2	2.5 µl	Biolegend
FceR1a	APC	AER-37	2.5 µl	eBioscience

Table 5. Antibody mix used to assess NK cells in NSCLC patients.

Specificity	Fluorophore	Clone	Volume	Manufacturer
CD3	A488	UCHT1	2.5 µl	Biolegend
CD19	BV605	HIB19	2.5 µl	Biolegend
CD56	PE	HCD56	2.5 µl	Biolegend
CD16	APC	3G8	2.5 µl	Biolegend
CD14	APC/Cy7	HCD14	2.5 µl	Biolegend
CD45	Pacific Blue	HI30	2.5 µl	Biolegend

Table 6. Antibody mix used to assess T cells and PD-1 expression in NSCLC patients

Specificity	Fluorophore	Clone	Volume	Manufacturer
CD3	A488	UCHT1	2.5 µl	Biolegend
CD4	PE	OKT4	2.5 µl	Biolegend
CD8	APC/Cy7	SK1	2.5 µl	Biolegend
CD19	A700	HIB19	1 µl	Biolegend
PD-1	BV510	EH12.2H7	2.5 µl	Biolegend
CD45	Pacific Blue	HI30	2.5 µl	Biolegend
CD45RO	APC	UCHL1	2.5 µl	Biolegend
CD45RA	PE/Cy7	HI100	2.5 µl	Biolegend

Table 7. Antibody mix for PD-1 Isotype control

Specificity	Fluorophore	Clone	Volume	Manufacturer
CD3	A488	UCHT1	2.5 µl	Biolegend
CD4	PE	OKT4	2.5 µl	Biolegend
CD8	APC/Cy7	SK1	2.5 µl	Biolegend
CD19	A700	HIB19	1 µl	Biolegend
IgG1,k Isotype Control	BV510	EH12.2H7	2.5 µl	Biolegend
CD45	Pacific Blue	HI30	2.5 µl	Biolegend
CD45RO	APC	UCHL1	2.5 µl	Biolegend
CD45RA	PE/Cy7	HI100	2.5 µl	Biolegend

4.3.4 Protocol for cytometer calibration for analysis of immune cells from NSCLC patients

We used a BD LSRFortessa cytometer to analyse immune cells isolated from the samples. BD LSRFortessa is equipped with four lasers, blue, red, violet and yellow-green, and it can detect 18 different fluorophores. The computer connected to the cytometer is equipped with BD FACSDiva software and this software is used to help compensate for spectral overlap and control data acquisition.

The cytometer is set to detect area, height and width of forward scatter (FSC) and, side scatter (SSC) parameters, and area of 10 fluorophores (PI, Alexa Fluor 488, APC/Cy7, PE/Cy7, APC, PE, Brilliant Violet 605, Alexa Fluor 700, Pacific Blue and Briliant Viollet 510). 10 different channels are used to detect 10 fluorophores (Table 8). Channels are mainly named after the fluorophore they detect except for PerCP channel which is used to detect PI emission and AmCyan channel which is used to detect Brilliant Violet 510 emission. Voltage in each channel is kept constant for all experiments (Table 8) and threshold on the cytometer is set to 2500. To correct for spillover between channels, spectral overlap values are measured for all fluorophores and in all detectors via single stained controls. The compensation is then calculated automatically by the BD FACSDiva software.

Table 8. Cytometer settings

Channel	Fluorophore	Type	Voltage
FSC	FSC	A,H,W	225
SSC	SSC	A,H,W	270
PerCP	PI	A	599
Alexa Fluor 488	Alexa Fluor 488	A	457
APC/Cy7	APC/Cy7	A	515
PE/Cy7	PE/Cy7	A	520
APC	APC	A	560
PE	PE	A	460
Brilliant Violet 605	Brilliant Violet 605	A	595
Alexa Fluor 700	Alexa Fluor 700	A	512
Pacific Blue	Pacific Blue	A	459
AmCyan	Brilliant Violet 510	A	490

4.3.5 Protocol for preparation of single stains

Before running the samples, the cytometer was calibrated it by use of single stained PBMCs from the blood of healthy donors. The blood was obtained from the blood bank at Ullevål hospital in Oslo. The PBMCs were isolated from blood using the same protocol as for isolation of PBMCs from blood of patients. Protocol for single staining of PBMCs from healthy donor is similar to the protocol for staining of samples, and it was done simultaneously.

1. One million PBMCs are stained with only one antibody. One sample for each fluorophore used in the experiment, and one sample for unstained control.

2. PBMCs are incubated for 20 minutes on ice, and in the dark

3. Following the incubation PBMCs were centrifuged at 420g at 4^{o}C for 6 minutes. The supernatant was discarded and the pellet was resuspended in 150µl Flow buffer. This step is repeated twice

4. The PBMCs were centrifuged one last time at 410g at 4^{o}C for 6 minutes. The supernatant was discarded and the pellet was resuspended in 200µl of Flow buffer.

4.3.6 Protocol for immunohistochemistry staining

Paraffin embedded tumor tissue and lung tissue were sectioned in 4 µm tick tissue sections, and stained in Ventana Benchmark, XT automated slide stainer (Ventana Medical). The staining procedure is automated and it starts with deparafinisation of the tissue sections. After deparafinisation, the samples are cooked in tris-EDTA to retrieve epitopes masked by paraffin. Once the epitopes are made available the primary anti CD45 antibody (clone 12B11 & PD7/26 Ventana) is added to the sections. The sections were incubated for 30 minutes followed by washing step and incubation with secondary antibody, conjugated with horseradish peroxidase. Excess secondary antibody was washed away and diaminobenzene was added to the slides. Horseradish peroxidase catalyses conversion of diaminobenzene into a brown coloured product. This gives brown colour to the sites of primary antibody binding. Tissues sections were counterstained with haematoxylin to visualize cell nuclei.

4.4 Statistical analysis of data

Statistical data was gathered from the analysis of cells in FlowJo v10 software. The values acquired from FlowJo were used for statistical analysis in Graph Pad prism 6.0. We analysed percentages of $CD45^{+}$ live leukocytes in single cells and percentage of different cell types in $CD45^{+}$ live leukocytes. To determine if the difference between three or more group means we used non-parametric, Kruskal-Wallis analysis of variance and post hoc Dunn's multiple comparison test. Results were considered statistically significant if Dunn's test showed a p value of less than 0.05. In the case where we only had only two groups we used non-paired two-tailed Mann-Whitney test, and results were considered statistically significant if p value was below 0.05.

5 Results

5.1 Flow cytometry analysis and statistical comparison of immune cells

The flow cytometry data acquired in this study was analysed in two dimensional dot plots and one dimensional histograms. For each staining, the same gating strategy was used for each tissue, and in all patients, to be able to compare the results. Threshold for all gate in each type of cells was established based on matched-antibody isotype controls in each tissue type.

There are three gates that are used in gating strategies for all types of cells: (I) nucleated cell gate, (II) single cell gate and (III) live leukocytes gate. The fourth gate (IV) which defines lymphocytes, is not present in all gating strategies, but it is present in T cells, B cells, NK cells and in the gating strategy for PD-1 expression. These four gates will be discussed in this part of the thesis. Other gates are specific to each of the gating strategy and cell type, and will be explained in their own specific sections.

(I) Nucleated cell gate is used to remove debris, non-cell events, and it is placed in a plot with SSC and FSC (Figure 3A). SSC is a measure of complexity of the event (shows how granulated the cell is) and FSC is a measure of size of the event. Combination of these two parameters allows the exclusion of events that are too small to be cells. The threshold of this gate is set by backgating the smallest cells we study, and those are the naive T cells. This backgating showed that all events under 70K can be excluded from the analysis.

(II) Single cell gate is set in a FSC-H/FSC-A graph. FSC is measure of size of the event, presented in the histogram. In the histogram FSC-H is the measure of height of the peak of the event and FSC-A is a measure of the area of the event under the peak. Because of the linear correlation between FSC-H and FSC-A parameters, single cells will appear along the diagonal of the graph and the doublets will appear outside the diagonal. This allowed us to exclude the doublets from the analysis by setting a single cell gate.

(III) From the single cell gate leukocytes are further gated as $CD45^+PI^-$ in the live leukocytes gate. All leukocytes are $CD45^+$, and PI will stain dead cells by penetrating the cell membrane and intercalating between nuclear bases of DNA. This marks live leukocytes as PI^-.

(IV) Leukocytes are further gated in a lymphocyte gate based on the size and granularity of cells. The lymphocyte gate includes $CD45^+$ lymphocytes but does not exclude all other types of cells. This gate will exclude most granulocytes, some of the dendritic cells and some monocytes/macrophages. This is why the lymphocyte gate is omitted in APC and granulocyte gating strategy.

We used the data collected with flow cytometry to do statistical analysis between the tissues and in different clinicopathological parameters. First we did comparison of immune cells between the four tissues: tumor, distant lung, lymph node and PBMCs. This comparison was done to examine possible difference of immune cells infiltration between the tumor tissue and distant lung. When analyzing immune cells in different tissues, patients were divided in two groups; one group of patients was diagnosed with adenocarcinoma and the other group was diagnosed with squamous cell carcinoma. The second analysis compared immune cells between the different tumor types, to examine if different histological type of tumor have influence on immune response. The third analysis compared cells in different stages of the disease to examine if the disease progression influences immune response. Finally we compared immune cell infiltration in tumor in patients with different smoking histories, to see if smoking influences immune response to tumor.

We also investigate PD-1 expression on T cells to (1) examine difference in PD-1 expression between tumor and distant lung and (2) to investigate expression profile between the patients.

5.2 Analysis of live leukocytes

In order to determine the percentages of all populations of live leukocytes we made use of the counted events in the nucleated cell gates, single cell gate and live leukocyte gate (Figure 9 A, B). Percentages of live leukocytes were obtained by calculating the percentage of $CD45^{+}PI^{-}$ cells in single cell population (Figure 9C). We examined percentages of live leukocytes in different tissues from patients diagnosed with

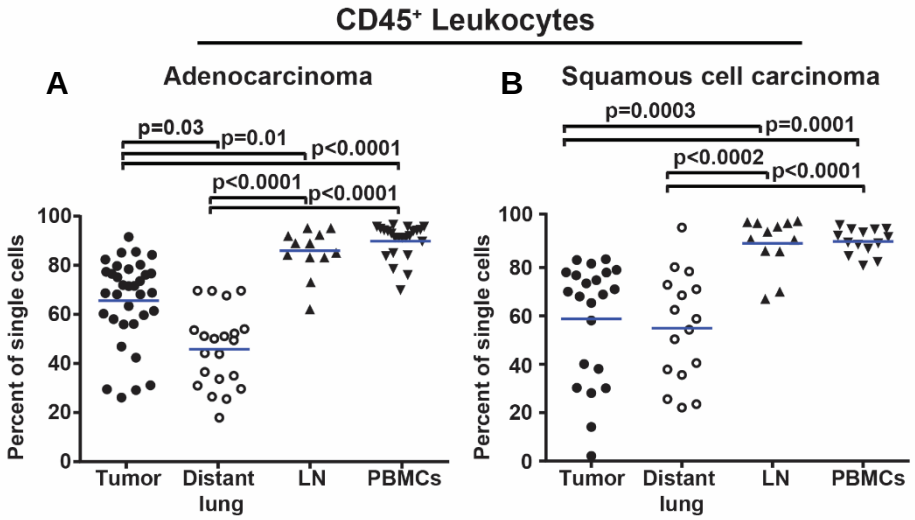

Figure 6. Characterization of live leukocyte population in tumor, distant lung, lymph node and PBMCs. Kruskal-Wallis analysis of live leukocytes in single cell population in four different tissues from patients diagnosed with **A**. adenocarcinoma and **B**. squamous cell carcinoma. Statistically significant differences between group means are obtained through Dunn's test. Each symbol represents data collected from one patient, as a percentage of single cells. LN = lymph node and PBMCs = peripheral blood nucleated cells.

adenocarcinoma and squamous cell carcinoma (Figure 6). Statistical analysis of live leukocytes in adenocarcinoma patients (Figure 6A) shows higher percentage in tumor than in distant lung (p=0.03), while leukocytes in squamous cell carcinoma (Figure 6B) show no significant difference between tumor and distant lung.

Comparison of leukocyte percentages in different tumor stages (Figure 7A), and in patients with different smoking histories (Figure 7B) showed that neither tumor stage nor different smoking histories had impact on percent of $CD45^+$ leukocyte in tumor tissue. Analysis of leukocytes in different histological tumor types indicates that adenocarcinoma had statistically significant higher percent of leukocytes than carcinoid tumor, however, only three patients with carcinoid tumors could be analysed (Figure 7 C). Other types of tumor could not be evaluated due to the small number of patients. Looking at Figure 7A, 7B and even 7C we observed that there is a tendency of leukocytes separating into two groups; one group with low and one with high percentages of leukocytes.

We further analysed $CD45^+$ cells using immunocytochemistry to confirm the infiltration of leukocytes in tumor, and to investigate which part of the tumor they infiltrate.

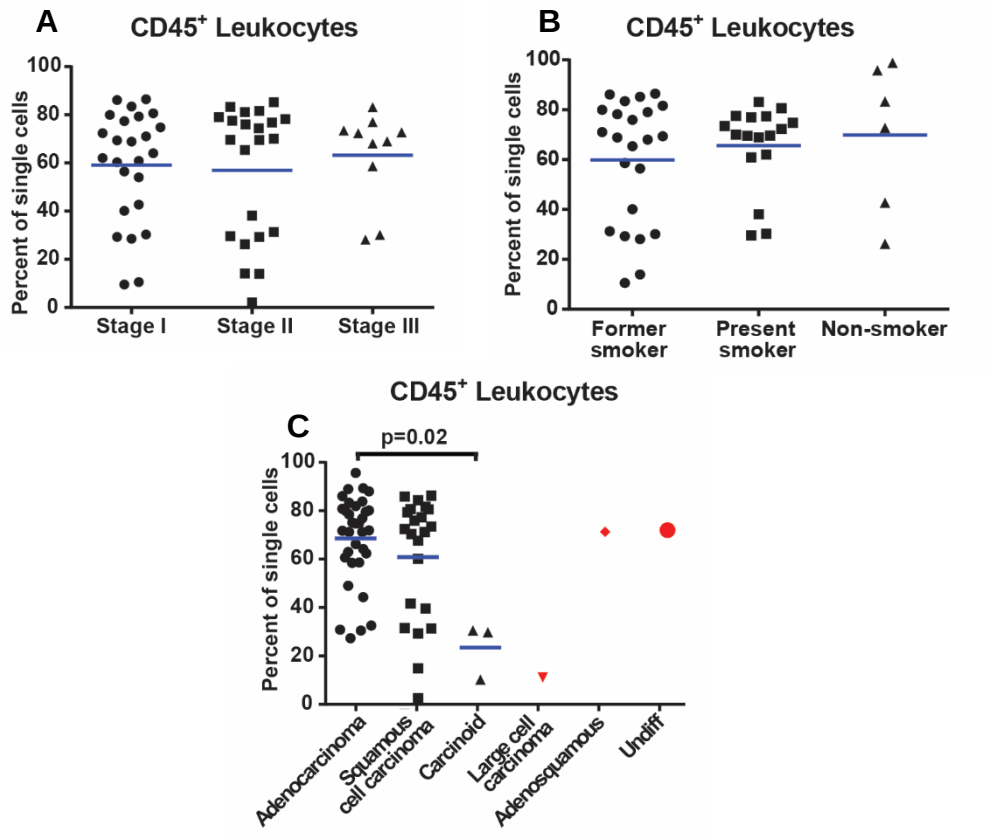

Figure 7. Characterization of $CD45^+$ in different clinicopathological parameters. Kruskal-Wallis analysis of live leukocytes in tumor tissue with respect to **A.** tumor stage, **B.** smoking history, and **C.** histological type of tumor. Kruskal-Wallis test was followed by Dunn's post hoc test. Each symbol represents data collected from one patient, as a percentage of single cells. LN lymph node and PBMCs means peripheral blood mononuclear cells.

We found tumor infiltrating leukocytes both in adenocarcinoma (Figure 8A) and in squamous cell carcinoma (Figure 8B). Leukocytes infiltrated both tumor stroma and tumor islets, but stroma is infiltrated in higher degree (Figure 8).

Since our flow cytometry analysis of $CD45^+$ live leukocytes revealed high level of individual differences between patients (Figure 6) we chose six random patients and compared microscopy analysed immunostained sections with flow cytometry data for $CD45^+$ leukocytes in tumor. Our semi-quantitative analysis revealed that percentages of leukocytes obtained by flow cytometry grossly correlated with immunohistochemistry staining (example in Figure 8A). Patients with high percent of $CD45^+$ leukocytes analysed by flow, showed high numbers of leukocytes in stained tissue sections as well. However, flow cytometry analysis tends to show higher percentages than what is observed in the sections (data not shown). This could be due to the methodological differences, for example some of the non-immune cells could be lost during cell isolation from tissues.

To illustrate the correlation between findings from flow cytometry analysis and immunohistochemistry stainings we chose two patients, one with 86% of leukocytes in single cell gate and the other with 38% of leukocytes in single cell population and compared flow cytometry analysis with immunohistochemistry analysis in these patients. Results are shown in Figure 8.

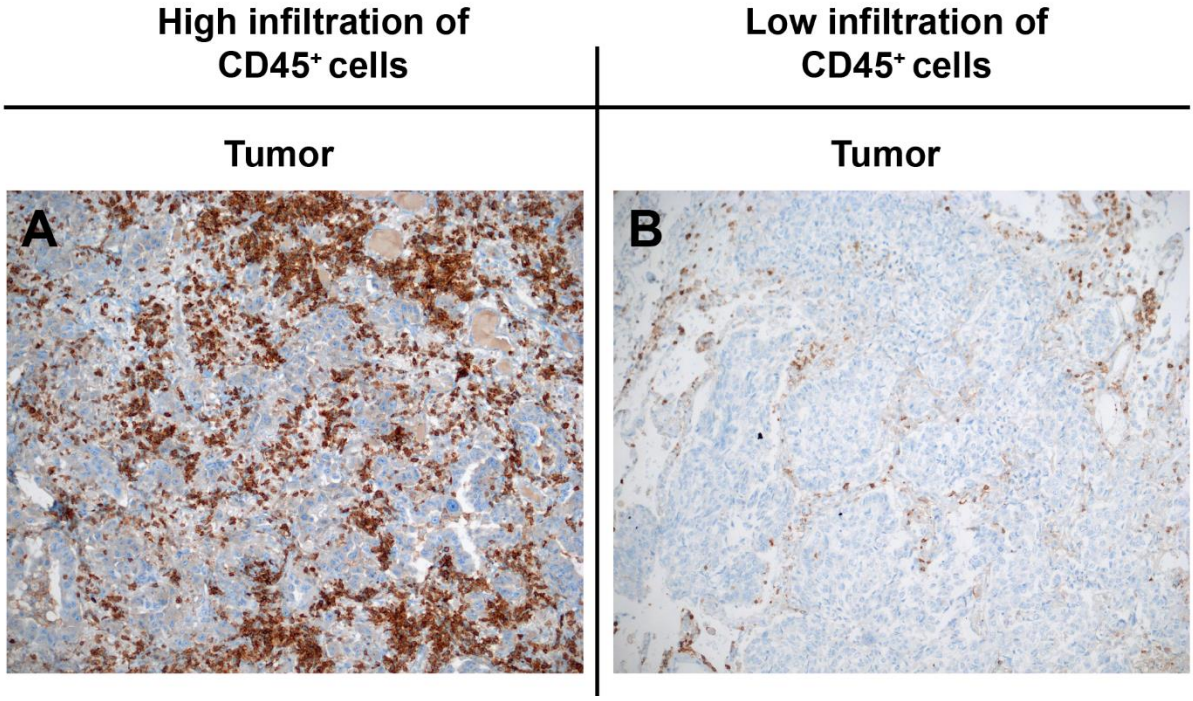

Figure 8. High and low infiltration of $CD45^+$ leukocytes in immunostained tissue sections from tumors of two patients. A. Microscopic picture of representative area of adenocarcinoma type, in 100x magnification in the patient that by flow cytometry showed 86% of $CD45^+$ cells in tumor. **B.** Microscopic picture of representative area of NSCLC of squamous cell carcinoma type, in 100x magnification in patients that showed 38% of $CD45^+$ cells in tumor in flow cytometry analysis.

5.2.1 Analysis of T cells

In the flow cytometry analysis of T cell all events were first gated in nucleated cell gate (SSC/FSC plot), then events from this gate were plotted in single cell gate to exclude doublets (FSC-H/FSC-A graph). Single cells were further gated in live leukocytes gate to exclude dead cells and non-leukocytes (Figures 9-12 A, B and C). Then a strict lymphocyte gate was set in FSC-A/SSC-H plot in order to, as much as possible, exclude non lymphocytes (Figures 9-12 D). In lymphocyte populations we observed: $CD19^-CD3^+$ T cells, $CD19^+CD3^-$ B cells and a double negative population. The T cell population was investigated for CD4, and CD8 expression, and three populations were observed: $CD4^+$, $CD8^+$, and $CD4^-CD8^-$ double negative (DN) (Figures 9-12 F). Each of the T cell populations was separated into $CD45RO^-CD45RA^+$ naive subset, and $CD45RO^+CD45RA^-$ memory subset (Figures 9-12 G, H, I). All T cells defined by the flow cytometry analysis are presented in table 9.

All the thresholds for the gates in flow cytometry analysis were set based on the staining with isotype controls of the relevant tissues. Percentages in the Figures 9-12 represent mean value of each cell type in the $CD45^+PI^-$ population – live leukocytes. Mean for each cell population is calculated from percentages gathered from all patients stained for T cells. Mean is calculated for each tissue separately.

Table 9. Definition of T cell subsets by flow cytometry

Cell population	Molecular marker
T cells	$CD45^+PI^-CD3^+CD19^-$
$CD4^+$T cells	$CD45^+PI^-CD3^+CD19^-CD8^-CD4^+$
$CD4^+$ Naive cells	$CD45^+PI^-CD3^+CD19^-CD8^-CD4^+CD45RA^+CD45RO^-$
Memory $CD4^+$ T cells	$CD45^+PI^-CD3^+CD19^-CD8^-CD4^+CD45RA^-CD45RO^+$
$CD8^+$ T cell	$CD45^+PI^-CD3^+CD19^-CD8^+CD4^-$
$CD8^+$ Naive T cell	$CD45^+PI^-CD3^+CD19^-CD8^+CD4^-CD45RA^+CD45RO^-$
Memory $CD8^+$ T cell	$CD45^+PI^-CD3^+CD19^-CD8^-CD4^+CD45RA^-CD45RO^+$

The data acquired in flow cytometry analysis was used to perform statistical analysis of T cells, and compare T cell infiltration between different tissues, different histological types of tumor, different stages of tumor and between patients with different smoking histories.

Analysis of $CD3^+$ T cells in different tissues did not show significant differences between any of the tumor types and distant lung tissue (Figure 13 A and B). $CD3^+$ T cells in tumor tissue of both adenocarcinoma and squamous cell carcinoma showed great individual variations between the patients. The only significant difference in $CD3^+$ T cells

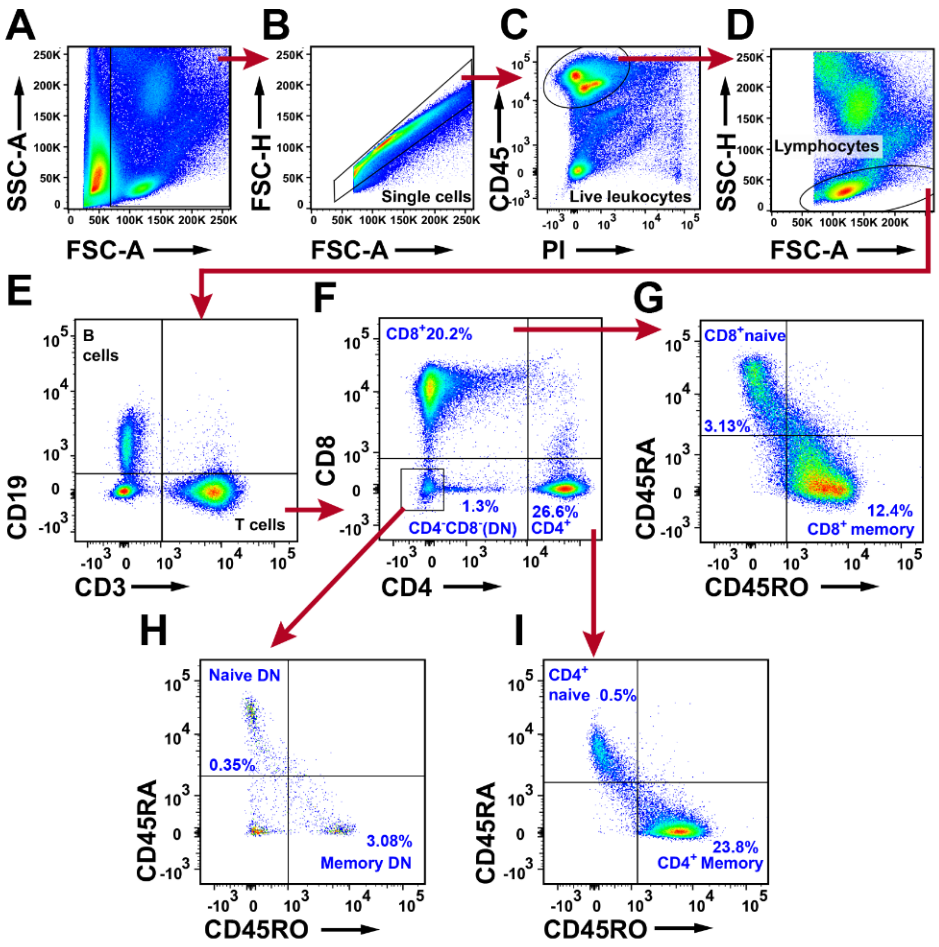

Figure 9. Flow cytometry analysis of T cells in tumor in NSCLC patients. A. SSC and FSC plot used to generate the nucleated cell gate. Debris was gated out by the left rectangle, and the remaining cells were assumed to be nucleated. **B.** FSC-A and FSC-H plot used to gate single cells. **C.** Live leukocyte gate, drawn by circle. Live leukocytes are defined as $CD45^+PI^-$. **D.** Lymphocyte gate. **E.** T cells are defined as $CD19^-CD3^+$ population and further divided in **F.** $CD4^+$ population, $CD8^+$ population and $CD4^-CD8^-$ populations. Each subset was examine for $CD45RA^+CD45RO^-$ naive phenotype and $CD45RA^-CD45RO^+$ memory phenotype. **G.** Naive/Memory phenotyping of $CD8^+$ T cells. **H.** Naive/Memory phenotyping of $CD4^-CD8^-$ T cells. **I.** Naive/Memory phenotyping of $CD4^+$ T cells. Percentages of presented in the figure are average percent of total live leukocytes, calculated from all patients stained for T cells. DN – $CD4^-CD8^-$ double negative T cells.

was observed between squamous cell carcinoma and lymph node, where lymph node had higher percentages of $CD3^+$ T cells (Figure 13B).

Investigation of $CD4^+$T cells in different tissue types revealed individual differences between the patients, but no differences were observed between tumor tissues and distant lung tissue (Figure 13 C and D). Analysis of the memory $CD4^+$ T cells in adenocarcinoma showed no significant difference between any of the tissues (Figure 14A). The naive $CD4^+$ T cells were more prominent in PBMC and lymph node than in adenocarcinoma, as expected (figure14 C, D). In squamous cell carcinoma naive $CD4^+$ T cells showed higher infiltration in lymph node compared to tumor, but no significant difference between the tumor and the distant lung was observed (Figure 14B).

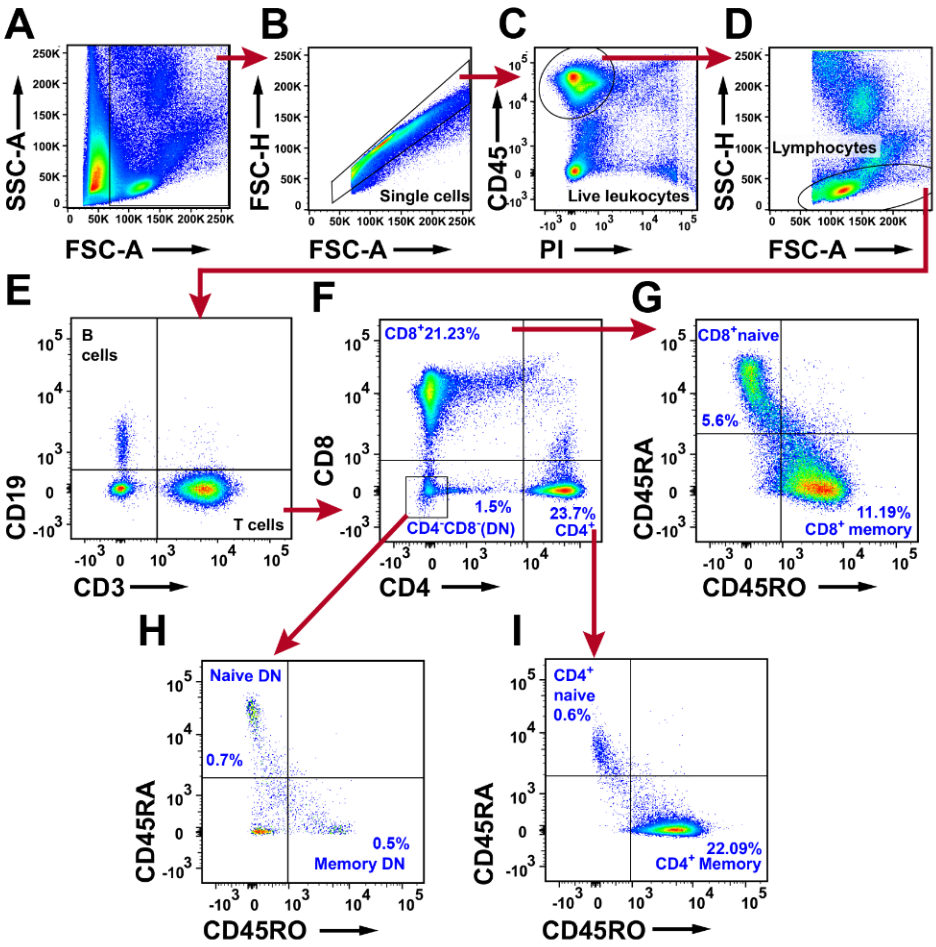

Figure 10. Flow cytometry analysis of T cells in distant lung in NSCLC patients. A. SSC and FSC plot used to generate the nucleated cell gate. Debris was gated out by the left rectangle, and the remaining cells were assumed to be nucleated. **B.** FSC-A and FSC-H plot used to gate single cells. **C.** Live leukocyte gate, drawn by circle. Live leukocytes are defined as $CD45^{+}PI^{-}$. **D.** Lymphocyte gate. **E.** T cells are defined as $CD19^{-}CD3^{+}$ population and further divided in **F.** $CD4^{+}$ population, $CD8^{+}$ population and $CD4^{-}CD8^{-}$ populations. Each subset was examine for $CD45RA^{+}CD45RO^{-}$ naive phenotype and $CD45RA^{-}CD45RO^{+}$ memory phenotype. **G.** Naive/Memory phenotyping of $CD8^{+}$ T cells. **H.** Naive/Memory phenotyping of $CD4^{-}CD8^{-}$ T cells. **I.** Naive/Memory phenotyping of $CD4^{+}$ T cells. Percentages of presented in the figure are average percent of total live leukocytes, calculated from all patients stained for T cells. DN – $CD4^{-}CD8^{-}$ double negative T cells.

Analysis of $CD8^{+}$T cells in different tissue types revealed that adenocarcinoma has higher percentages of these cells compared to the lymph node (p= 0.0004; Figure 13 E). The higher percentages of $CD8^{+}$ T cells in adenocarcinoma were mainly due to the increased percentage of memory population of $CD8^{+}$ T cells in tumor compared to lymph node (p= 0.0003; Figure 15 A). Analysis of $CD8^{+}$ T cells in squamous cell carcinoma showed no significant difference between the tumor tissue and the distant lung (Figure 13F). Memory subset of $CD8^{+}$ T cells showed higher percentages in squamous cell carcinoma compared to PBMCs while naive subset had lower percentages in tumor compared to the PBMCs (Figure 15 B, D)

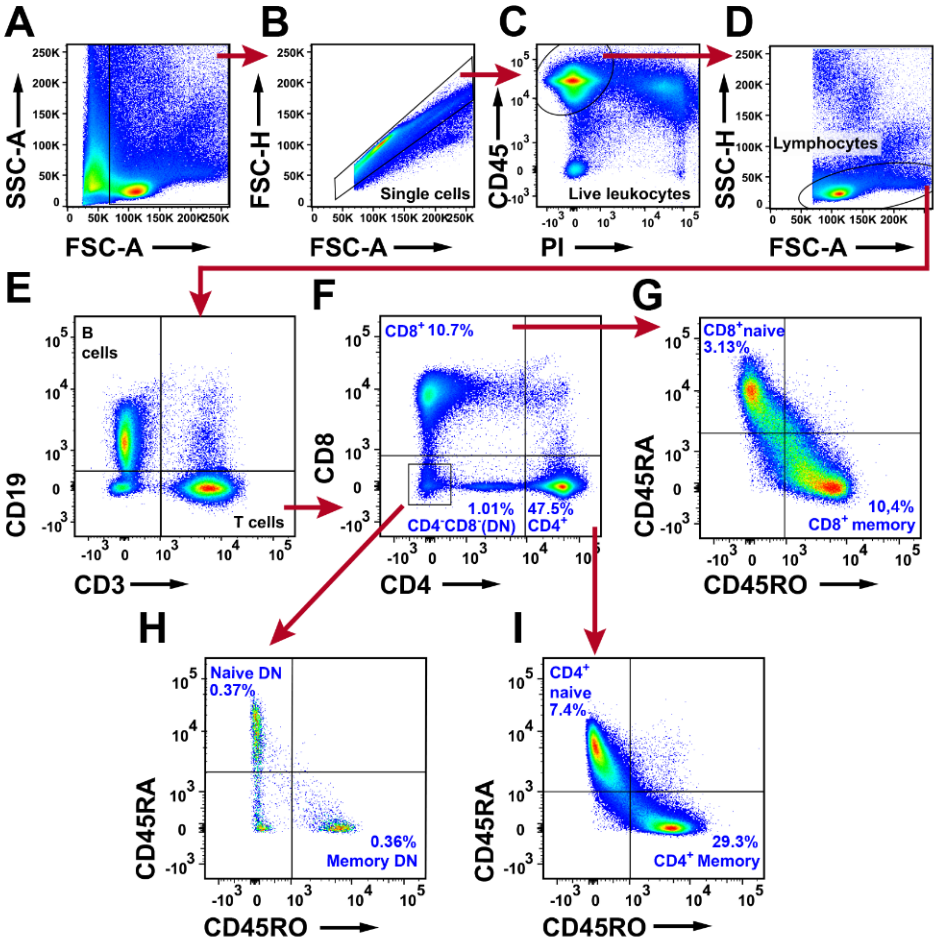

Figure11. Flow cytometry analysis of T cells in lymph node in NSCLC patients. A. SSC and FSC plot used to generate the nucleated cell gate. Debris was gated out by the left rectangle, and the remaining cells were assumed to be nucleated. **B.** FSC-A and FSC-H plot used to gate single cells. **C.** Live leukocyte gate, drawn by circle. Live leukocytes are defined as $CD45^{+}PI^{-}$. **D.** Lymphocyte gate. **E.** T cells are defined as $CD19^{-}CD3^{+}$ population and further divided in **F.** $CD4^{+}$ population, $CD8^{+}$ population and $CD4^{-}CD8^{-}$ populations. Each subset was examine for $CD45RA^{+}CD45RO^{-}$ naive phenotype and $CD45RA^{-}CD45RO^{+}$ memory phenotype. **G.** Naive/Memory phenotyping of $CD8^{+}$ T cells. **H.** Naive/Memory phenotyping of $CD4^{-}CD8^{-}$ T cells. **I.** Naive/Memory phenotyping of $CD4^{+}$ T cells. Percentages of presented in the figure are average percent of total live leukocytes, calculated from all patients stained for T cells. DN – $CD4^{-}CD8^{-}$ double negative T cells.

Analysis of $CD4^{-}CD8^{-}$ T cells, as well as their memory and naive subsets, between different tissues in adenocarcinoma and squamous cell carcinoma shows no differences between the means (Figure 16). Analysis of T cells in different stages of the disease, between the patients with different smoking histories and between different tumor types showed that these clinicopathological parameters had no influence on T cell infiltration in tumor (Figures 17 and 18).

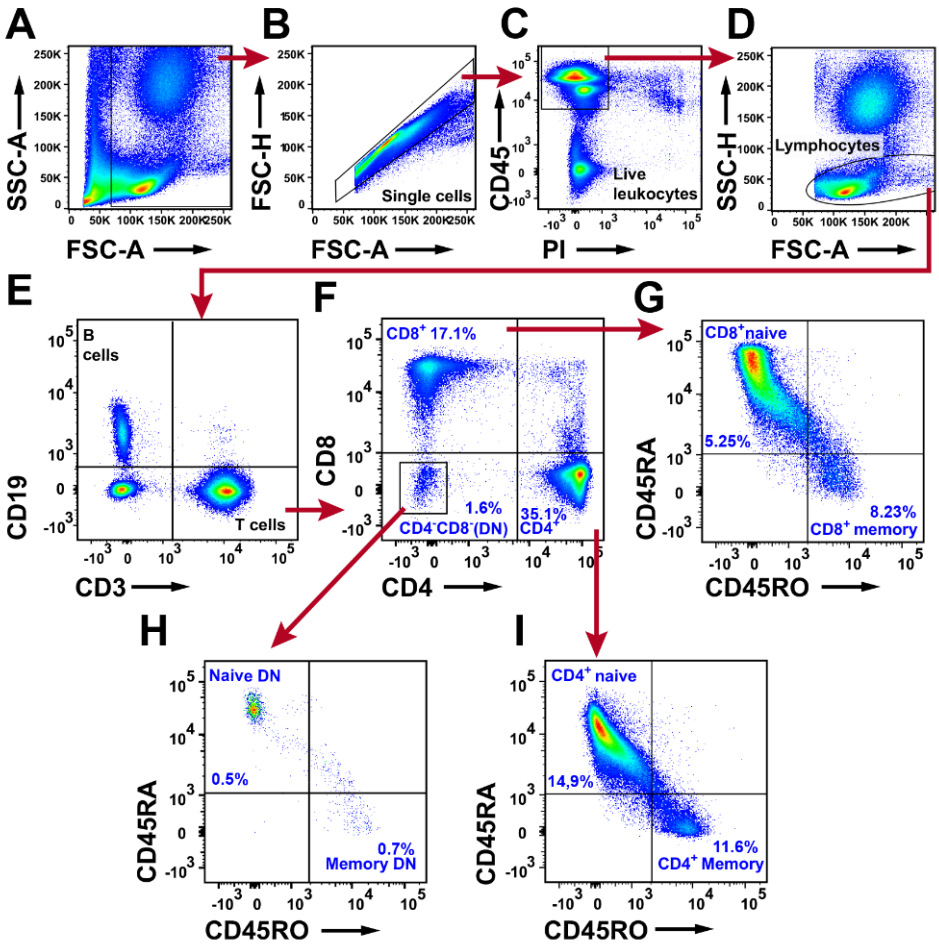

Figure 12. Flow cytometry analysis of T cells in PBMCs in NSCLC patients. A. SSC and FSC plot used to generate the nucleated cell gate. Debris was gated out by the left rectangle, and the remaining cells were assumed to be nucleated. **B.** FSC-A and FSC-H plot used to gate single cells. **C.** Live leukocyte gate, drawn by circle. Live leukocytes are defined as $CD45^{+}PI^{-}$. **D.** Lymphocyte gate. **E.** T cells are defined as $CD19^{-}CD3^{+}$ population and further divided in **F.** $CD4^{+}$ population, $CD8^{+}$ population and $CD4^{-}CD8^{-}$ populations. Each subset was examine for $CD45RA^{+}CD45RO^{-}$ naive phenotype and $CD45RA^{-}CD45RO^{+}$ memory phenotype. **G.** Naive/Memory phenotyping of $CD8^{+}$ T cells. **H.** Naive/Memory phenotyping of $CD4^{-}CD8^{-}$ T cells. **I.** Naive/Memory phenotyping of $CD4^{+}$ T cells. Percentages of all populations are average percent of total live leukocytes for all patients stained for T cells. DN – $CD4^{-}CD8^{-}$ double negative T cells.

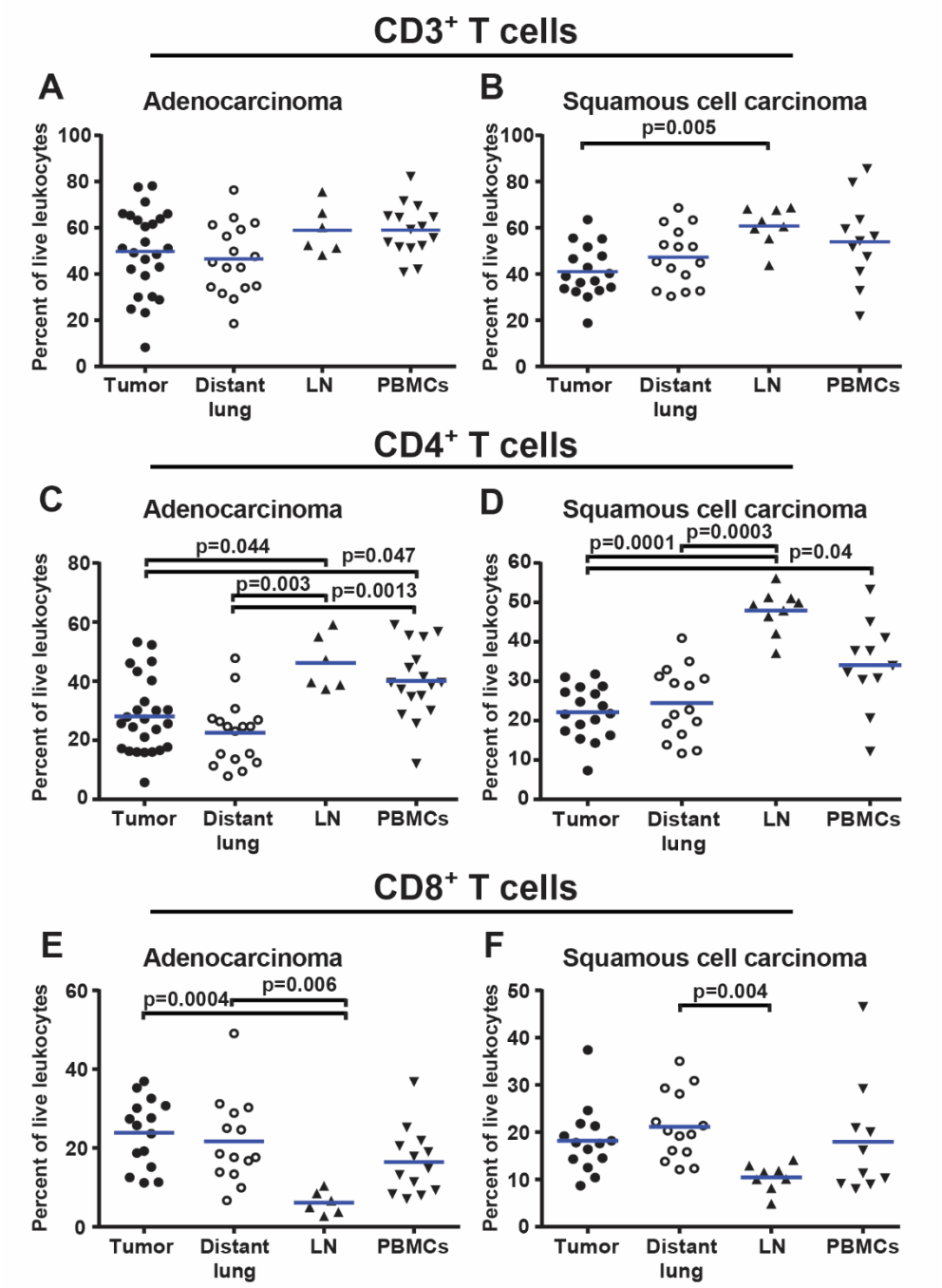

Figure 13. Percentage of CD3⁺, CD4⁺ and CD8⁺ T cells in different tissues in adenocarcinoma and squamous cell carcinoma patients. Comparison of CD3⁺ T cells in tissues of patients diagnosed with **A.** adenocarcinoma and **B**. squamous cell carcinoma. Comparison of CD4⁺ T cells in tissues from patients diagnosed with **C.** adenocarcinoma patients and **D.** squamous cell carcinoma. Comparison of CD8⁺ T cells in tissues of patients diagnosed with **E.** adenocarcinoma patients and **F.** squamous cell carcinoma. Kruskal-Wallis test and Dunn's multiple comparison were used to detect differences between means. The presented values in percentages were calculated from the total number of cells in live leukocyte population. Each symbol represents data collected from one patient, as a percentage of live leukocyte population and the mean is represented by the blue line. Abbreviation meaning: LN = lymph node, and PBMCs = peripheral blood mononuclear cells.

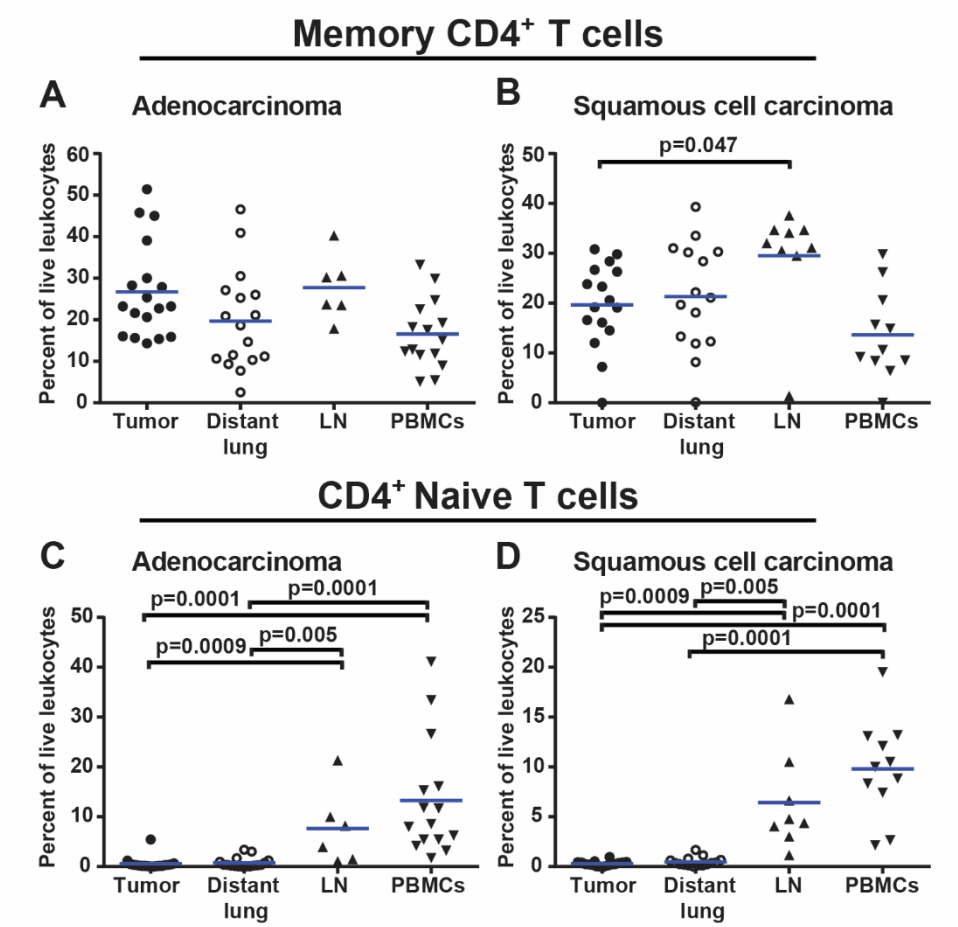

Figure 14. Percent of memory and naive subsets of CD4⁺ T cells in different tissues of patients diagnosed with adenocarcinoma and squamous cell carcinoma. Comparison of the memory CD4⁺ T cells in tissues form patients diagnosed with **A.** adenocarcinoma and **B.** squamous cell carcinoma patients. Comparison of the naive CD4⁺ T cells in **C.** adenocarcinoma and **D.** squamous cell carcinoma. Kruskal-Wallis test and Dunn's multiple comparison were used to detect differences between means. The presented values in percentages were calculated from the total number of cells in live leukocyte population. Each symbol represents data collected from one patient, as a percentage of live leukocyte population and the mean is represented by the blue line. LN = lymph node, PBMCs = peripheral blood mononuclear cells.

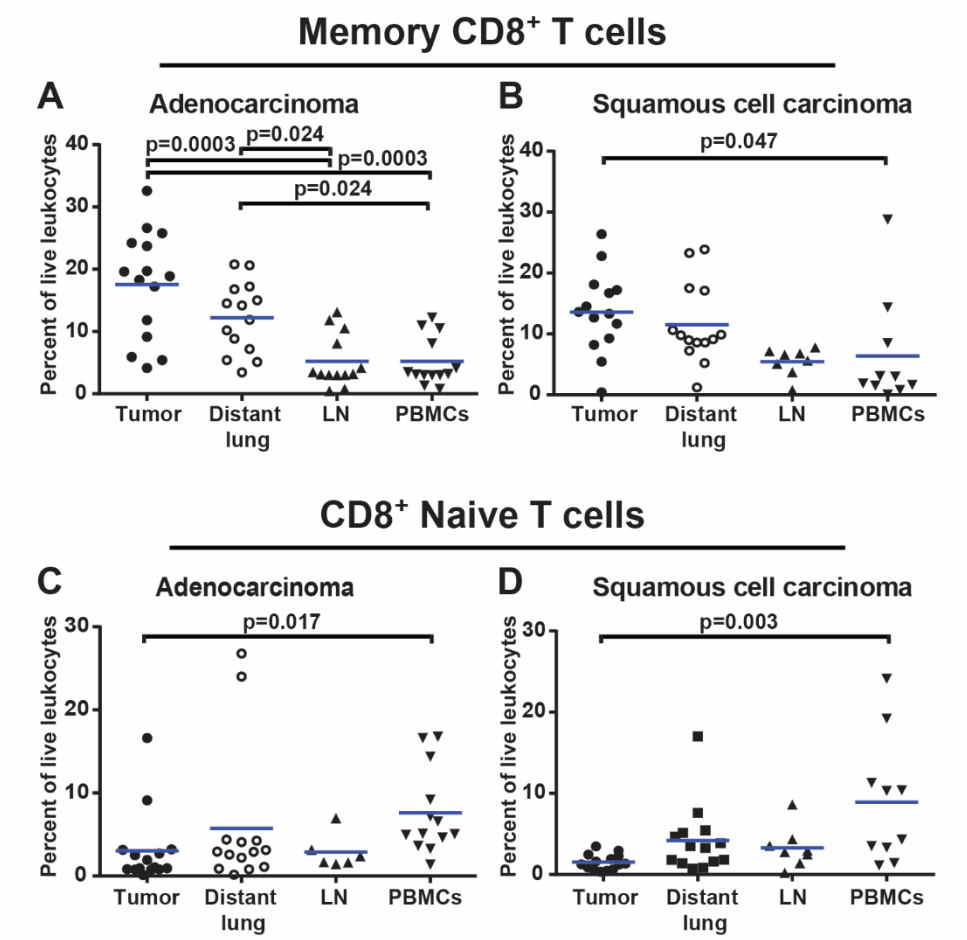

Figure 15. Characterization of naive and memory subsets of CD8⁺ T cells in different tissues of patients diagnosed with adenocarcinoma and squamous cell carcinoma. Comparison of memory CD8⁺ T cells in tissues of patients diagnosed with **A.** adenocarcinoma and **B.** squamous cell carcinoma. Comparison of naive CD8⁺ T cells in tissues of patients diagnosed with **C.** adenocarcinoma and **D.** squamous cell carcinoma. Kruskal-Wallis test and Dunn's multiple comparison were used to detect differences between means. The presented values in percentages were calculated from the total number of cells in live leukocyte population. Each symbol represents data collected from one patient, as a percentage of live leukocyte population and the mean is represented by the blue line. LN = lymph node, PBMCs = peripheral blood mononuclear cells.

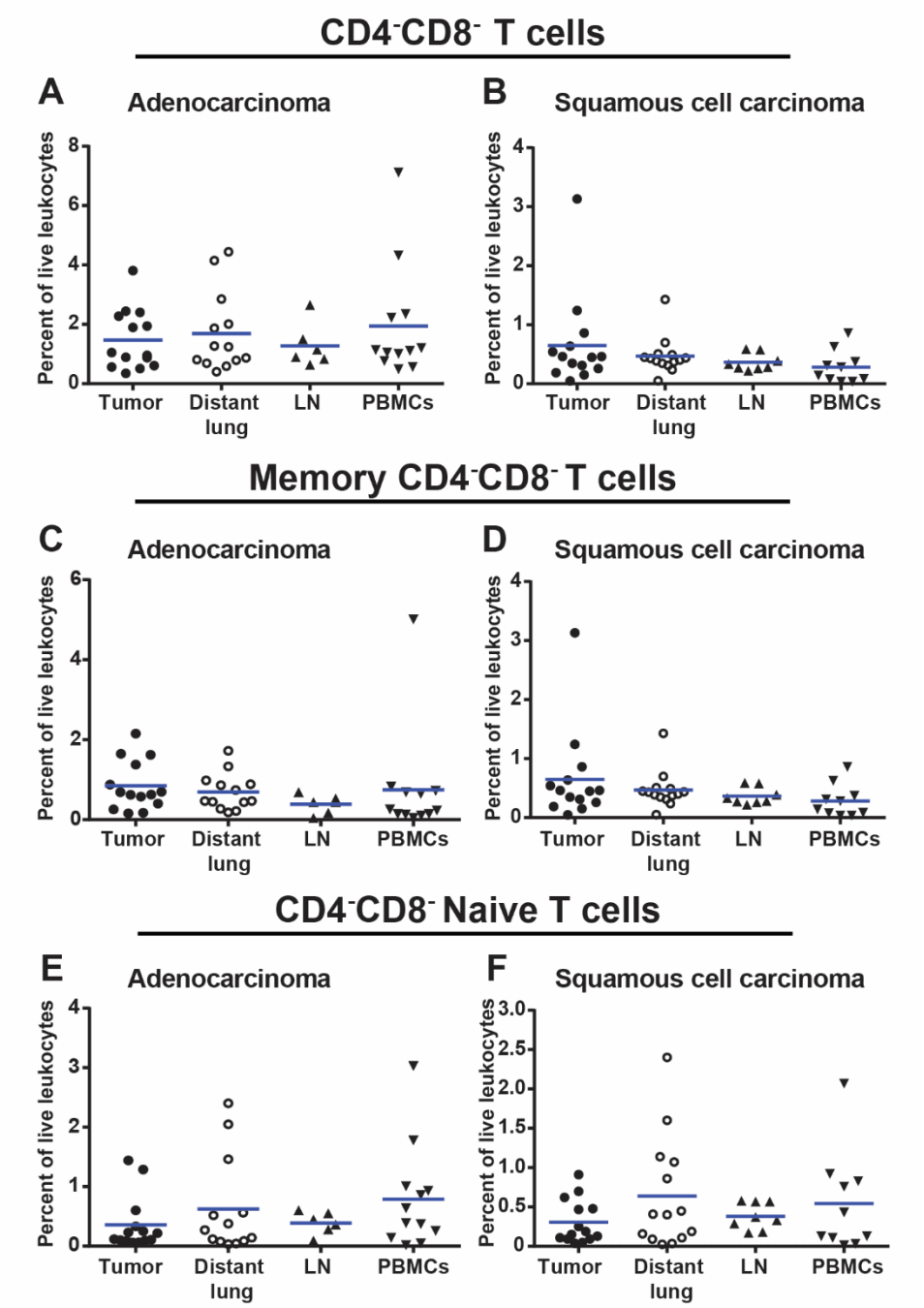

Figure 16. Percent of CD4$^-$CD8$^-$ T cell and their memory and naive subsets in different tissues of patiets diagnosed with adenocarcinoma and squamous cell carcinoma. Comparison of CD4$^-$CD8$^-$ T cells in tissues of patients diagnosed with **A.** adenocarcinoma, and **B.** squamous cell carcinoma. Comparison of memory subset of CD4$^-$ CD8$^-$ T cells in tissues of patients diagnosed with **C.** adenocarcinoma patients **D.** squamous cell carcinoma. Comparison of naive subset of CD4$^-$CD8$^-$ T cells in tissues of patients diagnosed with **E.** adenocarcinoma and **F.** squamous cell carcinoma. Kruskal-Wallis test and Dunn's multiple comparison were used to detect differences between means. The presented values in percentages were calculated from the total number of cells in live leukocyte population. Each symbol represents data collected from one patient, as a percentage of live leukocyte population and the mean is represented by the blue line. Abbreviation meaning: LN = lymph node, PBMCs = peripheral blood mononuclear cells.

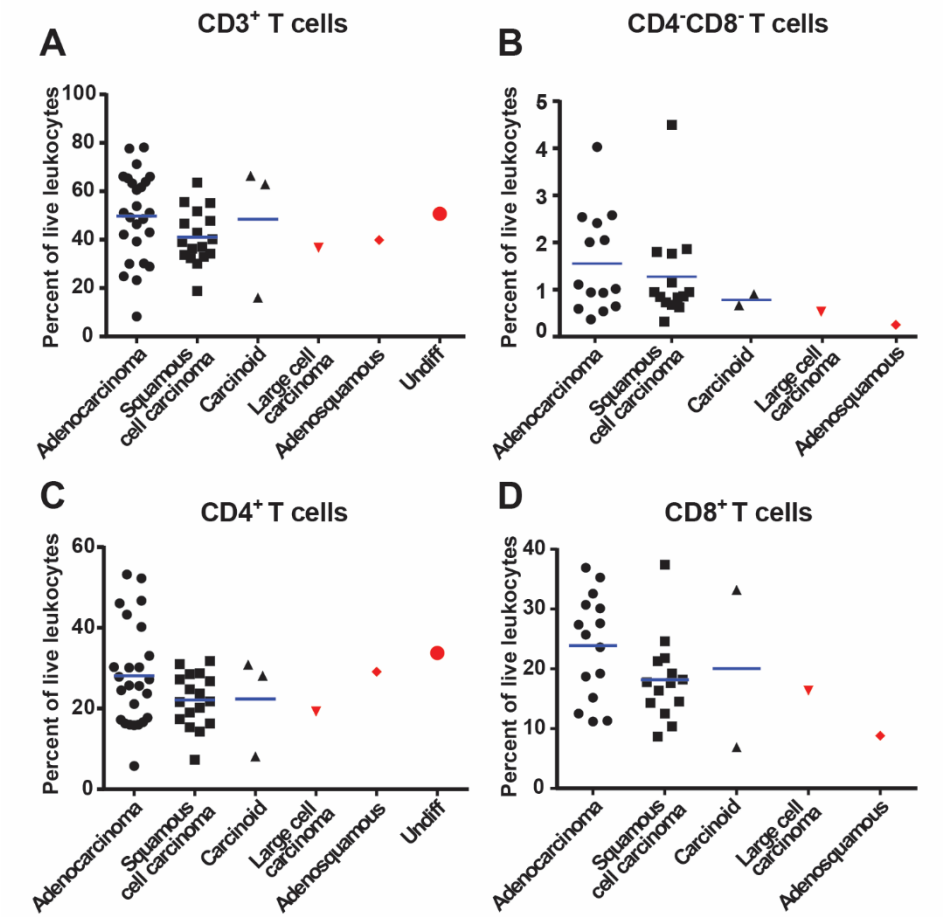

Figure 17. Percent of $CD3^+$ $CD4^+$, $CD8^+$ and, $CD4^-CD8^-$ T cells in different histological types of tumor. Comparison of tumor infiltrating **A.** $CD3^+$ T cells **B.** $CD4^+$ T cells **C.** and $CD8^+$ T cells and **D.** $CD4^-CD8^-$ T cells in adenocarcinoma, squamous cell carcinoma, carcinoid tumor, large cell carcinoma, adenosquamous tumor and undifferentiated tumor. Kruskal-Wallis test and Dunn's multiple comparison were used to detect differences between means. The presented values in percentages were calculated from the total number of cells in live leukocyte population. The presented values in percentages were calculated from the total number of cells in live leukocyte population. Each symbol represents data collected from one patient, as a percentage of live leukocyte population and the mean is represented by the blue line. Abbreviation meaning: LN = lymph node, PBMCs = peripheral blood mononuclear cells.

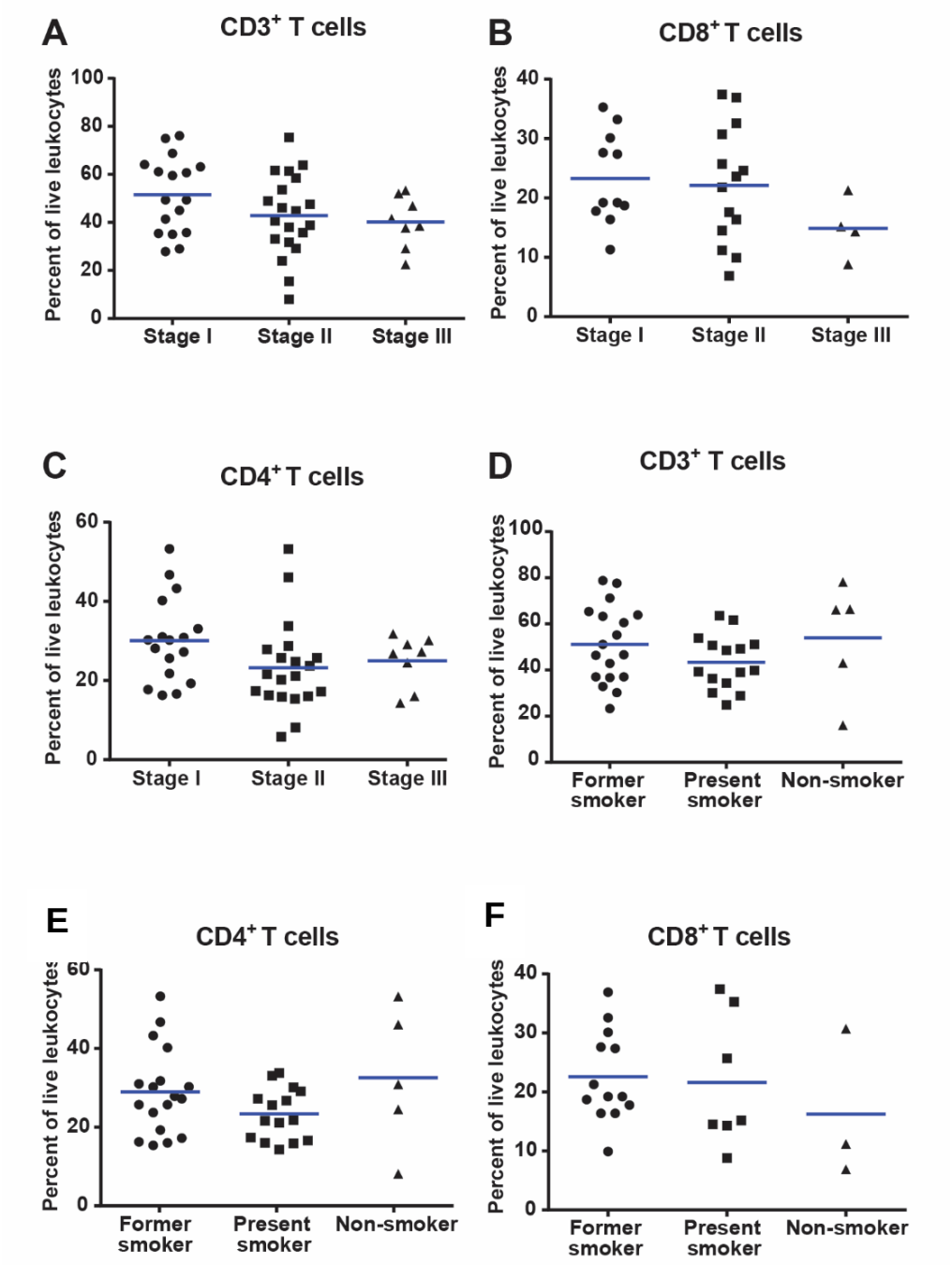

Figure 18. Percent of CD3⁺ CD4⁺ and CD8⁺ T cells in different tumor stages and patients with different smoking histories. Comparison of tumor infiltrating **A.** CD3⁺ T cells **B.** CD8⁺ T cells and **C.** and CD4⁺ T cells in stages I, II and III of NSCLC. Comparison of **D.** CD3⁺ T cells, **E.** CD4⁺ T cells, and **F.** CD8⁺ T cells in patients with different smoking history. Kruskal-Wallis test and Dunn's multiple comparison were used to detect differences between means. The presented values in percentages were calculated from the total number of cells in live leukocyte population. The presented values in percentages were calculated from the total number of cells in live leukocyte population. Each symbol represents data collected from one patient, as a percentage of live leukocyte population and the mean is represented by the blue line. Abbreviation meaning: LN = lymph node, PBMCs = peripheral blood mononuclear cells.

To gain a deeper understanding of mutual relationship of T cell subsets we analyzed their percentages in $CD3^+$ T cell population. The most abundant subset of $CD3^+$ T cells in tumors was $CD4^+$ memory T subset, followed by $CD8^+$ memory T cells (Figure 19). The naive subset of $CD4^+$ T cells were very scars in the tumor tissues, while naive $CD8^+$ T cells are more abundant. Analysis of of the T cell subsets show that there was no significant difference in percentages between the tumor tissue and the distant lung (Figures 20 and 21). Double negative (DN) subsets represent very small parts of $CD3^+$ T cells and show no significant difference between the tissues (Figures 20 and 21 G, H, I). These results are obtained from analysis of five patients and to conclude with certainty that there is no statistically significant difference higher number of patients need to be analyzed. Summary of T cell ratio in a $CD3^+$ T cell population is shown in Figure 19.

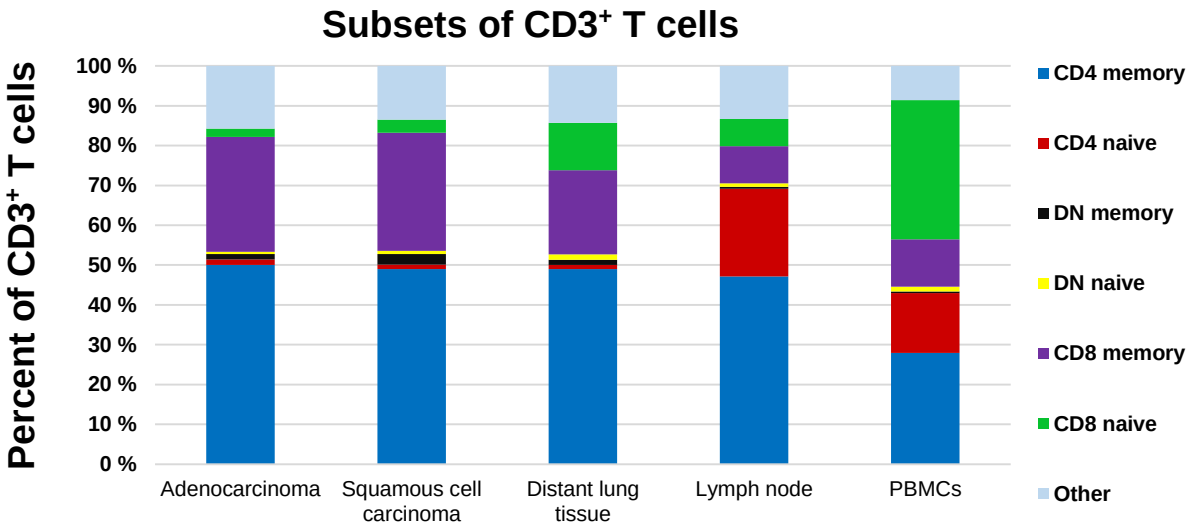

Figure 19. T cell subsets in different tissues. The graph presents T cell subsets in adenocarcinoma, squamous cell carcinoma, distant lung, lymph node and PBMCs form NSCLC patients. All percentages in the graph were obtained from mean values of T cell subsets, calculated from gated $CD3^+$ T cells presented in figures 9-12 E. DN $CD4^-CD8^-$ double negative T cells.

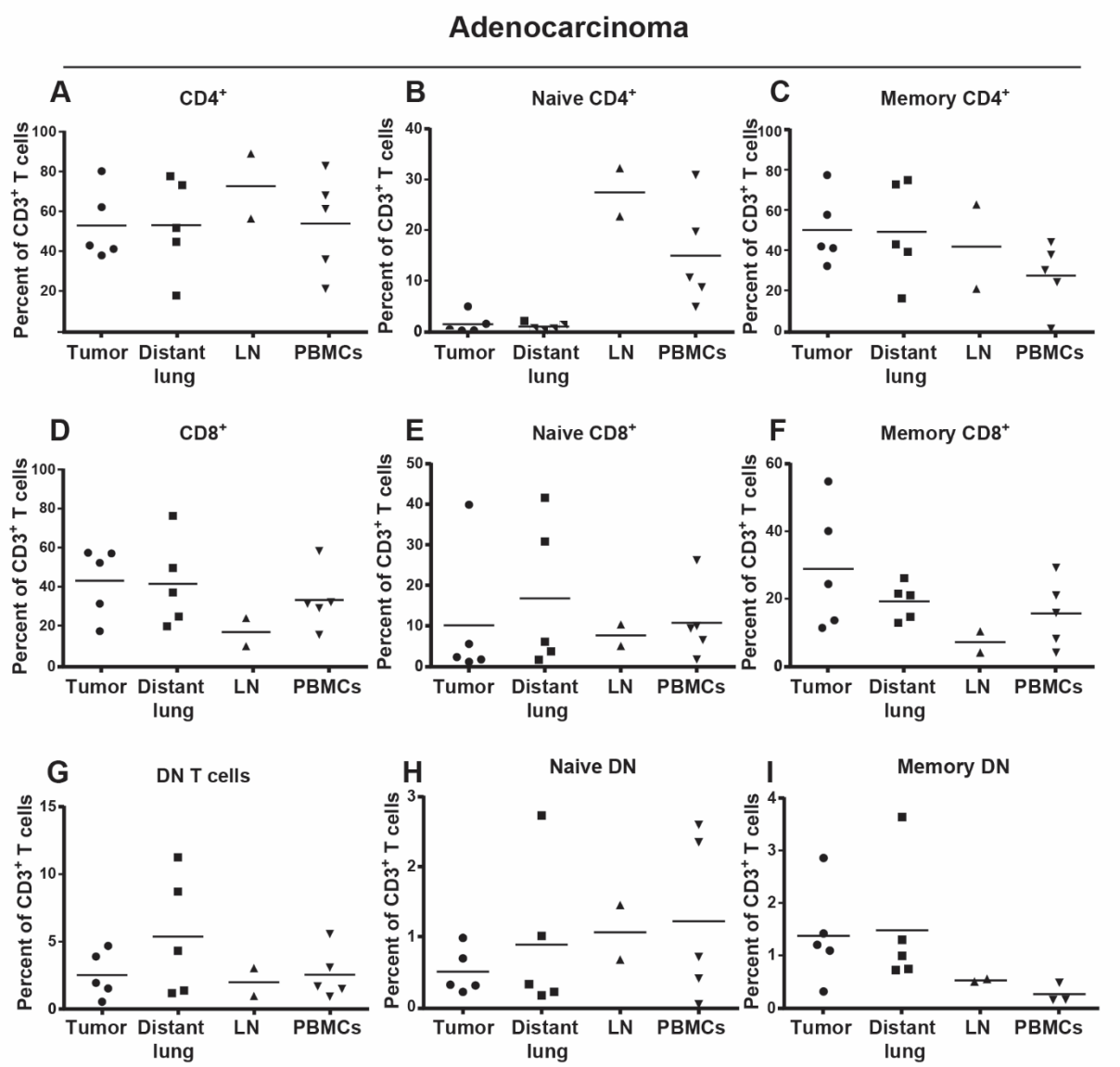

Figure 20. Percent of CD4$^+$, CD8$^+$ and, CD4$^-$CD8$^-$ T cells and their memory and naive subsets in adenocarcinoma, calculated from CD3$^+$ T cell population. Comparison of tumor infiltrating T cells as a percent of CD3$^+$ T cell population in tumor, distant lung, lymph node and PBMCs. **A.** CD4$^+$ T cells and their **B.** naive and **C.** memory subsets **D.** CD8$^+$ T cells and their **E.** naive and **F.** memory cubsets, and **G.** CD4$^-$CD8$^-$ T cells and their **H.** naive and **I.** subsets. Kruskal-Wallis test and Dunn's multiple comparison were used to detect differences between means. The presented values in percentages were calculated from the total number of cells in live leukocyte population. The presented values in percentages were calculated from the total number of cells in live leukocyte population. Each symbol represents data collected from one patient, as a percentage of live leukocyte population and the mean is represented by the blue line. Abbreviation meaning: LN = lymph node, PBMCs = peripheral blood mononuclear cells.

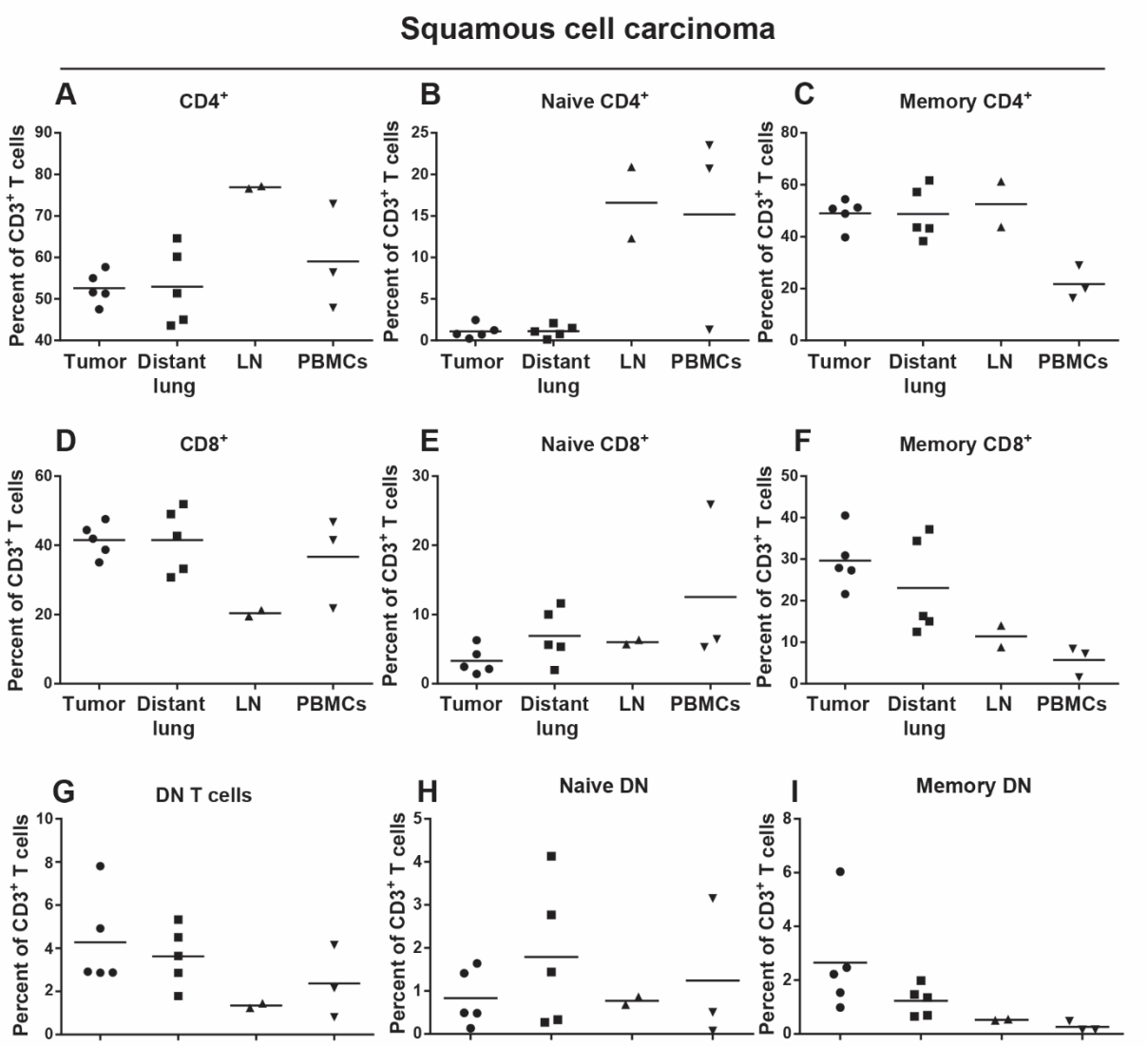

Figure 21. Percent of $CD4^+$, $CD8^+$ and, $CD4^-CD8^-$ T cells and their memory and naive subsets in squamous cell carcinoma, calculated from $CD3^+$ T cell population. Comparison of tumor infiltrating T cells as a percent of $CD3^+$ T cell population in tumor, distant lung, lymph node and PBMCs. **A.** $CD4^+$ T cells and their **B.** naive and **C.** memory subsets **D.** $CD8^+$ T cells and their **E.** naive and **F.** memory cubsets, and **G.** $CD4^-CD8^-$ T cells and their **H.** naive and **I.** subsets. Kruskal-Wallis test and Dunn's multiple comparison were used to detect differences between means. The presented values in percentages were calculated from the total number of cells in live leukocyte population. The presented values in percentages were calculated from the total number of cells in live leukocyte population. Each symbol represents data collected from one patient, as a percentage of live leukocyte population and the mean is represented by the blue line. Abbreviation meaning: LN = lymph node, PBMCs = peripheral blood mononuclear cells.

5.2.2 Analysis of B cells

In the flow cytometry analysis of B cell the first three gates were set as previously described (Results section 5.1, page 27; Figures 22-25 A, B, C). The lymphocyte gate is not set as strict as in T cell analysis. Some of the B cell subsets, like plasma cells, have increased in size and have higher FSC and SSC. Therefore, to ensure that plasma cells are included, the lymphocyte gate for B cells was wider (Figures 22-25 D). Events from the lymphocyte gate were further plotted to exclude $CD14^+$ cells (Figures 22-25 E). $CD14^+$ population contains mainly macrophages and some mast cells. These cells express Fcγ-receptor and may thereby bind to Fc part of antibodies and lead to false positive events. We therefore excluded $CD14^+$ population. The $CD14^-$ population was plotted into a CD19/CD3 graph. Here we observed two major lymphocyte populations: $CD3^+CD19^-$ T cells and $CD3^-CD19^+$ B cells (Figures 22-25 F). From the B cell population, B cell subsets were identified based on four surface markers: IgM, IgD, CD27 and CD38. IgM and IgD are expressed early on in B cell differentiation, while CD27 is only expressed in memory and plasma cells, and CD38 expression varies through B cell differentiation. CD38 is a marker that defines three populations: negative population ($CD38^-$), dim population ($CD38^+$) and bright population ($CD38^{++}$) [49].

All cells that expressed CD19, a pan-B cell marker, were examined for expression of IgM and IgD (Figures 22-25 H). This revealed three populations: IgM^+IgD^+, IgM^+IgD^-, and IgM^-IgD^- population. All three populations were further investigated for expression of CD38 and CD27. From the double positive, IgM^+IgD^+ population of B cells we defined naive B cells as $IgM^+IgD^+CD27^-CD38^{-/+}$ and non-conventional memory B cells as $IgM^+IgD^+CD27^+CD38^{-/+}$ (Figures 22-25 I). These latter cells are memory B cells that have not changed the immunoglobulin class expression. From the IgM^-IgD^-, double negative, B cell population we defined germinal centre B cells as $CD27^-CD38^+$, plasma cells as $CD27^+CD38^{++}$, and memory B cells that were $CD27^+CD38^{-/+}$. The IgM^+IgD^- population of B cells was examined for CD27 and CD38 expression and showed only one population that included events that were both positive and negative for CD27 and CD38, with no discrimination between positive and negative populations (data not shown).

All the thresholds for the gates in flow cytometry analysis were set based on the staining with isotype controls of the relevant tissues. Percentages in the Figures 22-25 represent mean value of each cell type in the $CD45^+PI^-$ population – live leukocytes. Mean for each cell population is calculated from percentages gathered from all patients stained for B cells. Mean is calculated for each tissue separately.

Table 10. Deffinition of B cell subsets by use of with flow cytometry

Cell population	Molecular markers
B cells	$CD45^+PI^-CD3^-CD14^-CD19^+$
Naive B cells	$CD45^+PI^-CD3^-CD19^+CD14^-IgM^+IgD^+CD38^{+/-}CD27^-$
Non-conventional memory B cell	$CD45^+PI^-CD3^-CD19^+CD14^-IgM^+IgD^+CD38^{+/-}CD27^+$
Memory B cells	$CD45^+PI^-CD3^-CD19^+CD14^-IgM^-IgD^-CD38^{+/-}CD27^+$
Plasma cells	$CD45^+PI^-CD3^-CD19^+CD14^-IgM^-IgD^-CD38^{++}CD27^+$
Germinal center cells	$CD45^+PI^-CD3^-CD19^+CD14^-IgM^-IgD^-CD38^+CD27^+$

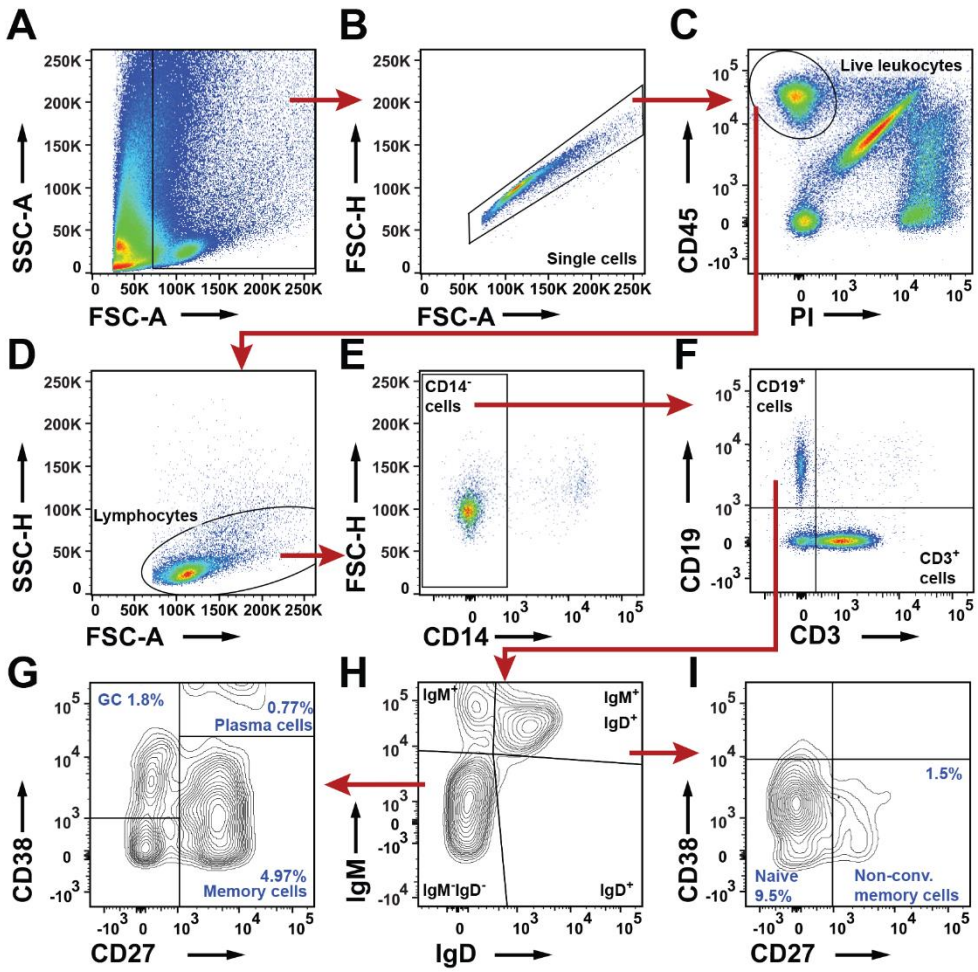

Figure 22. Flow cytometry analysis of B cell subsets in tumor in NSCLC patient.
A. Nucleated cell gate. Gating out debris. **B.** Single cell gate excluding doublets. **C.** Live leukocyte gate. Live leukocytes are defined as $CD45^+PI^-$. **D.** Lymphocyte gate **E.** B cell gate defining all B cell as CD19 and $CD3^-$. **F.** Gate excluding CD14 macrophages. **H.** Separating B cells according to IgM and IgD expression. **G**. Germinal centre B cells (GC) are defined as $CD27^-CD38$, Plasma cells are defined as $CD27^+CD38^{++}$ and Memory B cells are defined as $CD27^+CD38^{-/}$ **I.** Naive B cells are defined as $CD27^-CD38^{-/+}$ and Non- conventional memory B cells are defined as $CD27CD38^{-/+}$. Percentages of presented in the figure are average percent of total live leukocytes, calculated from all patients stained for B cells. GC= germinal center, Non-conv. = non-conventional memory B cells.

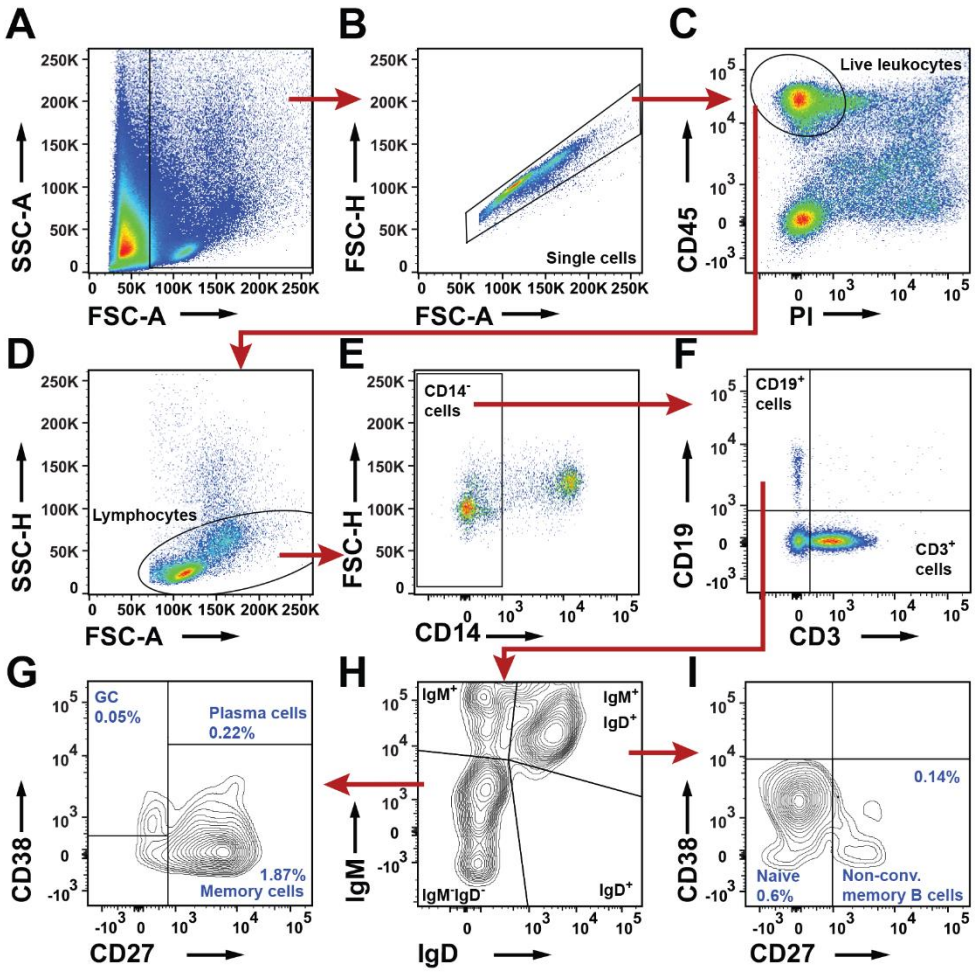

Figure 23. Flow cytometry analysis of B cells in distant lung in NSCLC patient.
A. Nucleated cell gate. Gating out debris. **B.** Single cell gate excluding doublets. **C.** Live leukocyte gate. Live leukocytes are defined as $CD45^{+}PI^{-}$. **D.** Lymphocyte gate **E.** B cell gate defining all B cell as CD19 and $CD3^{-}$. **F.** Gate excluding CD14 macrophages. **H.** Separating B cells according to IgM and IgD expression. **G**. Germinal centre B cells (GC) are defined as $CD27^{-}CD38$, Plasma cells are defined as $CD27^{+}CD38^{++}$ and Memory B cells are defined as $CD27^{+}CD38^{-/}$ **I.** Naive B cells are defined as $CD27^{-}CD38^{-/+}$ and Non- conventional memory B cells are defined as $CD27CD38^{-/+}$. Percentages of presented in the figure are average percent of total live leukocytes, calculated from all patients stained for B cells. GC= germinal center, Non-conv. = non-conventional memory B cells.

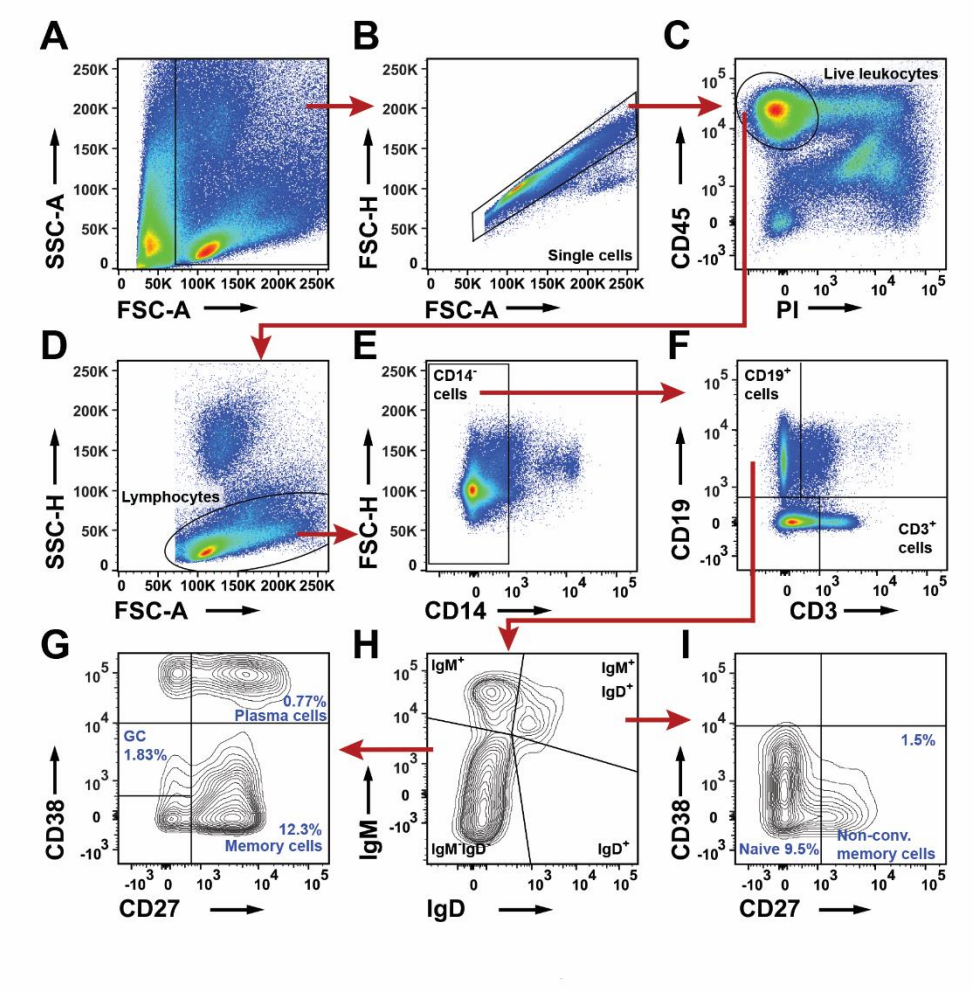

Figure 24. Flow cytometry analysis of B cells in lymph node in NSCLC patient.
A. Nucleated cell gate. Gating out debris. **B.** Single cell gate excluding doublets. **C.** Live leukocyte gate. Live leukocytes are defined as $CD45^{+}PI^{-}$. **D.** Lymphocyte gate **E.** B cell gate defining all B cell as CD19 and $CD3^{-}$. **F.** Gate excluding CD14 macrophages. **H.** Separating B cells according to IgM and IgD expression. **G**. Germinal centre B cells (GC) are defined as $CD27^{-}CD38$, Plasma cells are defined as $CD27^{+}CD38^{++}$ and Memory B cells are defined as $CD27^{+}CD38^{-/}$ **I.** Naive B cells are defined as $CD27^{-}CD38^{-/+}$ and Non- conventional memory B cells are defined as $CD27CD38^{-/+}$. Percentages of presented in the figure are average percent of total live leukocytes, calculated from all patients stained for B cells. GC= germinal center, Non-conv. = non-conventional memory B cells.

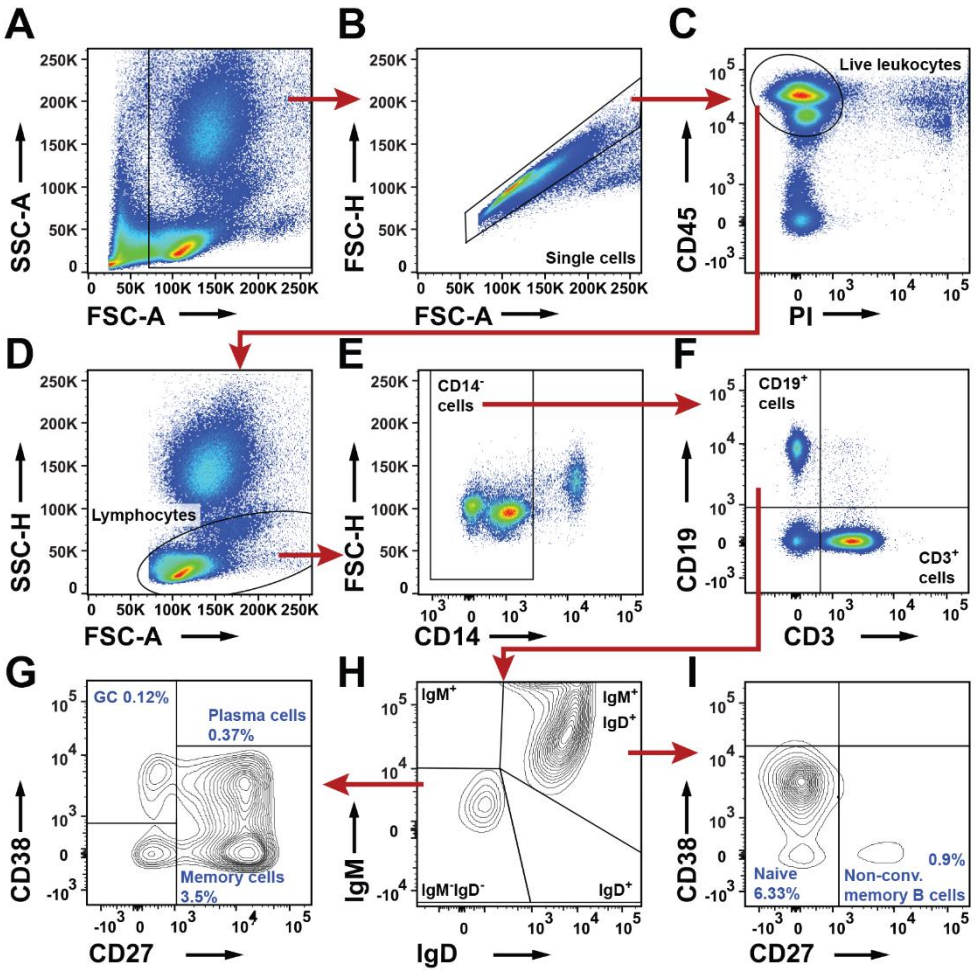

Figure 25. Flow cytometry analysis of B cell subsets in PBMCs in NSCLC patient.
A. Nucleated cell gate. Gating out debris. **B.** Single cell gate excluding doublets. **C.** Live leukocyte gate. Live leukocytes are defined as $CD45^{+}PI^{-}$. **D.** Lymphocyte gate **E.** B cell gate defining all B cell as CD19 and $CD3^{-}$. **F.** Gate excluding CD14 macrophages. **H.** Separating B cells according to IgM and IgD expression. **G**. Germinal centre B cells (GC) are defined as $CD27^{-}CD38$, Plasma cells are defined as $CD27^{+}CD38^{++}$ and Memory B cells are defined as $CD27^{+}CD38^{-/+}$ **I.** Naive B cells are defined as $CD27^{-}CD38^{-/+}$ and Non- conventional memory B cells are defined as $CD27CD38^{-/+}$. Percentages of presented in the figure are average percent of total live leukocytes, calculated from all patients stained for B cells. GC= germinal center, Non-conv. = non-conventional memory B cells.

In addition to identification of B cell subsets in NSCLC patients, we also performed statistical analysis of B cells and their subsets. Percentages obtained from flow cytometry were used to compare means of populations between different tissues, different histological types of tumor, different tumor stages and between patients with different smoking histories.

Analysis of $CD19^{+}$ B cells, between different tissues, revealed high individual variation in the tumor and lymph node. Percentages of $CD19^{+}$ B cells in distant lung and blood were more constant. $CD19^{+}$ B cells showed statistically significant increase in adenocarcinoma compared to distant lung ($p=0.0001$; Figure 26 A). Looking into $CD19^{+}$B cells in squamous cell carcinoma we noticed less individual variation in percentages of

CD19⁺ B cells in tumor tissue, compared to adenocarcinoma. CD19⁺ B cells in squamous cell carcinoma had significantly higher percentages in the tumor compared to the distant lung. (p=0.006; Figure 26 B). This suggests that B cells are recruited more strongly to tumor microenvironment compared to other leukocytes.

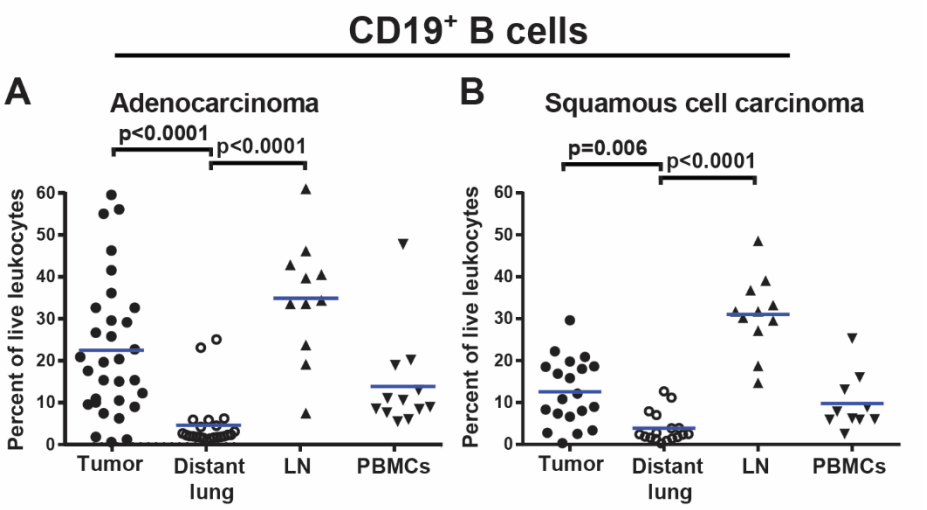

Figure 26. Percent of CD19⁺B cells in different tissues from NSCLC patients. Comparison of CD19⁺B cells in tissues of patients diagnosed with **A.** adenocarcinoma and **B.** squamous cell carcinoma. Kruskal-Wallis test and Dunn's multiple comparison were used to detect differences between means. Each symbol represents data collected from one patient, as a percentage of live leukocyte population and the mean is represented by the blue line. Abbreviation meaning: LN = lymph node and PBMCs = peripheral blood mononuclear cells.

Looking into subsets of B cells in different tissues we noticed general higher percentage of naive B cells in PBMCs compared to tumor (Figure 27 A). This ratio is expected considering that, unlike other tissues, PBMCs contain mainly naive circulating leukocytes. Non-conventional memory B cells showed individual variations between patients in adenocarcinoma while in squamous cell carcinoma, distant lung, lymph node and PBMCs, distribution of these cells were more constant. We also observed a trend of increased percentages of non-conventional memory B cells in adenocarcinoma compared to distant lung (Figure 28 A, B). This trend might reach statistical significance if more patients are included.

Memory B cells showed a higher concentration in adenocarcinoma compared to distant lung tissue (p=0.04; Figure 28 C). In patients with squamous cell carcinoma there was no statistically significant difference between the tumor and the distant lung (**Figure 28**Figure 28 D). Analysis of plasma cells showed no difference between the tissues in adenocarcinoma or squamous cell carcinoma.

Statistical analysis of B cells and their subsets, between different histological types of tumor revealed no significant difference between the groups (Figure 29). However it is obvious that there are big individual differences between the patients diagnosed with adenocarcinoma. More analysis is necessary for less common types of tumor to perform adequate statistical analysis.

For the analysis of B cell subsets, in different histological types of tumor, there was enough data only for analysis of adenocarcinoma and squamous cell carcinoma (Figure 29 B-F). We did not notice any significant difference between the B cell subsets in these two types of tumor (Figure 28 B-F).

The stage of tumor did not show to have effect on infiltration of $CD19^+$ B cells in the tumor (Figure 30). However we have very little data on the B cell subsets, and in order to conclude, with certainty, that there is no correlation between tumor stage and B cell infiltrate we need to acquire more data. For analysis of influence of smoking history on B cell infiltration we had no data for the B cell subsets because all of the patients stained for B cell subsets were former smokers. We did analysis of $CD19^+$ B cells in patients with different smoking history and found that smoking history has no influence on B cell infiltration in tumor tissue (Figure 31).

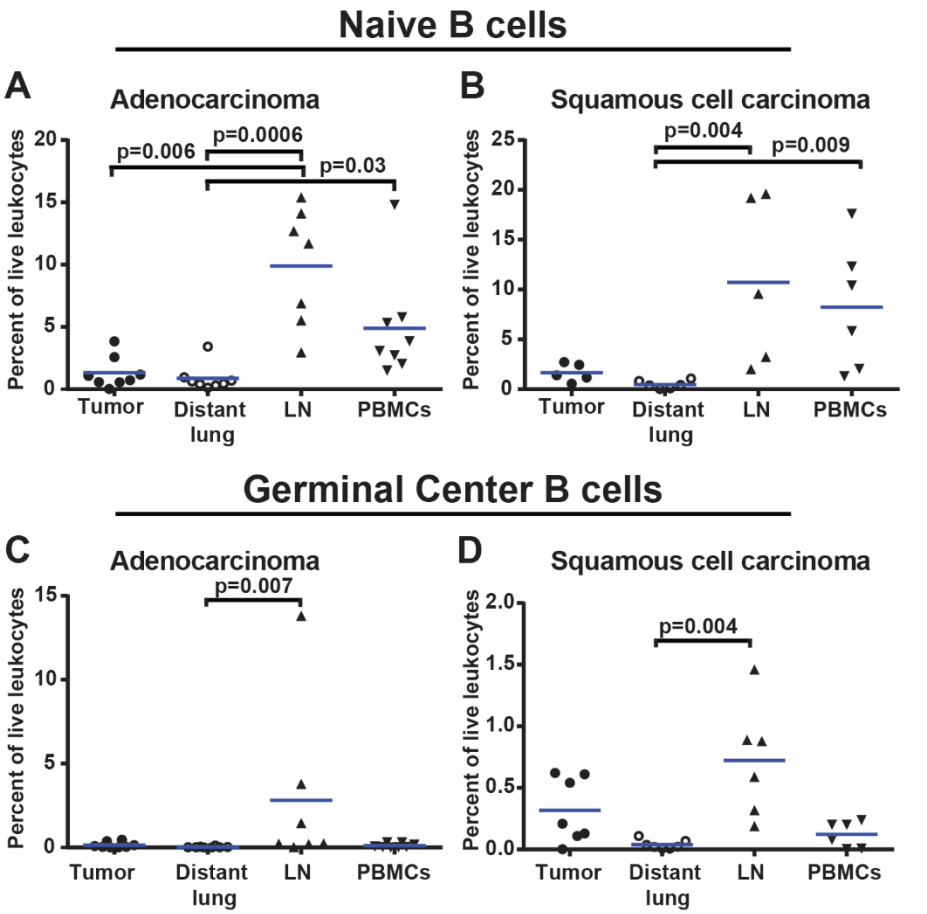

Figure 27. Percent of naive B cells and germinal center B cells in different tissues from NSCLC patients Comparison of naive cells in tissues of patients diagnosed with **A.** adenocarcinoma and **B.** squamous cell carcinoma. Comparison of germinal centre B cells in tissues of patients diagnosed with **C.** adenocarcinoma and **D.** squamous cell carcinoma. Kruskal-Wallis test and Dunn's multiple comparison were used to detect differences between means. Each symbol represents data collected from one patient, as a percentage of live leukocyte population and the mean is represented by the blue line. Abbreviation meaning: LN = lymph node and PBMCs = peripheral blood mononuclear cells.

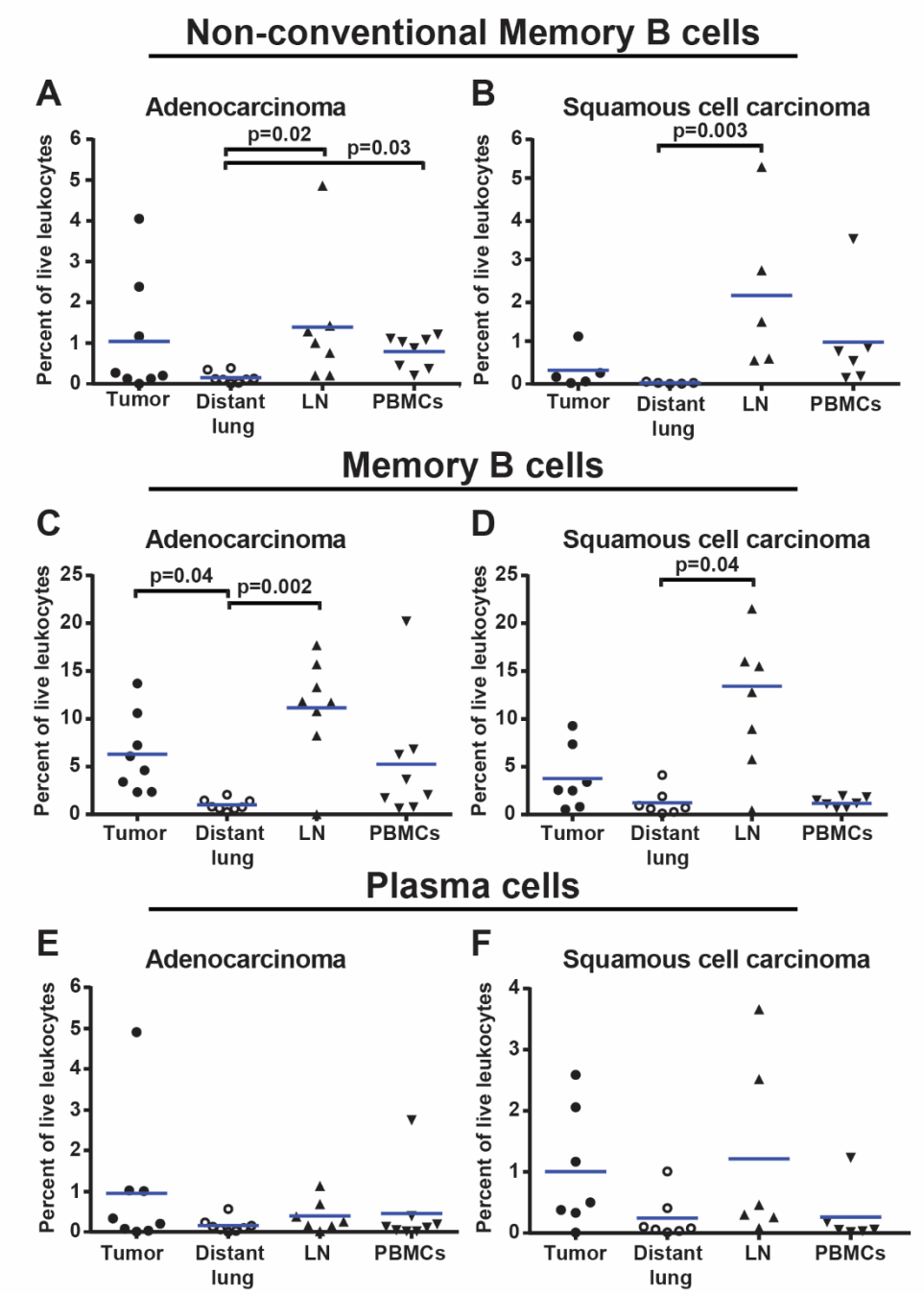

Figure 28. Percent of non-conventional memory, memory and plasma cells in different tissues from NSCLC patients Comparison of non-conventional memory B cells in tissues of patients diagnosed with **A.** adenocarcinoma and **B.** squamous cell carcinoma. Comparison of memory B cells in tissues of patients diagnosed with **C.** adenocarcinoma and **D.** squamous cell carcinoma. Kruskal-Wallis test and Dunn's multiple comparison were used to detect differences between means. Each symbol represents data collected from one patient, as a percentage of live leukocyte population and the mean is represented by the blue line. Abbreviation meaning: LN = lymph node and PBMCs = peripheral blood mononuclear cells.

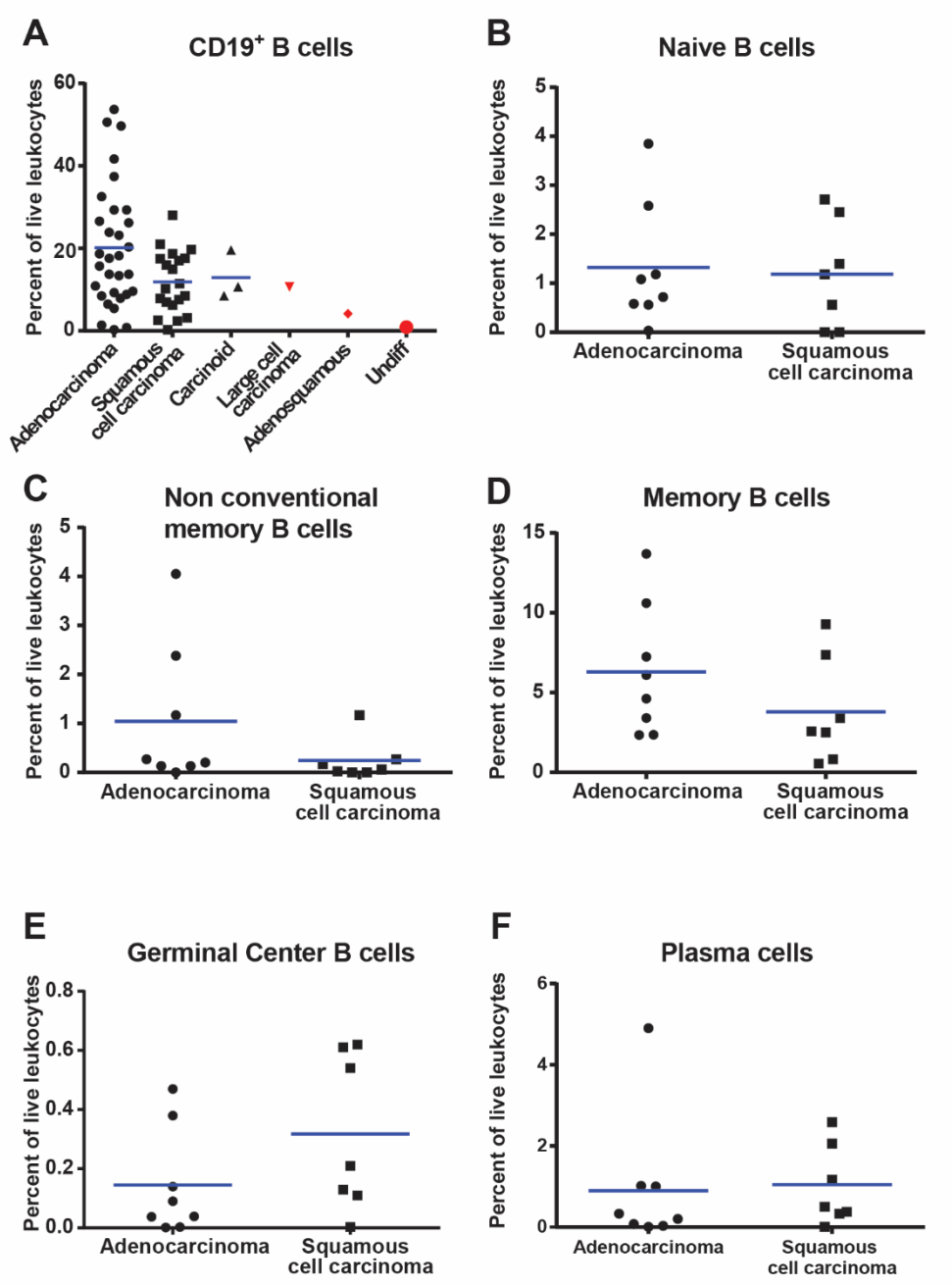

Figure 29. Percent of B cells and their subsets in different histological types of NSCLC. A. Kruskal-Wallis analysis of CD19⁺ B cells in adenocarcinoma, squamous cell carcinoma, carcinoid tumor, large cell carcinoma, adenosquamous tumor and undifferentiated tumor. **B.** Mann-Whitney analysis of **B.** naive B cells, **C.** non-conventional memory B cells, **D.** memory B cells, **E.** germinal center B cells and **F.** plasma cells in adenocarcinoma and squamous cell carcinoma. Kruskal-Wallis test was followed by Dunn's multiple comparison. Each symbol represents data collected from one patient, as a percentage of live leukocyte population. Abbreviation meaning: Undiff. = undifferentiated tumor.

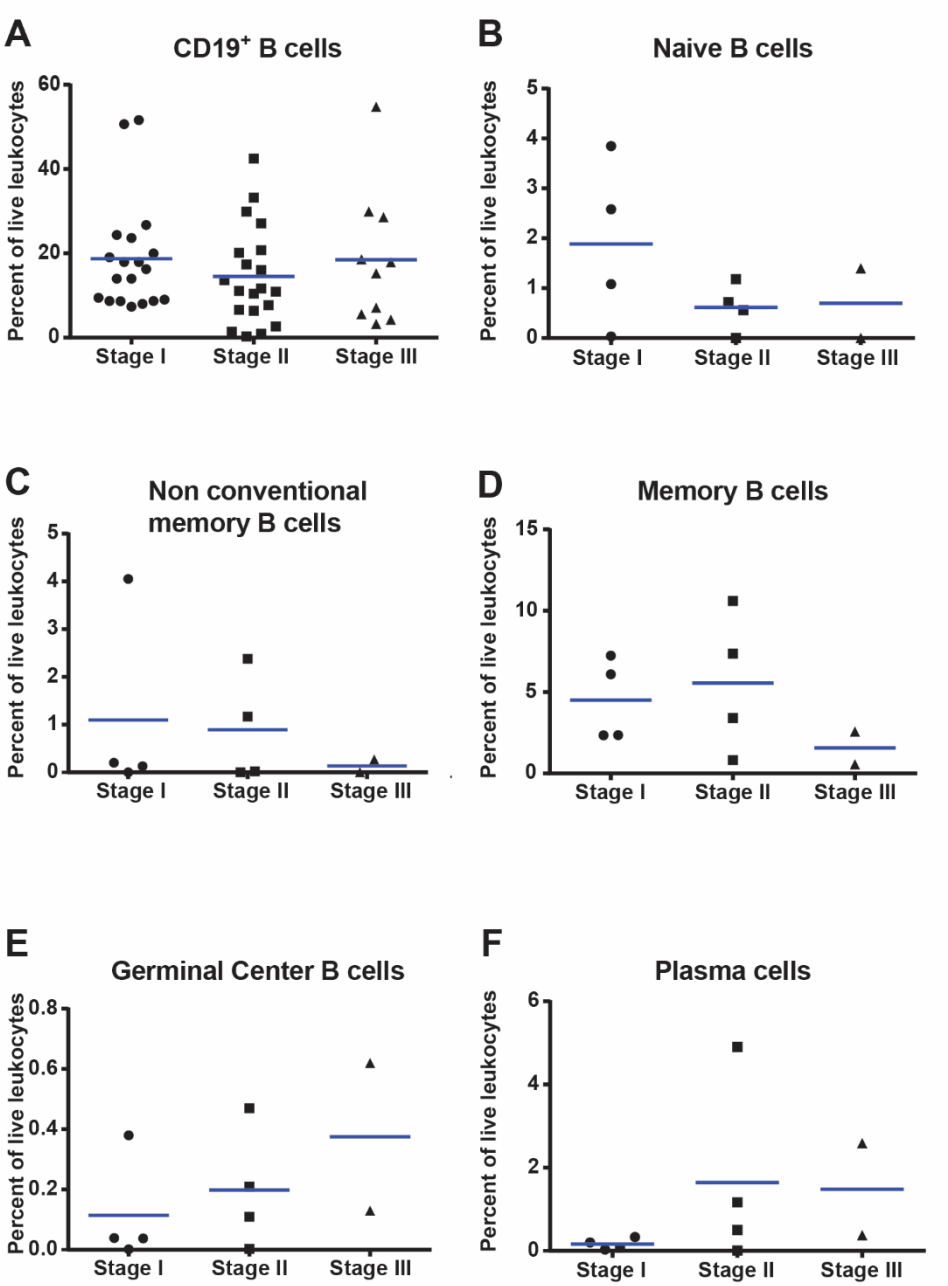

Figure 30. Percent of B cells and their subsets in different stages of NSCLC. Comparison of **A.** CD19^{+} B cells, **B.** naive B cells, **C.** non-conventional memory B cells **D.** memory B cells, **E.** germinal center B cells and, **F.** plasma cells in stages I, II and III of NSCLC. Kruskal-Wallis test and Dunn's multiple comparison were used to detect differences between means. Each symbol represents data collected from one patient, as a percentage of live leukocyte population and the mean is represented by the blue line.

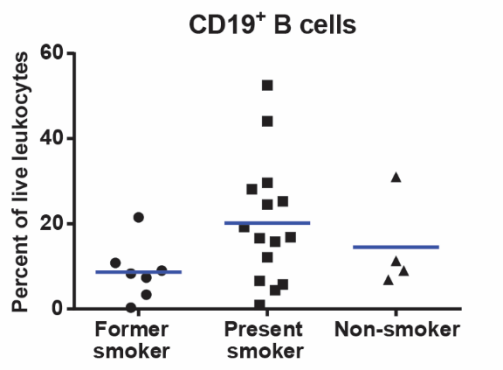

Figure 31. Percent of CD19⁺ B cells in patients with different smoking history. Comparison of CD19⁺ B cells between former smokers, present smokers and non-smokers. Kruskal-Wallis test and Dunn's multiple comparison were used to detect differences between means. Each symbol represents data collected from one patient, as a percentage of live leukocyte population and the mean is represented by the blue line.

To better understand the mutual ratio of B cell subsets, we analyzed their presence in CD19⁺ population. The largest population of B cell subsets, in CD19⁺ B cells, in both tumor types were memory B cells. The next most abundant population was plasma cells, closely followed by naive cells (Figure32). The next population by size was non-conventional memory B cells and the least abundant cells were germinal center cells. We also see a large population of "other" that are part of CD19⁺ B cells but which we did not define. This population includes IgM⁺IgD⁻ cells and possibly pre-germinal center cells that were not defined with our gating strategies. Analysis of B cell subsets in as CD19⁺ population, between the tissues showed no statistical significance (Figure 33).

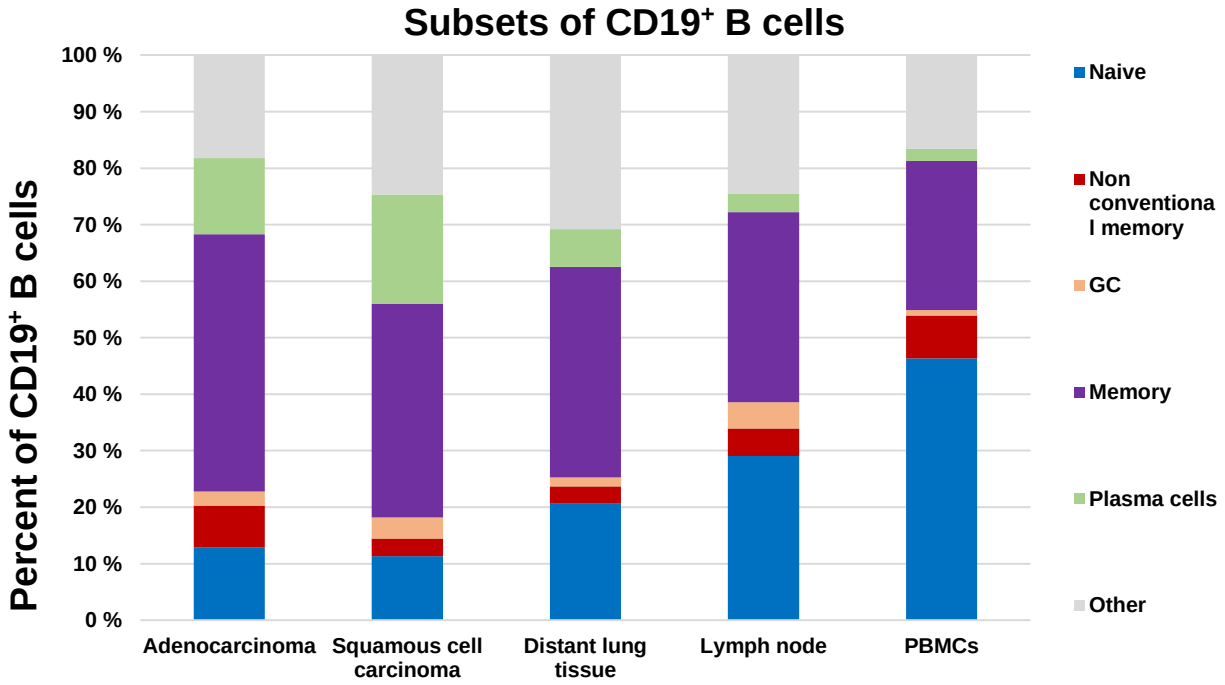

Figure 32. B cell subsets in different tissues. The graph represents B cell subsets in adenocarcinoma, squamous cell carcinoma, distant lung, lymph node and PBMCs. All percentages in the graph were obtained from a mean values of B cell subsets.

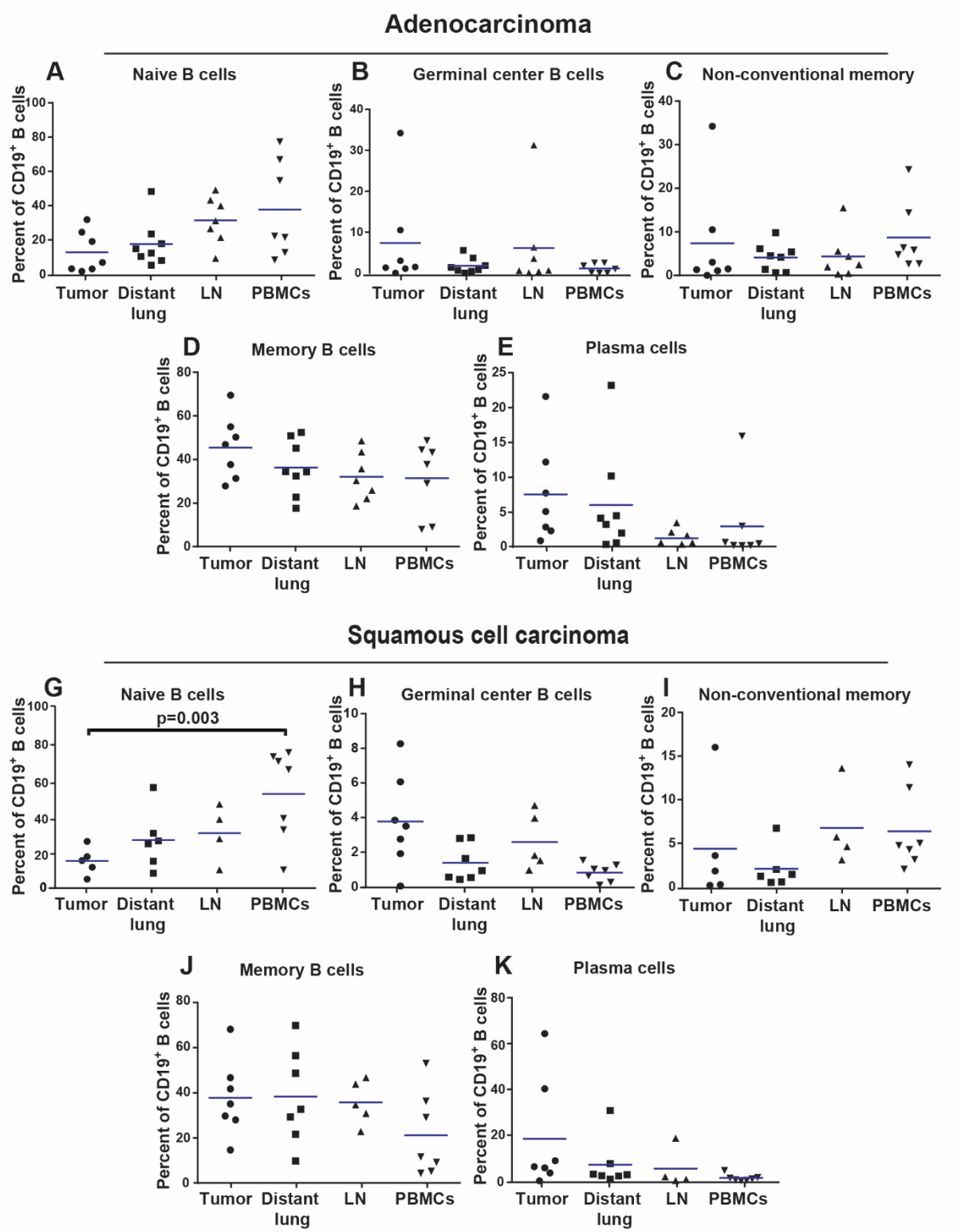

Figure 33. B cell subsets as a percent of CD19⁺ B cell population. Comparison of **A.** naive, **B.** germinal center, **C.** non-conventional memory, **D.** memory, and **E.** plasma cells in tissues of patients diagnosed with adenocarcinoma. Comparison of **G.** naive, **H.** germinal center, **I.** non-conventional memory, **J.** memory, and **k.** plasma cells in tissues of patients diagnosed with squamous cell carcinoma. Kruskal-Wallis test and Dunn's multiple comparison were used to detect differences between means. Each symbol represents data collected from one patient, as a percentage of live leukocyte population and the mean is represented by the blue line. Abbreviation meaning: LN = lymph node and PBMCs = peripheral blood mononuclear cells.

5.2.3 Analysis of APC

Flow cytometry analysis was used to define APC populations in tissues of NSCLC patients. For the APC gating strategy, cells were first gated in the nucleated cell gate to exclude debris. Next cells were gated in the single cell gate to exclude doublets, and finally single cells were gated in live leukocytes gate, where dead cells and cells that are not leukocytes were exclude (Figures 34-37 A, B, C). The live leukocytes were further gated by using $CD19^-$ gate to exclude B cells (Figures 34-37 E). B cells are excluded to avoid false positives due to unspecific binding of IgG to Fcγ receptor on B cells. From the $CD19^-$ gate cells are gated in three different populations, which is indicated by different colors of arrows (green, red and purple (Figures 34-37 E)).

The macrophages/monocytes represent a population of cells that are HLA-DR^{lo} to HLA-DR^{hi} and $CD14^+$ (green arrow; Figures 34-37 F). HLA-DR is a surface molecule (MHC class II) that is upregulated in tissue macrophages compared to monocytes. Due to this the macrophages in the tissues appeared higher on the graphs than the monocytes in the blood. Plasmacytoid dendritic cells (pDCs) were gated from $CD19^-$ gate to HLA-DR/CD123 gate (red arrow; Figures 34-37 H) where they form distinct HLA-DR^+CD123^+ population. This population was gated further to $CD11c^-$ and $CD14^-$ cells to exclude any possible contamination with myeloid DC and macrophages/monocytes (Figures 34-37 I). Myeloid DCs are first plotted in HLA-DR/CD11c graph (purple arrow; Figures 34-37 D). Population that is positive for both markers was selected. Similar to macrophages, dendritic cells upregulate HLA-DR in tissues. This causes variation in population appearance between blood and tissue (Figure 34-37 D). From the HLA-DR^+CD11c^+ population we further excluded $CD14^+$ cells (Figure 34-37 G). When excluding $CD14^+$ cells we set very strict gates aiming to exclude any macrophages. The HLA-$DR^+CD11c^+CD14^-$ population contains classical DCs, but it is not limited only to DCs. This population can also contain $CD14^-$ macrophages and granulocytes. And so to define DCs we used CD1c and CD141 markers (Figures 34-37 J). Use of these two markers revealed three populations: $CD141^-CD1c^+$ DCs, $CD141^+CD1c^-$ DCs and a third population that is double negative (DN). The double negative population was not investigated further, however it might be a heterogenic population of $CD1c^-$ DCs, activated macrophages, and granulocytes.

All the thresholds for the gates were set based on the staining with isotype controls of the relevant tissues. Percentages in the Figures 34-37 represent mean value of each cell type in the $CD45^+PI^-$ population – live leukocytes. Mean for each cell population is calculated from percentages gathered from all patients stained for APCs. Mean is calculated for each tissue separately.

Table 11. Deffinition of APCs by use of with flow cytometry.

Cell population	Molecular marker
Macrophages/Monocytes	$CD45^+PI^-CD19^-CD14^+$HLA-DR^+
Plasmacytoid dendritic cells	$CD45^+PI^-CD19^-CD14^+$HLA-$DR^+CD11c^-CD123^+$
$CD1c^+$ dendritic cells	$CD45^+PI^-CD19^-CD14^-CD11c^+CD1c^+CD141^-$
CD141 dendritic cells	$CD45^+PI^-CD19^-CD14^-CD11c^+CD1c^-CD141^+$

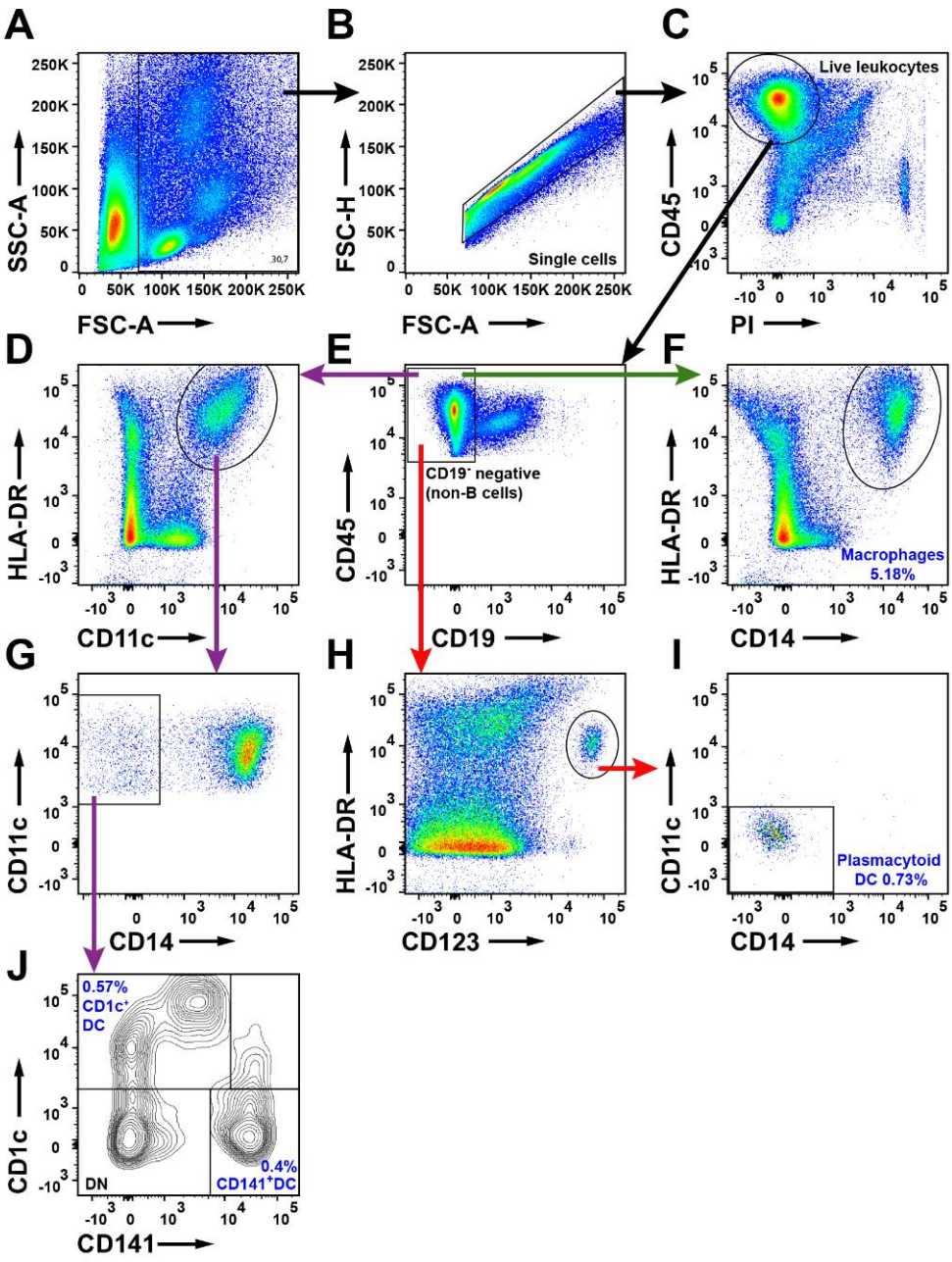

Figure 34. Flow cytometry analysis of APC cells in tumor from NSCLC patient.
A. Nucleated cell gate. Gating out apoptotic cells, necrotic cells and debris. **B.** Single cell gate excluding doublets. **C.** Live leukocyte gate. Live leukocytes are defined as $CD45^{+}PI^{-}$. **E.** $CD19^{-}$ - non B cell gate. Excluding B cells to decrease unspecific binding of antibodies to Fcγ receptor on B cells. **F**. Macrophages are defined as $HLA\text{-}DR^{+}CD14^{-}$ **H.** Plasmacytoid dendritic cells are $HLA\text{-}DR^{+}CD123^{+}$ but they are also **I.** $CD11c^{-}$ and $CD14^{-}$. **D.** Classical dendritic cells include $HLA\text{-}DR^{+}CD11c^{+}$ cells, but this population also includes macrophages. **G**. Dendritic cell gate, gating out $CD14^{+}$ macrophages. **J.** Three dendritic cell populations – $CD1c^{+}$ and $CD141^{+}$ and double negative population (DN). Percentages of all populations are average percent of total live leukocytes.

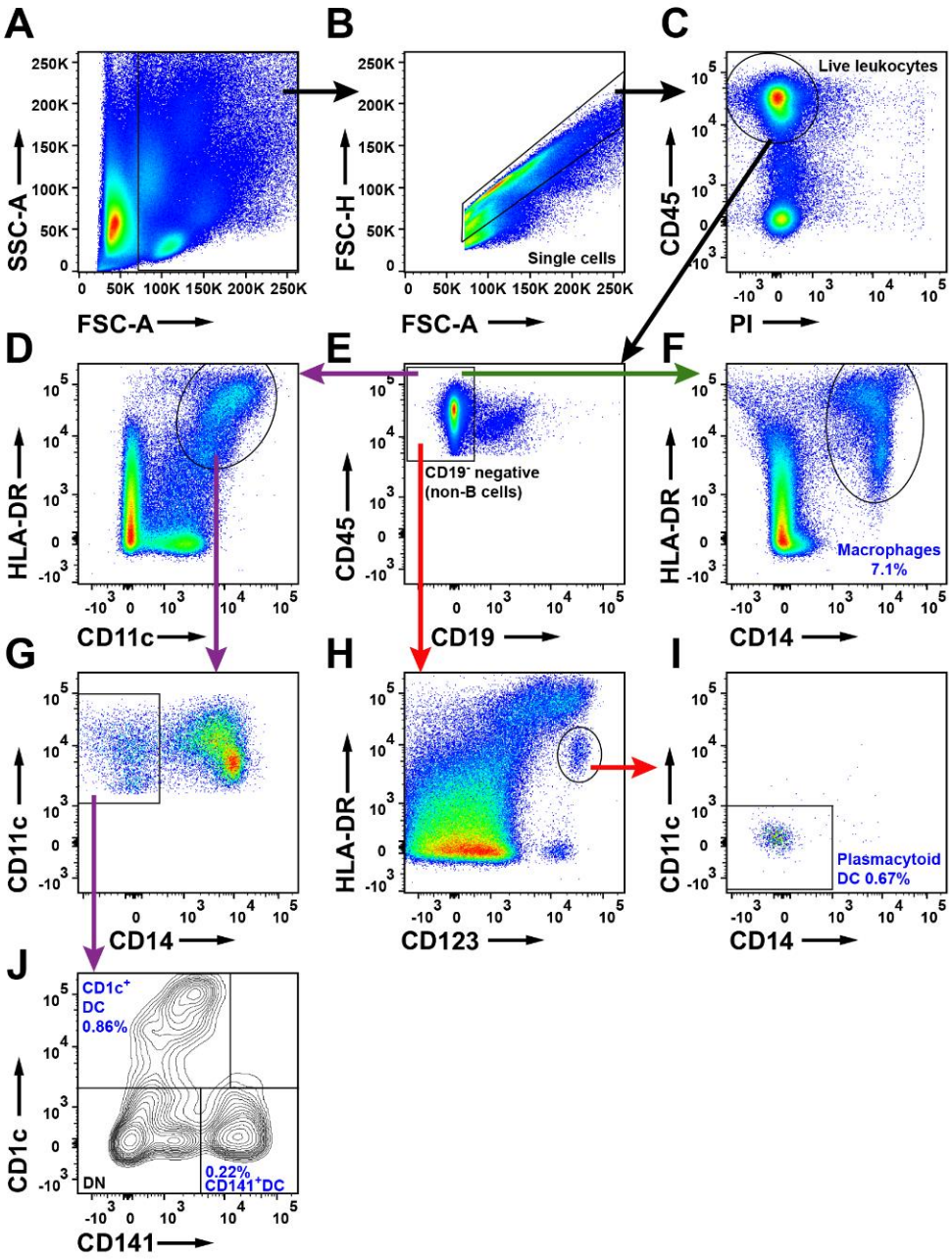

Figure 35. Flow cytometry analysis of APC cells in distant lung from NSCLC patient.
A. Nucleated cell gate. Gating out apoptotic cells, necrotic cells and debris. **B.** Single cell gate excluding doublets. **C.** Live leukocyte gate. Live leukocytes are defined as $CD45^{+}PI^{-}$. **E.** $CD19^{-}$ - non B cell gate. Excluding B cells to decrease unspecific binding of antibodies to Fcγ receptor on B cells. **F**. Macrophages are defined as $HLA\text{-}DR^{+}CD14^{-}$ **H.** Plasmacytoid dendritic cells are $HLA\text{-}DR^{+}CD123^{+}$ but they are also **I.** $CD11c^{-}$ and $CD14^{-}$. **D.** Classical dendritic cells include $HLA\text{-}DR^{+}CD11c^{+}$ cells, but this population also includes macrophages. **G**. Dendritic cell gate, gating out $CD14^{+}$ macrophages. **J.** Three dendritic cell populations – $CD1c^{+}$ and $CD141^{+}$ and double negative population (DN). Percentages of all populations are average percent of total live leukocytes.

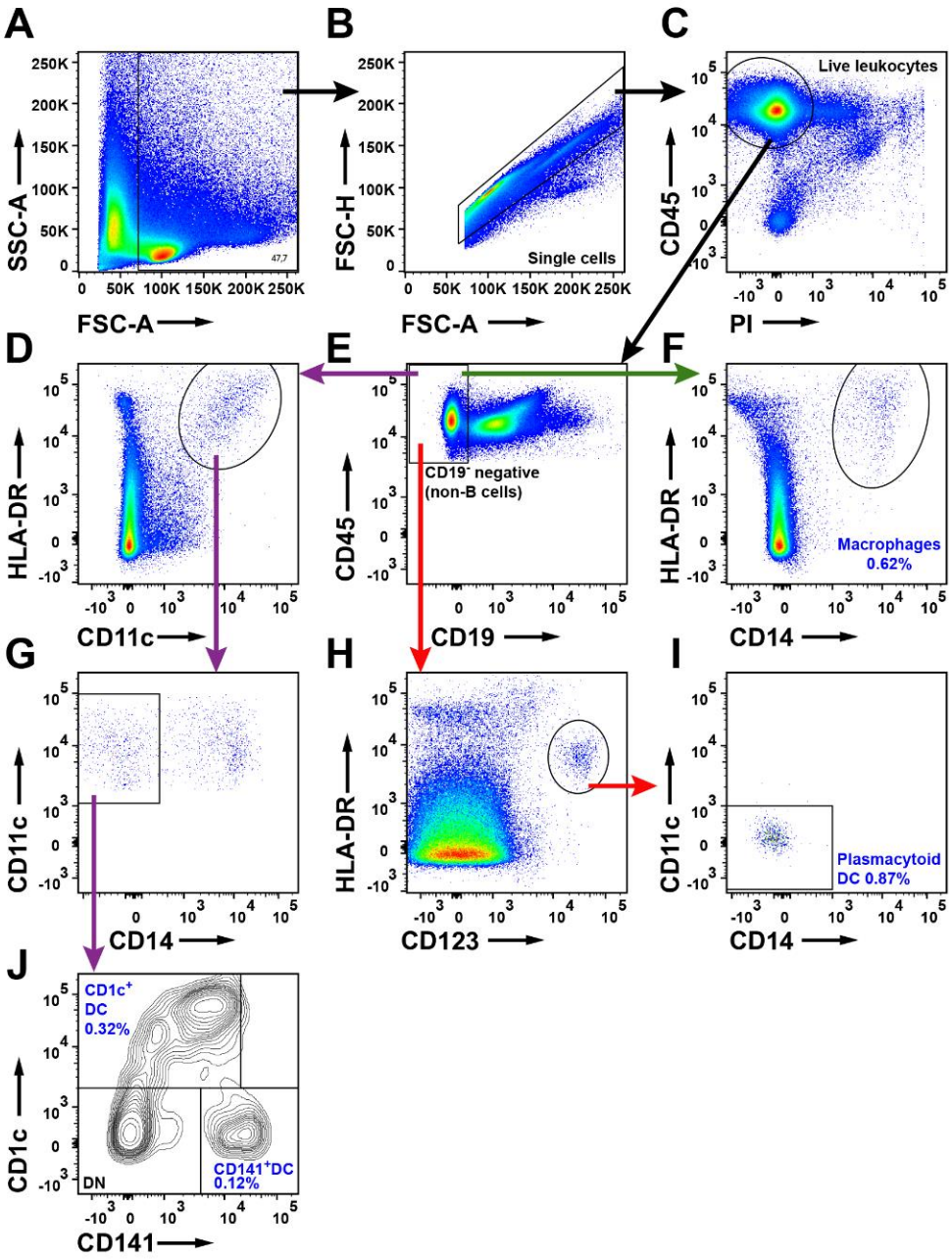

Figure 36. Flow cytometry analysis of APC cells in lymph node from NSCLC patient.
A. Nucleated cell gate. Gating out apoptotic cells, necrotic cells and debris. **B.** Single cell gate excluding doublets. **C.** Live leukocyte gate. Live leukocytes are defined as $CD45^{+}PI^{-}$. **E.** $CD19^{-}$ - non B cell gate. Excluding B cells to decrease unspecific binding of antibodies to Fcγ receptor on B cells. **F**. Macrophages are defined as $HLA\text{-}DR^{+}CD14^{-}$ **H.** Plasmacytoid dendritic cells are $HLA\text{-}DR^{+}CD123^{+}$ but they are also **I.** $CD11c^{-}$ and $CD14^{-}$. **D.** Classical dendritic cells include $HLA\text{-}DR^{+}CD11c^{+}$ cells, but this population also includes macrophages. **G**. Dendritic cell gate, gating out $CD14^{+}$ macrophages. **J.** Three dendritic cell populations – $CD1c^{+}$ and $CD141^{+}$ and double negative population (DN). Percentages of all populations are average percent of total live leukocytes.

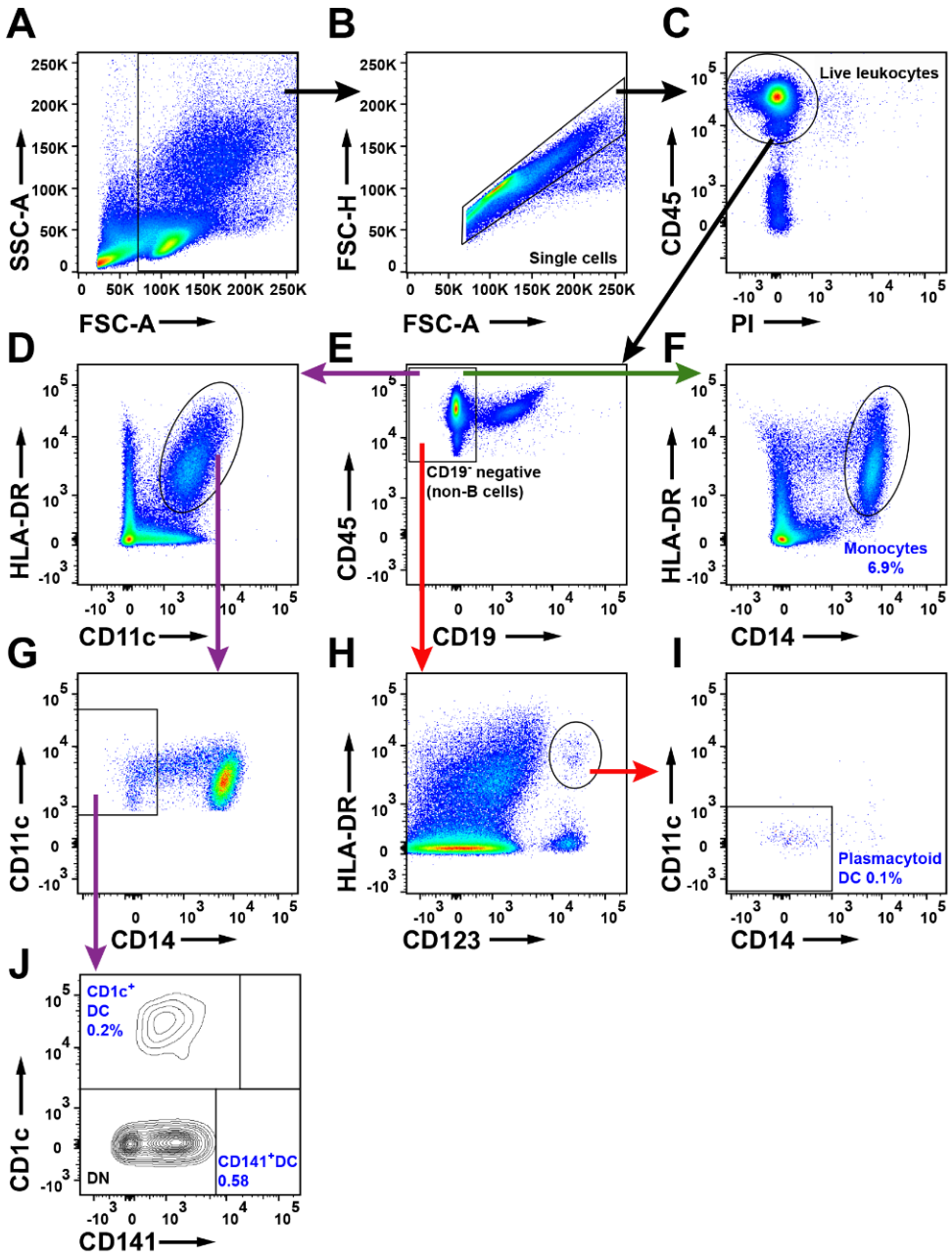

Figure 37. Flow cytometry analysis of APC cells in PBMCs from NSCLC patient.
A. Nucleated cell gate. Gating out apoptotic cells, necrotic cells and debris. **B.** Single cell gate excluding doublets. **C.** Live leukocyte gate. Live leukocytes are defined as $CD45^{+}PI^{-}$. **E.** $CD19^{-}$ - non B cell gate. Excluding B cells to decrease unspecific binding of antibodies to Fcγ receptor on B cells. **F**. Macrophages are defined as $HLA\text{-}DR^{+}CD14^{-}$ **H.** Plasmacytoid dendritic cells are $HLA\text{-}DR^{+}CD123^{+}$ but they are also **I.** $CD11c^{-}$ and $CD14^{-}$. **D.** Classical dendritic cells include $HLA\text{-}DR^{+}CD11c^{+}$ cells, but this population also includes macrophages. **G**. Dendritic cell gate, gating out $CD14^{+}$ macrophages. **J.** Three dendritic cell populations – $CD1c^{+}$ and $CD141^{+}$ and double negative population (DN). Percentages of all populations are average percent of total live leukocytes.

Statistical analysis of APC cells was performed in different tissue type and with respect to three different clinicopathological parameters: histological tumor type, stage of disease and smoking history of the patient. When performing analysis of APC cells in different tissues we separated patients in two groups: adenocarcinoma and squamous cell carcinoma patients. In the tumor of adenocarcinoma patients macrophages are present in lower degree than the monocytes in PBMCs (p=0.0028; Figure 38 A). In squamous cell carcinoma there is higher number of macrophages in tumor tissue than in lymph node (p=0.0082; Figure 38 B). There is a trend on higher number of macrophages in distant lung than in both tumors, however the trend was not strong enough to reach statistical significance.

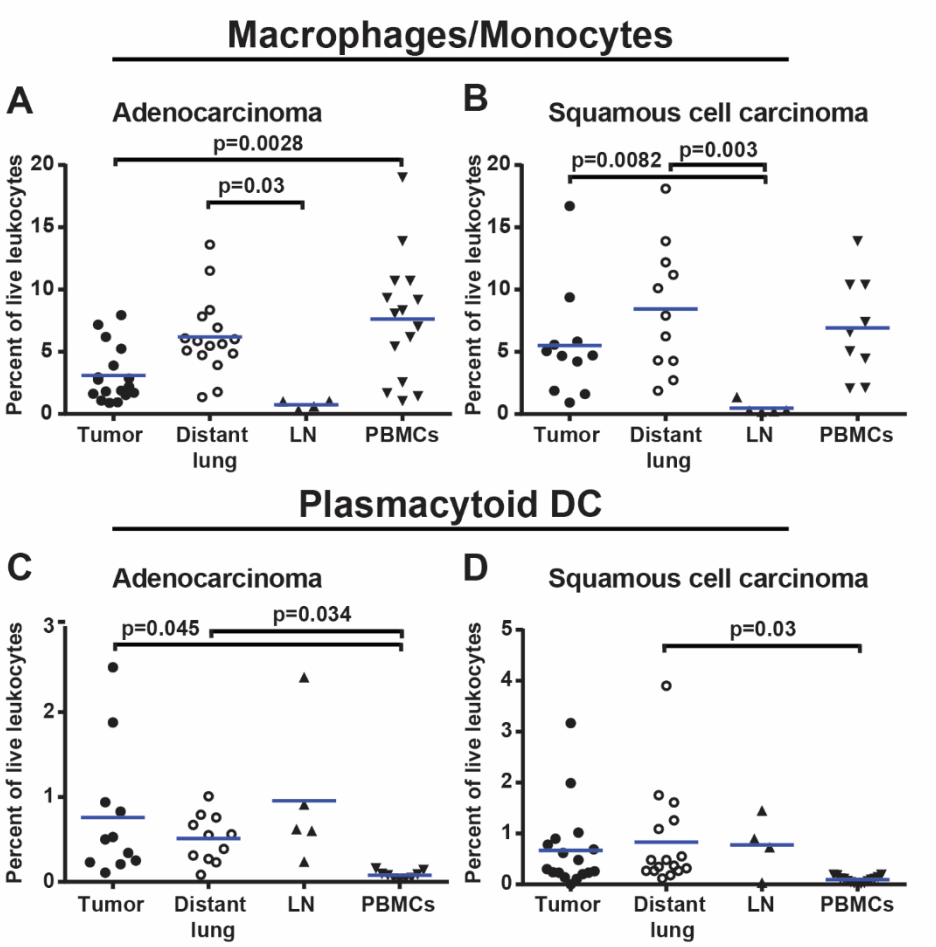

Figure 38. Percent of macrophages/monocytes and plasmacytoid dendritic cells in different tissues of NSCLC patients. Comparison of macrophages/monocytes in different tissues of patients diagnosed with **A.** adenocarcinoma and **B.** squamous cell carcinoma. Comparison of pDCs in different tissues of patients diagnosed with **C.** adenocarcinoma and **D.** squamous cell carcinoma. Kruskal-Wallis test and Dunn's multiple comparison were used to detect differences between means. Each symbol represents data collected from one patient, as a percentage of live leukocyte population and the mean is represented by the blue line. LN = lymph node and PBMCs = peripheral blood mononuclear.

Plasmacytoid DCs showed no significant difference between either of the tumors and the distant lung, but there was increase in adenocarcinoma compared to PBMCs (Figure 38 C and D). The CD1c$^+$ and the CD141$^+$ DCs show slightly higher means in distant lung tissue than in tumor tissue, however none reach statistical significance (Figure 39).

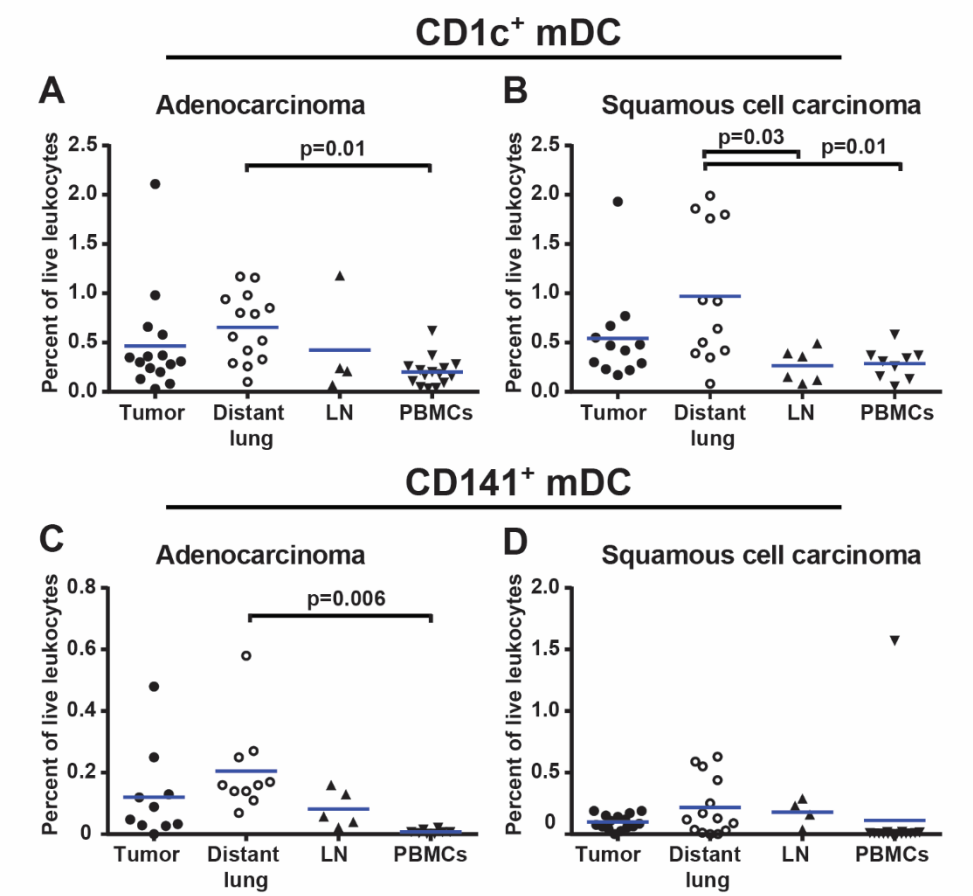

Figure 39. Percent of macrophages/monocytes and plasmacytoid dendritic cells in different tissues of NSCLC patients. Comparison of macrophages/monocytes in different tissues of patients diagnosed with **A.** adenocarcinoma and **B.** squamous cell carcinoma. Comparison of pDCs in different tissues of patients diagnosed with **C.** adenocarcinoma and **D.** squamous cell carcinoma. Kruskal-Wallis test and Dunn's multiple comparison were used to detect differences between means. Each symbol represents data collected from one patient, as a percentage of live leukocyte population and the mean is represented by the blue line. Abbreviation meaning: LN = lymph node and PBMCs = peripheral blood mononuclear.

Analysis of APC populations between different tumor types, showed no significant difference between the tumor and the distant lung. This analysis was done between adenocarcinoma, squamous cell carcinoma and carcinoid carcinoma. Other types of tumor had only one patients per group and did not allow analysis (Figure 40). Analysis of APCs in different stages of disease revealed no significant difference between the groups (Figures 41). APC analysis in patients with different smoking histories revealed difference in percentages of DCs in smokers and former smokers. The CD1c$^+$ DCs and CD141$^+$ DCs were more abundant in former smokers than in smokers (Figure 42 C, D). This suggests that cigarette smoke influences infiltration of myeloid DCs in tumor tissue.

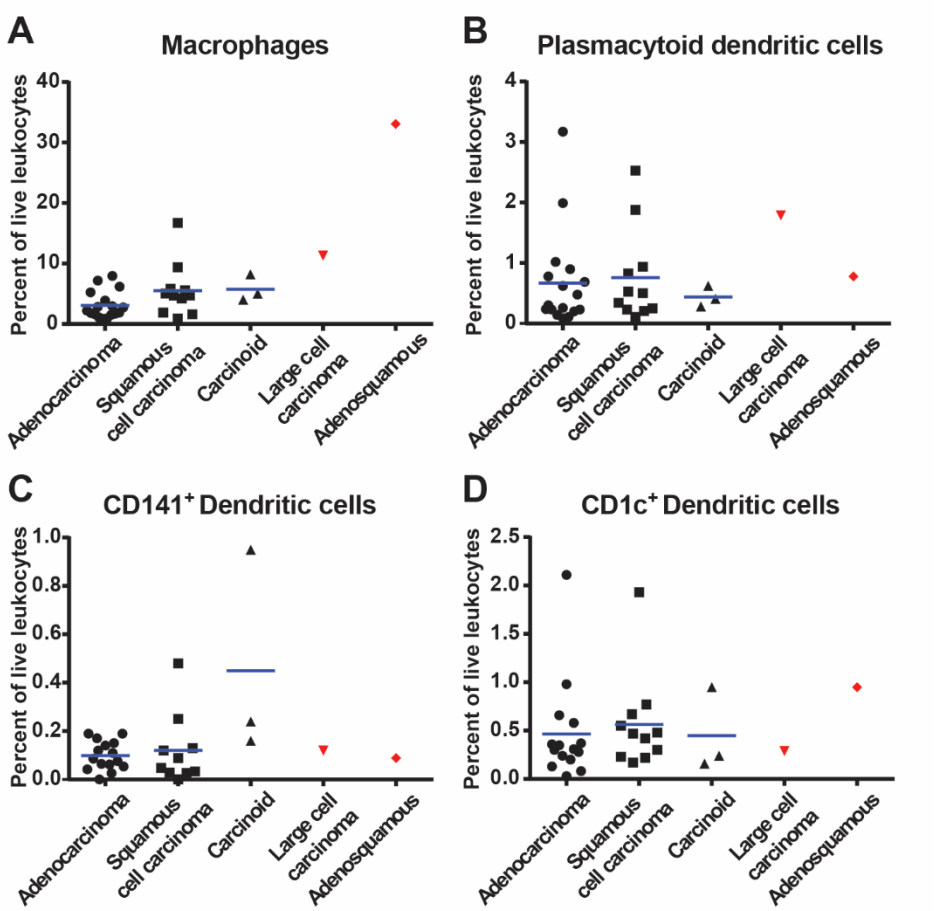

Figure 40. Percent of APC cells in different stages of NSCLC patients. Comparison of **A.** macrophages/monocytes **B.** plasmacytoid dendritic cells, **C.** CD141$^+$ dendritic cells and **D.** CD1c$^+$ dendritic cells in adenocarcinoma, squamous cell carcinoma, carcinoid tumor, large carcinoma and adenosquamous tumor. Kruskal-Wallis test and Dunn's multiple comparison were used to detect differences between means. Each symbol represents data collected from one patient, as a percentage of live leukocyte population and the mean is represented by the blue line.

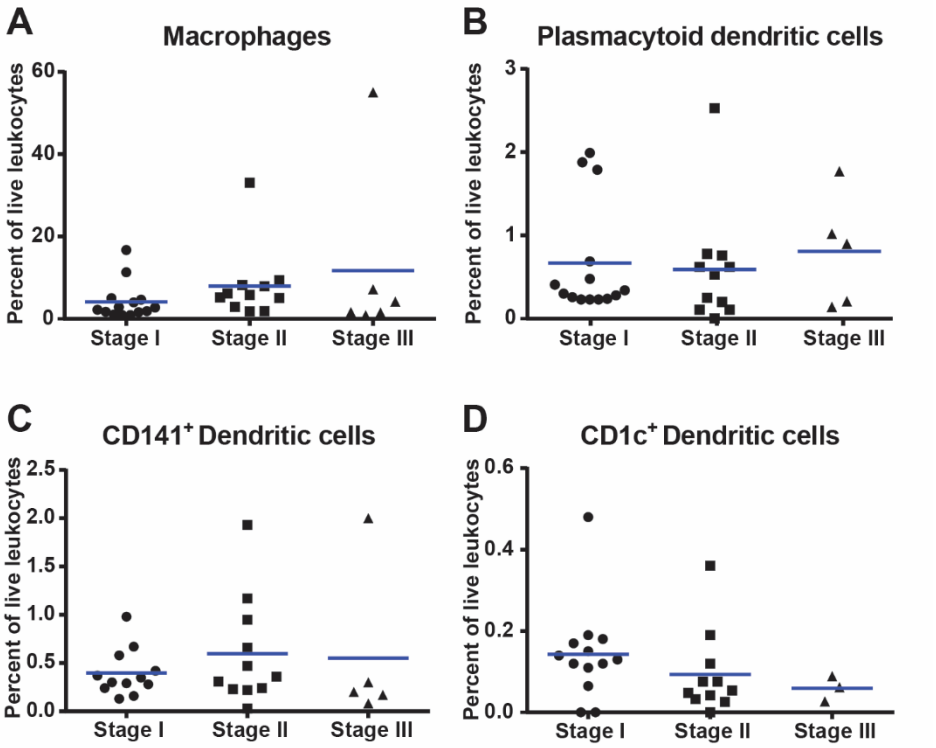

Figure 41. Percent of APC cells in different stages of NSCLC patients. Comparison of **A.** macrophages/monocytes **B.** plasmacytoid dendritic cells, **C.** CD141$^+$ dendritic cells and **D.** CD1c$^+$ dendritic cells in stage I, II and II of the disease. Kruskal-Wallis test and Dunn's multiple comparison were used to detect differences between means. Each symbol represents data collected from one patient, as a percentage of live leukocyte population and the mean is represented by the blue line.

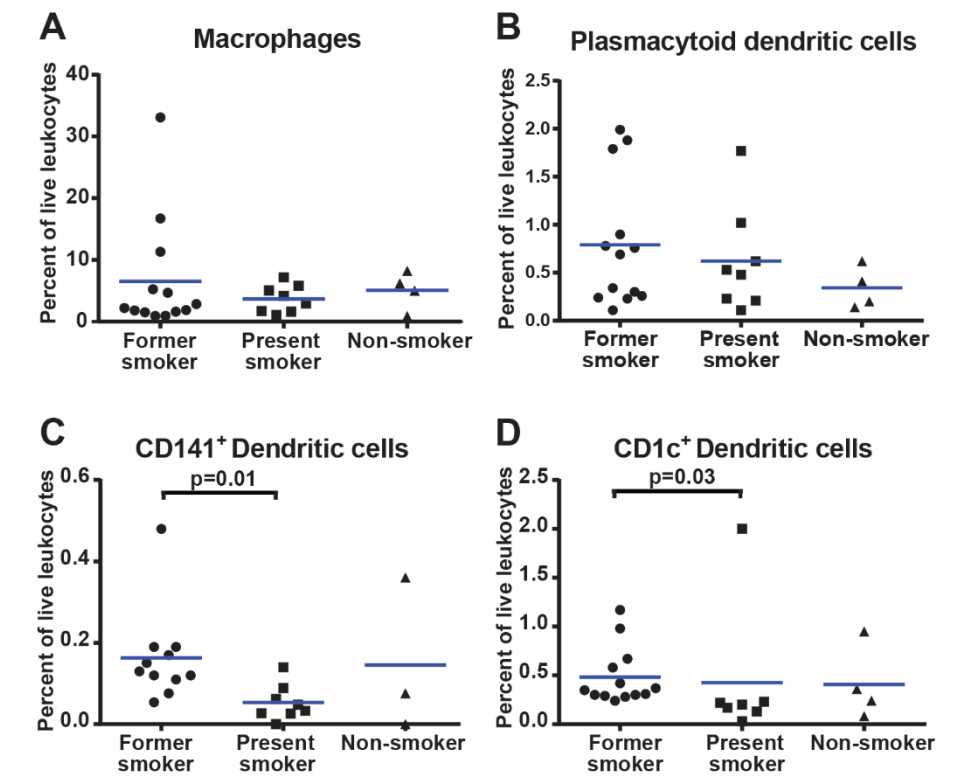

Figure 42. Percent of APC cells in different patients with different smoking history. Comparison of **A.** macrophages/monocytes **B.** plasmacytoid dendritic cells, **C.** CD141$^+$ dendritic cells and **D.** CD1c$^+$ dendritic cells in tumor tissue of patients with different smoking histories. Kruskal-Wallis test and Dunn's multiple comparison were used to detect differences between means. Each symbol represents data collected from one patient, as a percentage of live leukocyte population and the mean is represented by the blue line.

5.2.4 Analysis of NK cells and NKT cells

NK cells and NKT cells were analyzed by flow cytometry followed by statistical analysis of NK and NKT cells. NKT cells are in fact T cells, since they have TCR, and not NK cells. However since they were characterized using flow strategy for NK cells we will present their statistical analysis here, together with their flow cytometry characterization.

NK cells are a third population of lymphocytes and because of this the same gating strategy was used up until lymphocyte gate (Figures 43-46, sections A, B, C and D). From lymphocyte population we excluded B cells by selecting $CD19^-$ population (Figures 43-46 section E) and macrophages by selecting $CD14^-$ population (Figures 43-46 section F). B cells and macrophages were excluded to avoid false positive results. The cells were further plotted in CD3/CD56 graph to exclude $CD3^+CD56^-$ classical T cells, to define $CD56^+CD3^+$ NKT cells and $CD56^+CD3^-$ NK cells (Figures 43-46 section G). The NK cells were further investigated for expression of the CD16 marker and two NK cell subsets were found: $CD16^+$ cytotoxic NK cells and $CD16^-$ cytokine producing NK cells (Figures 43-46 section H). The $CD16^+$ population had dimmer expression of CD56 compared to $CD16^-$ population. Detailed characterization of all four cell types defined with flow cytometry analysis is shown in Table 12.

Table 12. Characterization of NK and NKT cells

Cell population	Molecular markers
NKT cells	$CD45^+PI^-CD19^-CD14^-CD3^+CD56^+$
NK cells	$CD45^+PI^-CD19^-CD14^-CD3^-CD56^+$
$CD16^+$ NK cells	$CD45^+PI^-CD19^-CD14^-CD3^-CD56^+CD16^+$
$CD16^-$ NK cells	$CD45^+PI^-CD19^-CD14^-CD3^-CD56^+CD16^-$

We analyzed NKT cells in different tissues of NSCLC patients and found that there was no significant difference between the tissues in either adenocarcinoma or squamous cell carcinoma. Analysis of NKT cells in different tumor types was only possible for adenocarcinoma and squamous cells carcinoma. We observed no significant difference of NKT cell concentration between these two tumor types (Figure 47). Analysis of NKT cells in tumor tissue in respect to the disease stage was only possible in stage I and II (Figure 48). This analysis did not show significant difference in NKT cell concentration between the tumor stages (Figure 48). However in order undoubtedly conclude that clinicopathological parameters have no influence on NKT infiltration in tumor tissues we need to acquire more data. This specially applies to smoking history where it was not possible to do analysis since all of the patients analyzed belonged to former smokers group.

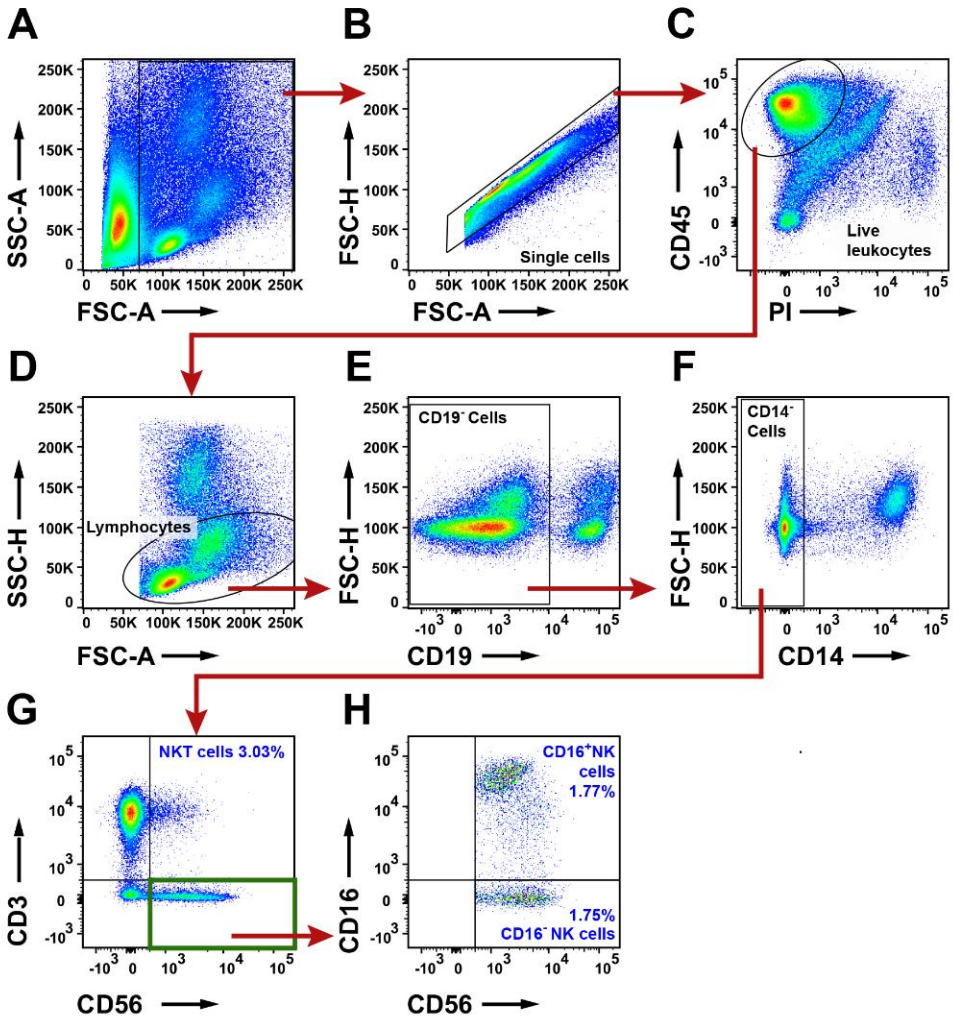

Figure 43. Flow cytometry analysis of NK cells in tumor in NSCLC patients. A. Nucleated cell gate. Gating out small apoptotic cells and debris. **B.** Single cell gate excluding doublets. **C.** Live leukocyte gate. Live leukocytes are defined as $CD45^{+}PI^{-}$. **D.** Lymphocyte gate **E.** Gating out B cells **F.** Gating out macrophages. **G.** NKT cells are $CD3^{+}CD56^{+}$ and NK cells are $CD3\text{-}CD56^{+}$. **H.** Two NK cell subsets are defined $CD16^{+}$ cytotoxic NK cells and CD16- cytokine producing NK cells. Percentages of all populations are average percent of total live leukocytes

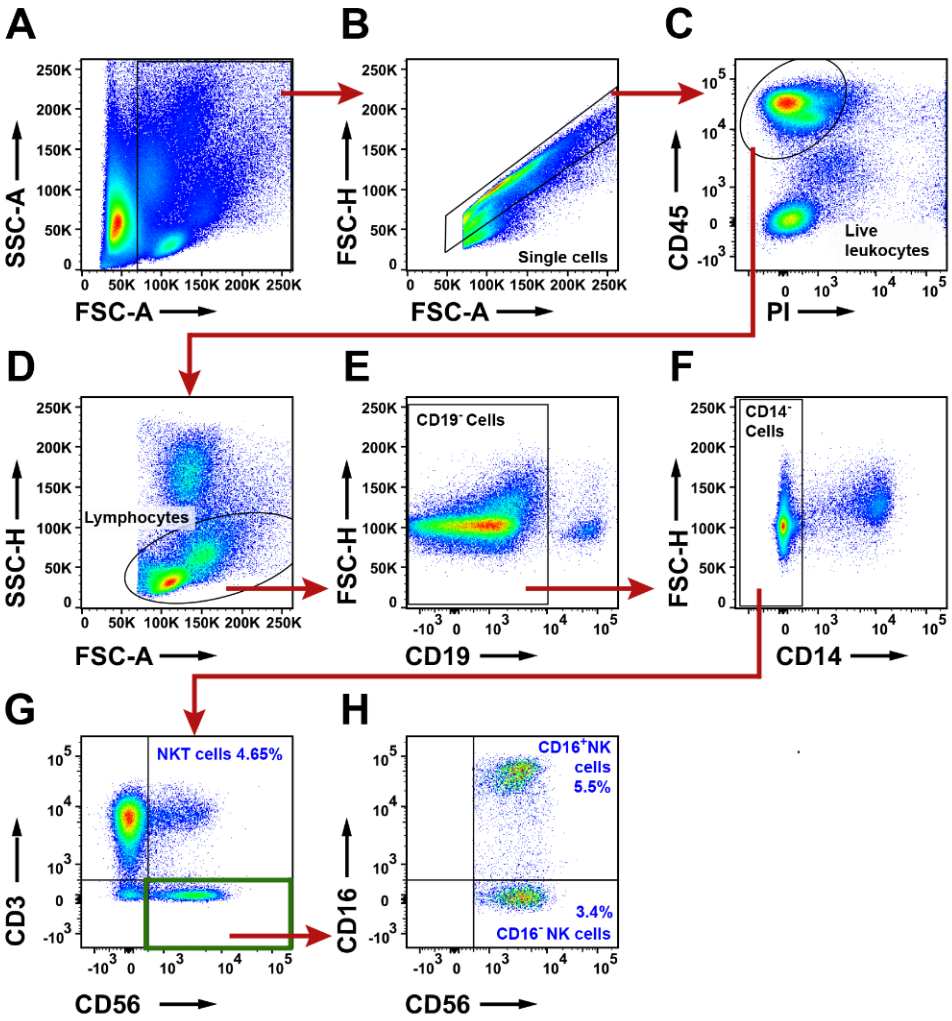

Figure 44. Flow cytometry analysis of NK cells in distant lung in NSCLC patients.
A. Nucleated cell gate. Gating out small apoptotic cells and debris. **B.** Single cell gate excluding doublets. **C.** Live leukocyte gate. Live leukocytes are defined as $CD45^{+}PI^{-}$. **D.** Lymphocyte gate **E.** Gating out B cells **F.** Gating out macrophages. **G.** NKT cells are $CD3^{+}CD56^{+}$ and NK cells are $CD3\text{-}CD56^{+}$. **H.** Two NK cell subsets are defined $CD16^{+}$ cytotoxic NK cells and CD16- cytokine producing NK cells. Percentages of all populations are average percent of total live leukocytes.

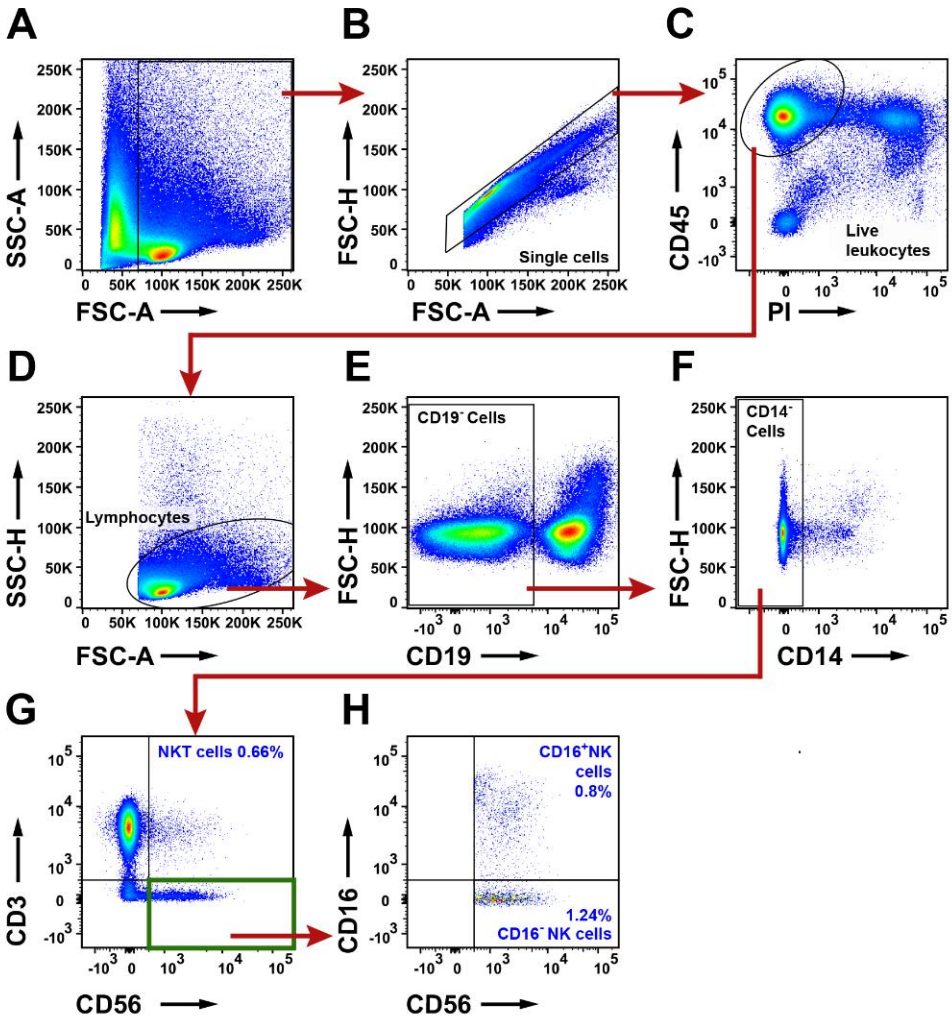

Figure 45. Flow cytometry analysis of NK cells in lymph node in NSCLC patients.
A. Nucleated cell gate. Gating out small apoptotic cells and debris. **B.** Single cell gate excluding doublets. **C.** Live leukocyte gate. Live leukocytes are defined as $CD45^{+}PI^{-}$. **D.** Lymphocyte gate **E.** Gating out B cells **F.** Gating out macrophages. **G.** NKT cells are $CD3^{+}CD56^{+}$ and NK cells are CD3-$CD56^{+}$. **H.** Two NK cell subsets are defined $CD16^{+}$ cytotoxic NK cells and CD16- cytokine producing NK cells. Percentages of all populations are average percent of total live leukocytes.

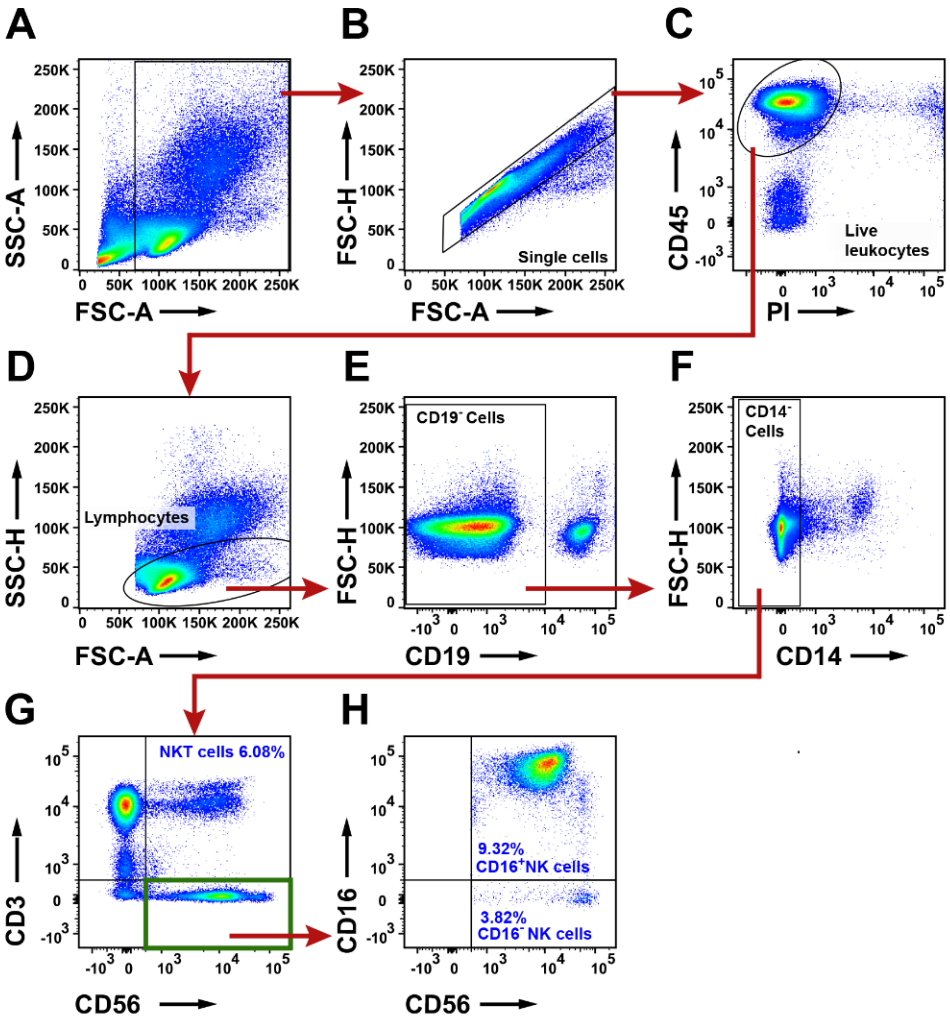

Figure 46: Flow cytometry analysis of NK cells in PBMCs in NSCLC patients. A. Nucleated cell gate. Gating out small apoptotic cells and debris. **B.** Single cell gate excluding doublets. **C.** Live leukocyte gate. Live leukocytes are defined as $CD45^{+}PI^{-}$. **D.** Lymphocyte gate **E.** Gating out B cells **F.** Gating out macrophages. **G.** NKT cells are $CD3^{+}CD56^{+}$ and NK cells are $CD3^{-}CD56^{+}$. **H.** Two NK cell subsets are defined $CD16^{+}$ cytotoxic NK cells and CD16- cytokine producing NK cells. Percentages of all populations are average percent of total live leukocytes.

Statistical analysis of $CD56^{+}$ NK cells, in different tissues of adenocarcinoma patients, revealed higher concentration of NK cell in distant lung compared to the tumor tissue (p=0.013; Figure 49 A). There was no significant difference between tissues in squamous cell carcinoma patients. Same analysis was performed in $CD16^{+}$ and $CD16^{-}$ subsets of NK cells. We observed significant decrease in $CD16^{+}$ subset in adenocarcinoma, where tumor had lower concentration of NK cells than distant lung (p=0.01; Figure 49 C). No such difference was present in squamous cell carcinoma (Figure 49D).

Analysis of NK cells in different stages of disease did not show significant difference between the groups (Figure 50 A). The subsets of NK cells also revealed no

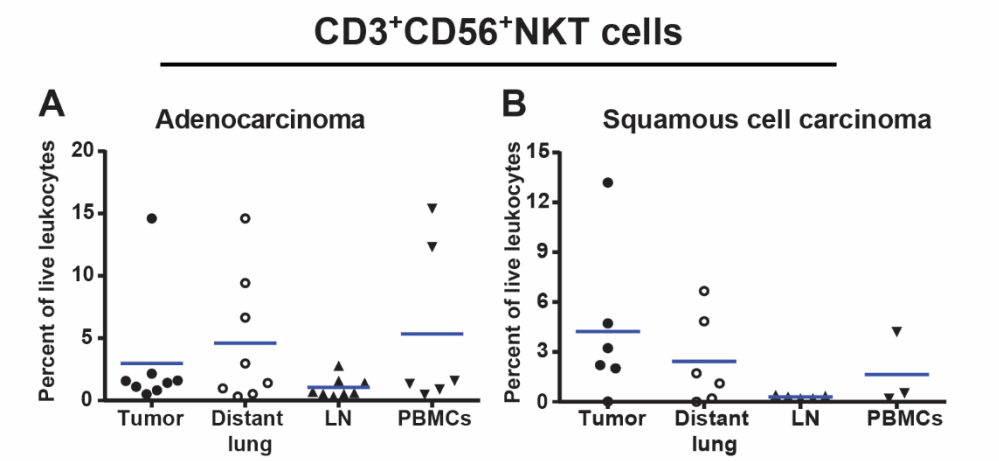

Figure 48. Characterization of NKT cells in different tissues of NSCLC patients. Comparison NKT cells in different tissues of patients diagnosed with **A.** adenocarcinoma and **B.** squamous cell carcinoma.. Kruskal-Wallis test and Dunn's multiple comparison were used to detect differences between means. Each symbol represents data collected from one patient, as a percentage of live leukocyte population and the mean is represented by the blue line. Abbreviation meaning: LN = lymph node and PBMCs = peripheral blood mononuclear cells.

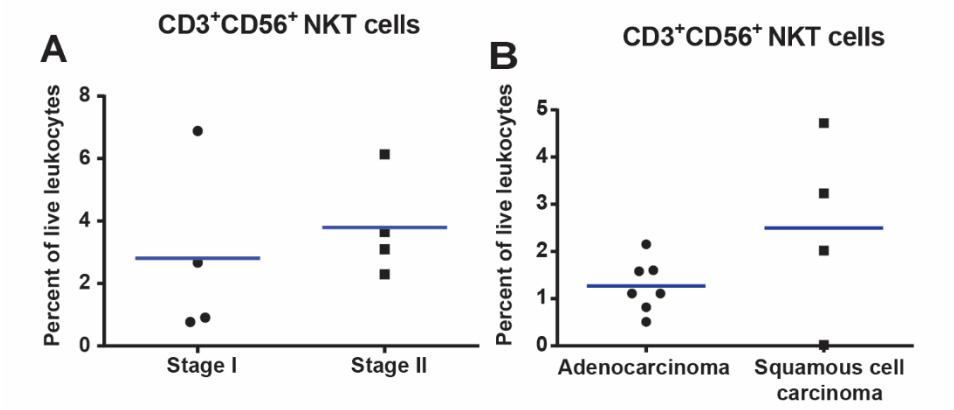

Figure 47. Characterization of $CD3^+$ $CD4^+$ and $CD8^+$ T cells in different clinicopathological parameters. Comparison of **A.** NKT cells in tumor tissue in stage I and II of the disease. **B.** Comparison of NKT cells in adenocarcinoma and squamous cell carcinoma **C.** Mann-Whitney test was used to detect differences between means. Each symbol represents data collected from one patient, as a percentage of live leukocyte population and the mean is represented by the blue line

difference between the groups in different stages of disease (50 B, C). Analysis of NK cells in different types of tumor was only possible in adenocarcinoma and squamous cell carcinoma. We did not observed any significant differences between the groups (Figure 50 D, E and F). Analysis of NK cells in patients with different smoking histories was not possible since all of the patients stained for NK cells were previous smokers

To gain a deeper understanding of mutual ratio of $CD16^+$ and $CD16^-$ NK cell we analyzed their percentages in $C56^+$ NK cell population. We observed that in distant lung majority of the cells were $CD16^+$, and the same was observed in adenocarcinoma. Contradictory to adenocarcinoma, in squamous cell carcinoma $CD16^-$ cells were most abundant (Figure 51). The percentages of NK cell subsets in $CD56^+$ NK cells were used

for statistical analysis in different tissues. This analysis showed no noticeable difference between the different tissues (Figure 52).

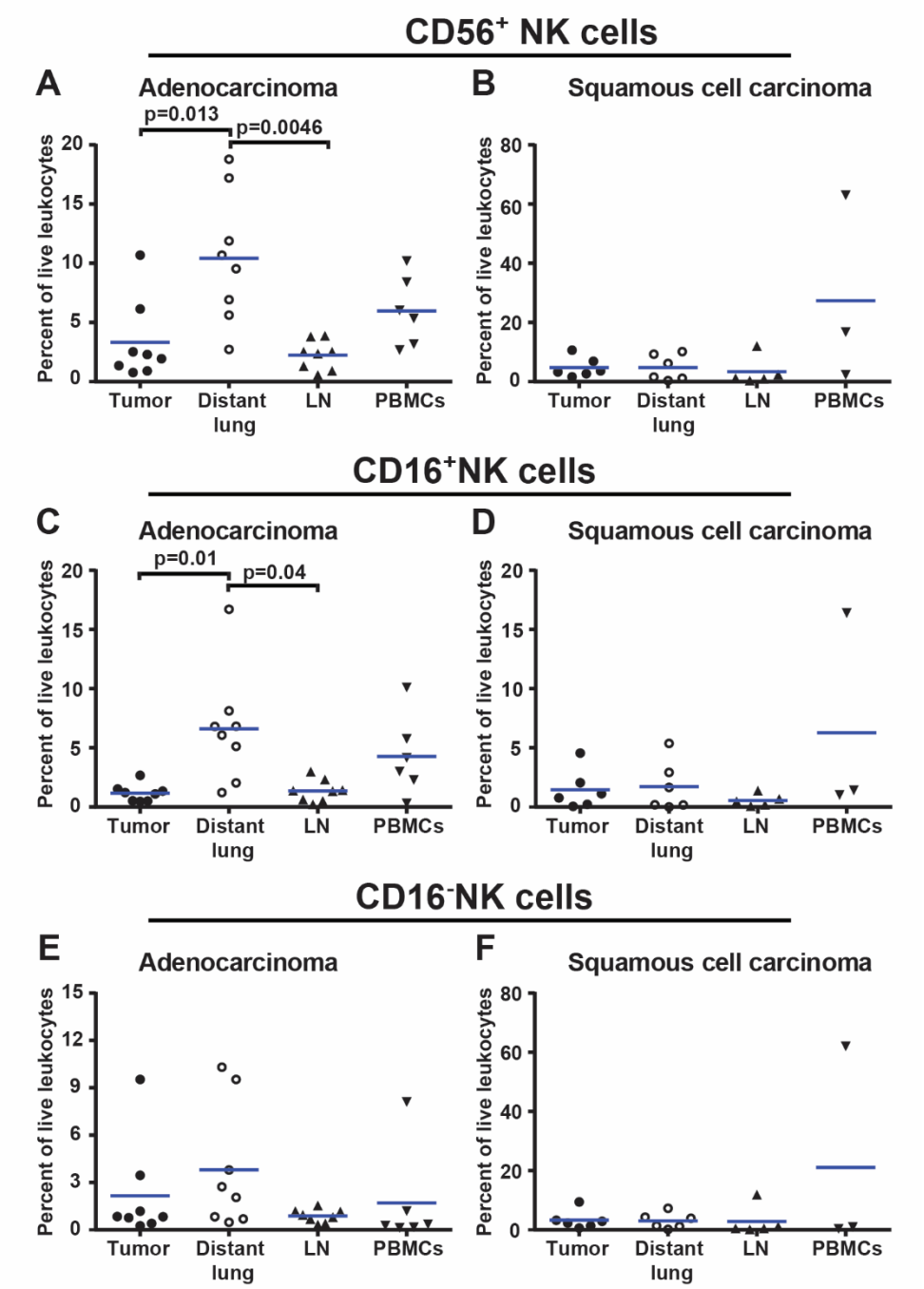

Figure 49. Characterization of NK cells in different tissues of NSCLC patients. Comparison of NK cells in different tissues of patients diagnosed with **A.** adenocarcinoma and **B.** squamous cell carcinoma. Comparison of $CD16^+$ NK cells in **C.** adenocarcinoma and **D.** squamous cell carcinoma. Comparison of $CD16^-$ NK cells in different tissues of patients diagnosed with **E.** adenocarcinoma and **F.** squamous cell carcinoma. Kruskal-Wallis test and Dunn's multiple comparison were used to detect differences between means. Each symbol represents data collected from one patient, as a percentage of live leukocyte population and the mean is represented by the blue line. Abbreviation meaning: LN = lymph node and PBMCs = peripheral blood mononuclear cells.

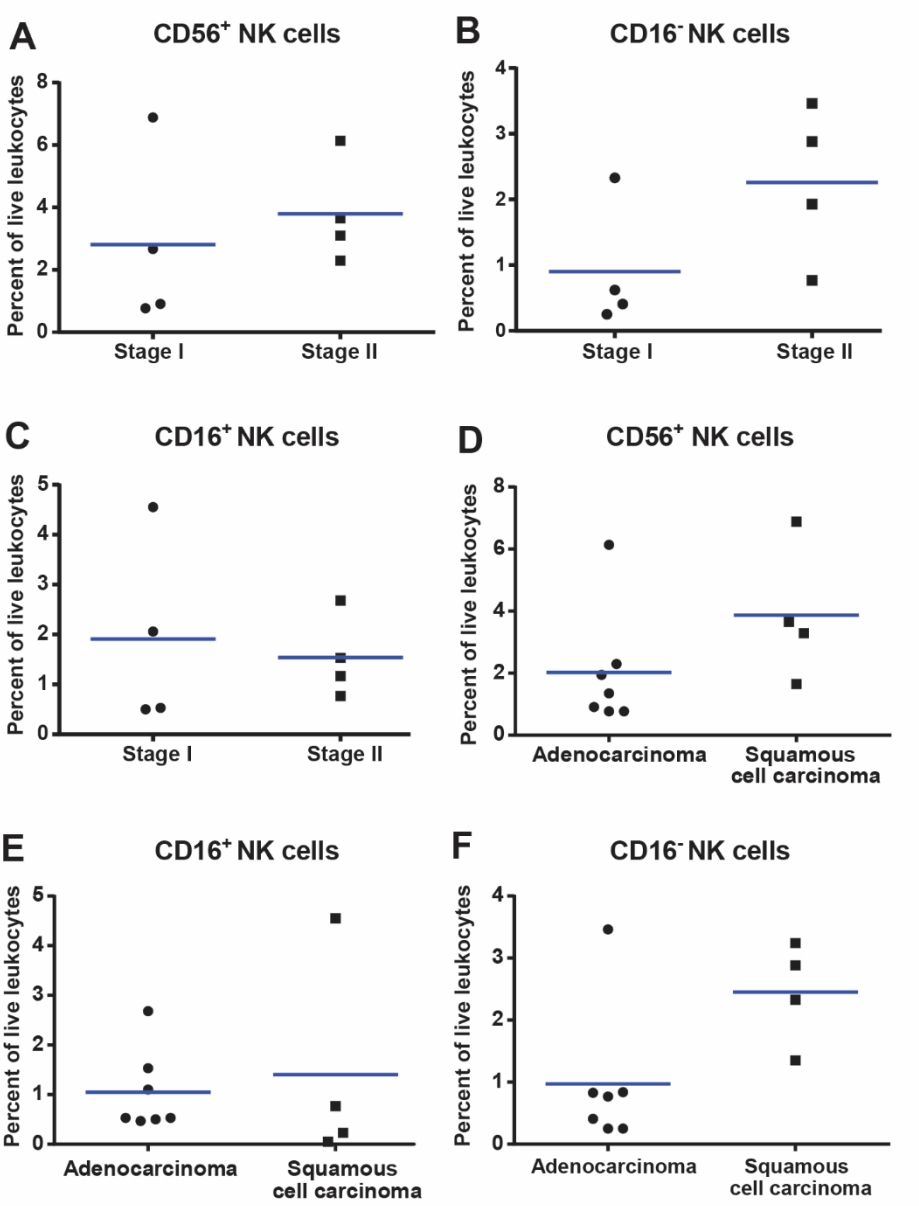

Figure 50 Characterization of NK cells in respect to different clinicopathological parameters. Comparison of **A.** NK cells, **B.** $CD16^+$ NK cells, and **C.** $CD16^-$ NK cells in tumor tissue in stage I and II of the disease. Comparison of **D.** NK cells, **E.** $CD16^+$ NK cells, and **F.** $CD16^-$ NK cells in adenocarcinoma and squamous cell carcinoma. Mann-Whitney test was used to detect differences between means. Each symbol represents data collected from one patient, as a percentage of live leukocyte population and the mean is represented by the blue line.

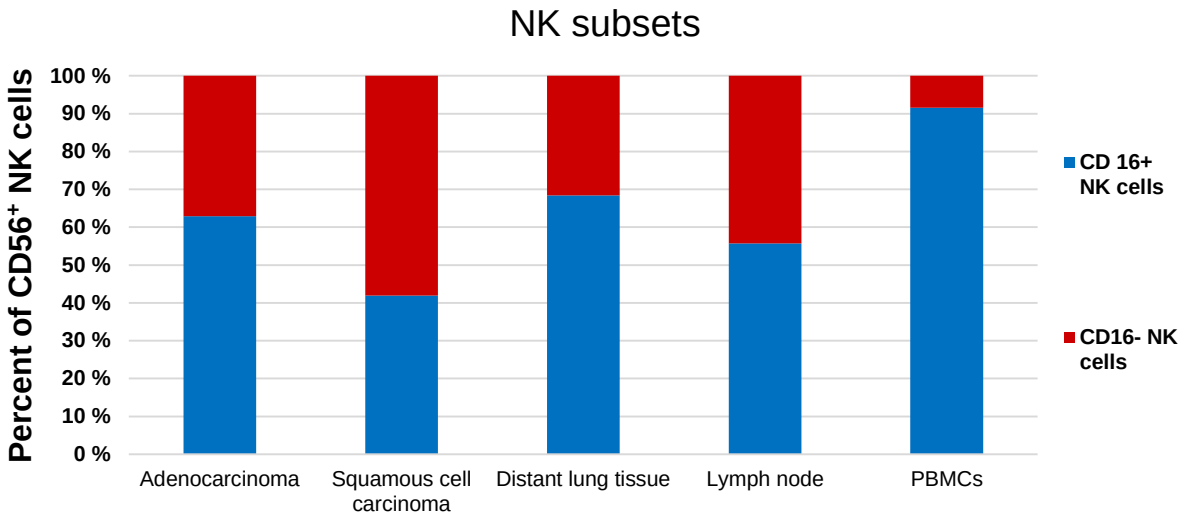

Figure 52. NK cell subsets in adenocarcinoma, squamous cell carcinoma, distant lung, lymph node and PBMCs. The graph represents NK cell subsets in adenocarcinoma, squamous cell carcinoma, distant lung, lymph node and PBMCs. All percentages in the graph were obtained from a mean values of NK cell subsets.

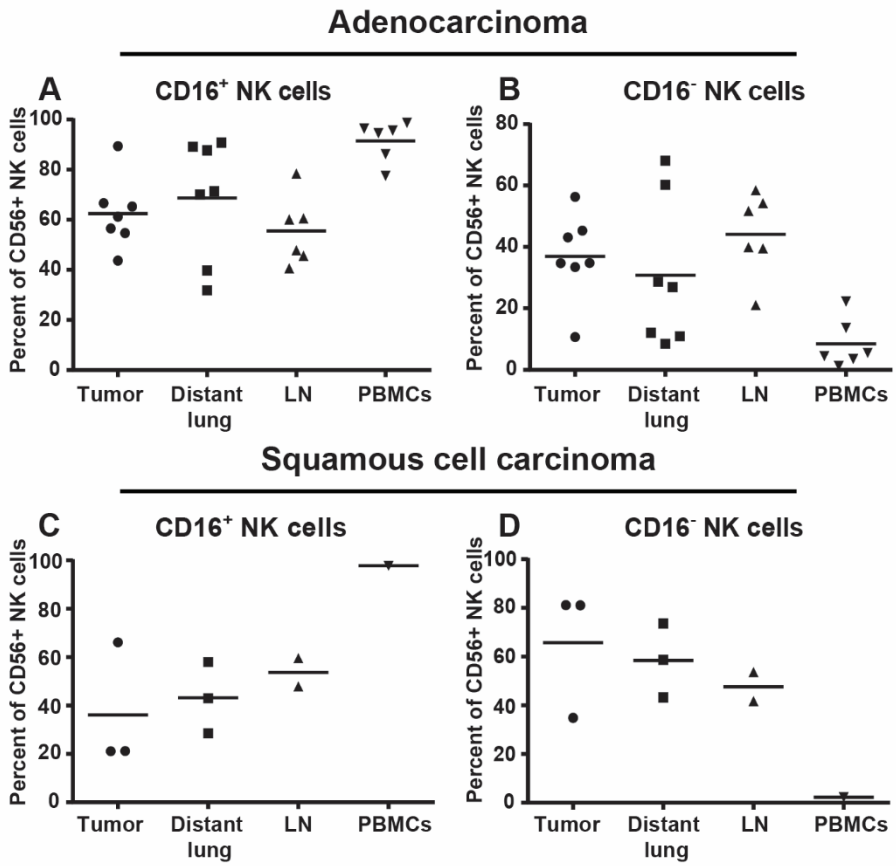

Figure 51. NK cell subsets as a percent of CD56$^+$ NK cells. Comparison of **A.** CD16$^+$ NK cells and **B.** CD16$^-$ NK cells in tissues of patients diagnosed with adenocarcinoma. Comparison of **C.** CD16$^+$ NK cells and **D.** CD16$^-$ NK cells in tissues of patients diagnosed with squamous cell carcinoma. The percent of B cell subset was calculated from CD56$^+$CD3$^-$ NK cell population. Kruskal-Wallis test and Dunn's multiple comparison were used to detect differences between means. Each symbol represents data collected from one patient, as a percentage of live leukocyte population and the mean is represented by the blue line. Abbreviation meaning: LN = lymph node and PBMCs = peripheral blood mononuclear cells.

5.2.5 Analysis of granulocyte populations

Granulocytes are population of leukocytes, so first three gates were the same as in all other gating strategies (Figures 53-56 A, B, C). Lymphocyte gate is omitted in this samples because most granulocytes have higher FSC and SSC than lymphocytes and would be excluded from the analysis if this gate was used. From the leukocyte gate we excluded $CD3^+$ and $CD19^+$ cells by selecting negative cells in CD3CD19 exclusion channel (Figures 53-56 D). Cells were further gated to exclude macrophages by excluding $CD14^+$ cells (Figures 53-56 E). Granulocytes were then divided into $CD11b^+$ and $CD11b^-$ populations (Figures 53-56 F). In $CD11b^+$ population we selected $CD15^+$ cells, and from this population we separated neutrophils from eosinophils based on CD49d expression (Figures 53-56 I, J). Neutrophils were defined as $CD49d^-$ and eosinophils were defined as $CD49d^+$. In $CD11b^-$ population we selected cells that expressed high-affinity IgE receptor (FcεR1α) and from this population we defined mast cells and basophils with CD49d and CD117 (Figures 49-52 G, H). Both basophils and mast cells were defined as $CD49d^+$. Mast cells were defined as $CD117^+$ and basophils were defined as $CD117^-$. Detailed characterization of granulocyte populations is presented in table 13.

Table 13. Characterization of granulocytes

Cell population	Molecular markers
Neutrophils	$CD45^+PI^-CD19^-CD3^-C14^-CD11b^+CD15^+CD49d^+$
Basophils	$CD45^+PI^-CD19^-CD3^-C14^-CD11b^-FcεR1α^+CD117^-CD49d^+$
Eosinophils	$CD45^+PI^-CD19^-CD3^-C14^-CD11b^+CD15^+CD49d^-$
Mast cells	$CD45^+PI^-CD19^-CD3^-C14^-CD11b^-FcεR1α^+CD117^-CD49d^+$

Flow cytometry analysis for all four granulocyte populations are presented in the figures 53-56. Populations are presented together with their mean values of live leukocytes. Mean values are calculated for each tissue separately. Each mean value is calculated from percentages for each patient stained for granulocyte populations.

Statistical analysis of the four granulocyte populations in different tissues in both adenocarcinoma and squamous cell carcinoma revealed that only mast cells in adenocarcinoma show significantly higher concentration in tumor compared to PBMCs and lymph node (Figure 58). This is not surprising since granulocytes are not expected to be found in lymph node and they are removed for the most part from the blood with density gradient used to purify PBMCs. Analysis of granulocyte populations in patients with different smoking histories was not possible because all of the patients stained for granulocyte populations were former smokers. The analysis of granulocytes in different tumor types was only possible for adenocarcinoma and squamous cell carcinoma. In this analysis we observed that neutrophils had higher concentrations in adenocarcinoma than in squamous cell carcinoma (Figure 59 C). The stage of the tumor showed no influence on tumor infiltration (Figure 60)

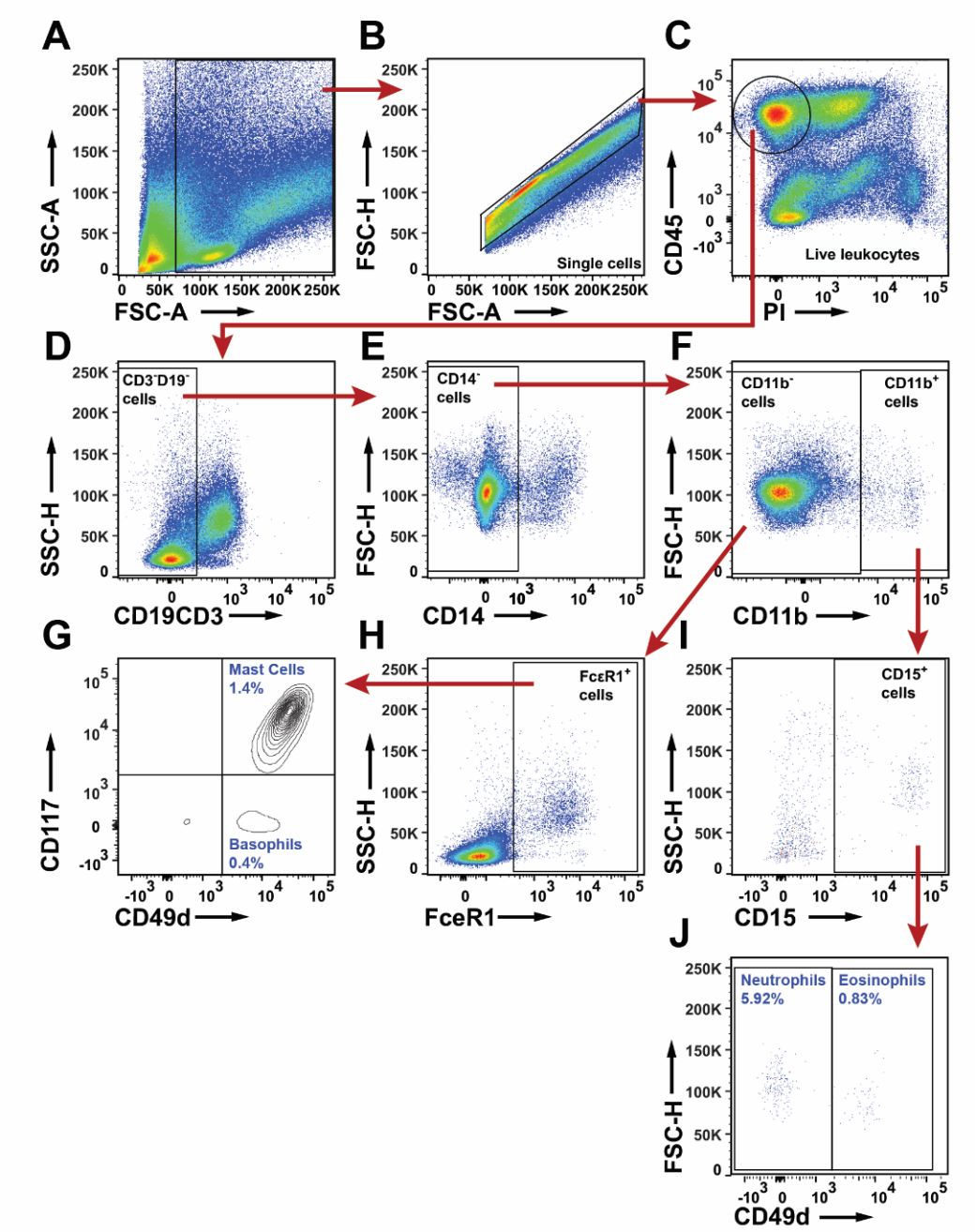

Figure 53. Flow cytometry analysis of granulocyte populations in tumor in NSCLC patient
A. Nucleated cell gate. Gating out apoptotic cells, necrotic cells and debris. **B.** Single cell gate excluding dublets. **C.** Live leukocyte gate. Live leukocytes are defined as CD45 positive and propidium iodide (PI) negative. **D.** Gatin for $CD3^-$ $CD19^-$ cells – excluding T cells and B cells. **E.** $CD14^-$ cells gate – gating out macrophages. **F.** $CD11b^-$ cells include mast cells and basophils, and CD11b cells include neutrophils and eosinophils. **H.** Mast cells and basophils are further defined as FceR1 population and **G.** CD49d population. Mast cells are CD117 and basophils are $CD117^-$. **I.** Neutrophils and eosinophils are defined as CD15 **J.** Neutrophils are further defined as $CD49d^-$ and eosinophils are defined as $CD49d^-$ Percentages of all populations are average percent of total live leukocytes.

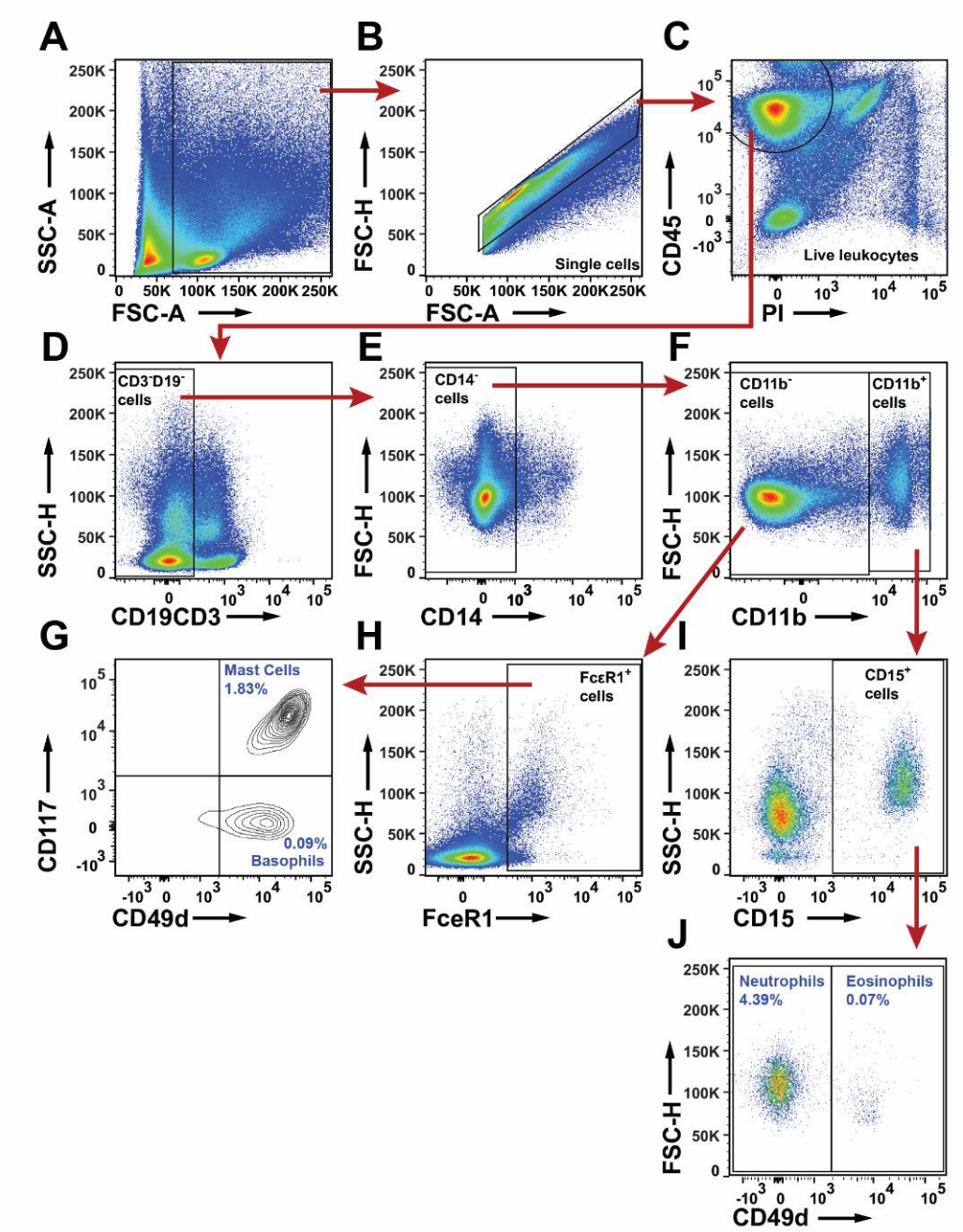

Figure 54. Flow cytometry analysis of granulocyte populations in distant lung in NSCLC patient **A.** Nucleated cell gate. Gating out apoptotic cells, necrotic cells and debris. **B.** Single cell gate excluding dublets. **C.** Live leukocyte gate. Live leukocytes are defined as CD45 positive and propidium iodide (PI) negative. **D.** Gatin for $CD3^-$ $CD19^-$ cells – excluding T cells and B cells. **E.** $CD14^-$ cells gate – gating out macrophages. **F.** $CD11b^-$ cells include mast cells and basophils, and CD11b cells include neutrophils and eosinophils. **H.** Mast cells and basophils are further defined as FceR1 population and **G.** CD49d population. Mast cells are CD117 and basophils are $CD117^-$. **I.** Neutrophils and eosinophils are defined as CD15 **J.** Neutrophils are further defined as $CD49d^-$ and eosinophils are defined as $CD49d^-$ Percentages of all populations are average percent of total live leukocytes.

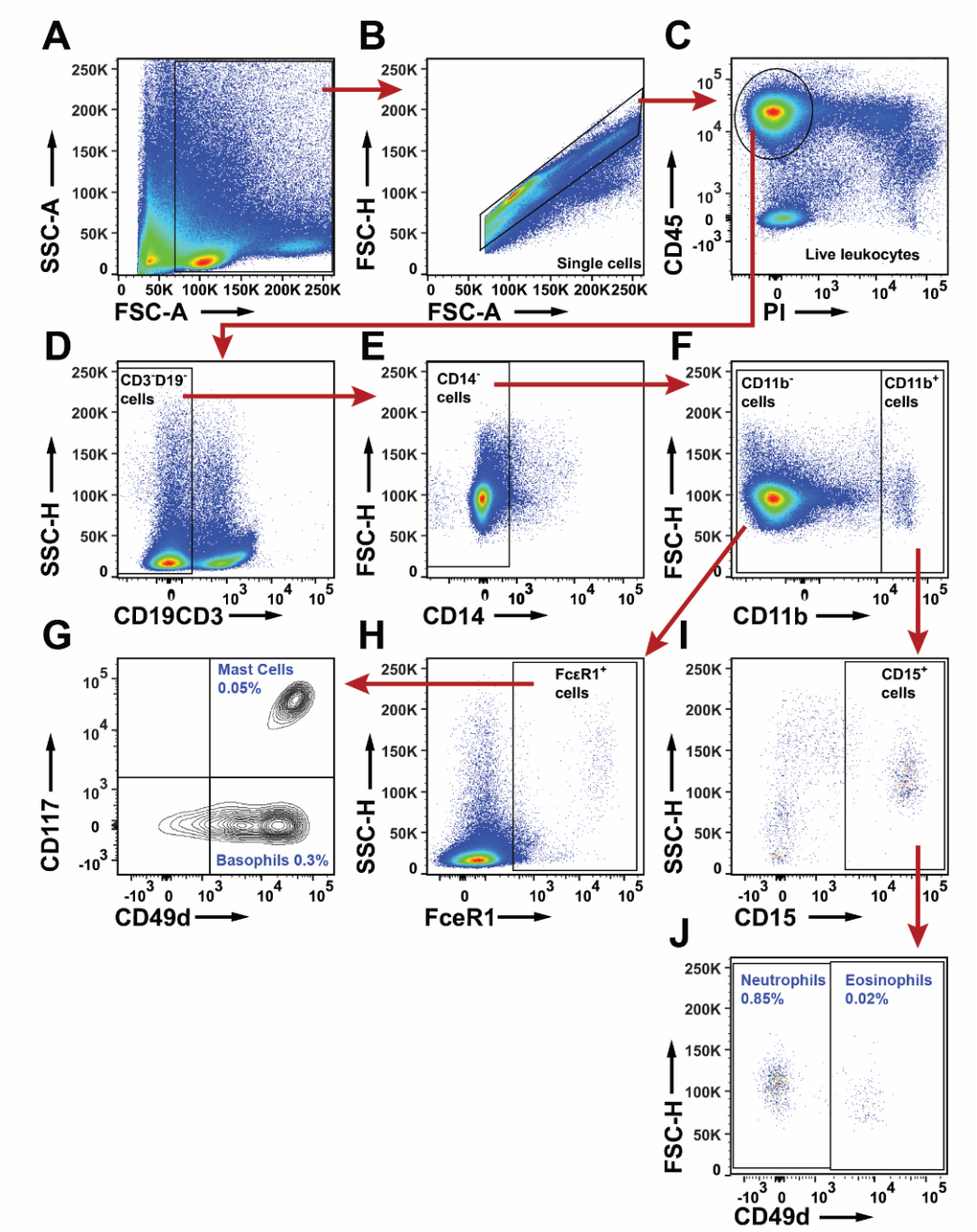

Figure 55. Flow cytometry analysis of granulocyte populations in lymph node in NSCLC patient **A.** Nucleated cell gate. Gating out apoptotic cells, necrotic cells and debris. **B.** Single cell gate excluding dublets. **C.** Live leukocyte gate. Live leukocytes are defined as CD45 positive and propidium iodide (PI) negative. **D.** Gatin for $CD3^{-}CD19^{-}$ cells – excluding T cells and B cells. **E.** $CD14^{-}$ cells gate – gating out macrophages. **F.** $CD11b^{-}$ cells include mast cells and basophils, and CD11b cells include neutrophils and eosinophils. **H.** Mast cells and basophils are further defined as FceR1 population and **G.** CD49d population. Mast cells are CD117 and basophils are $CD117^{-}$. **I.** Neutrophils and eosinophils are defined as CD15 **J.** Neutrophils are further defined as $CD49d^{-}$ and eosinophils are defined as $CD49d^{-}$ Percentages of all populations are average percent of total live leukocytes.

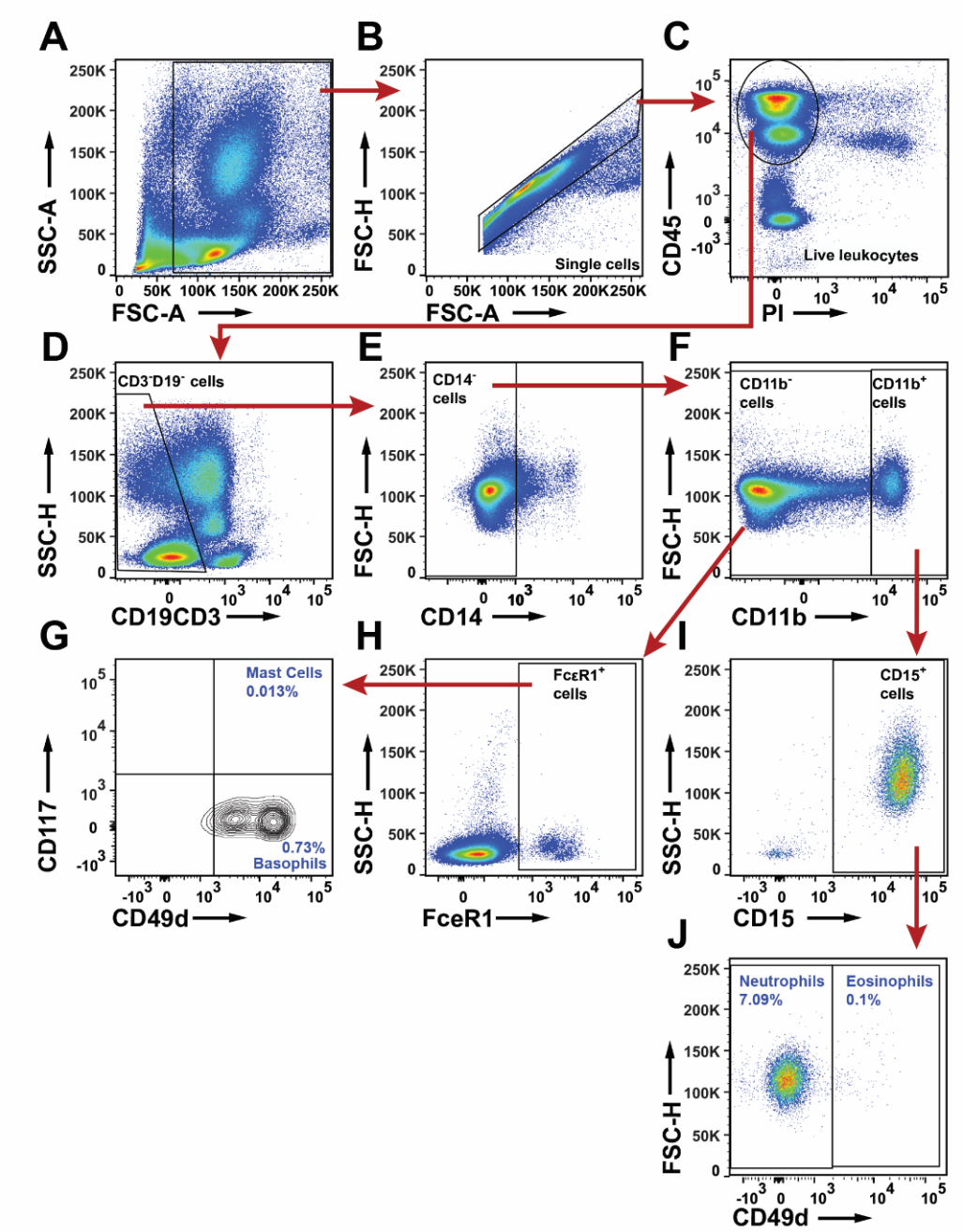

Figure 56. Flow cytometry analysis of granulocyte populations in PBMCs in NSCLC patient. A. Nucleated cell gate. Gating out small apoptotic cells and debris. **B.** Single cell gate excluding dublets. **C.** Live leukocyte gate. Live leukocytes are defined as CD45 positive and propidium iodide (PI) negative. **D.** Gatin for $CD3^{-}CD19^{-}$ cells – excluding T cells and B cells. **E.** $CD14^{-}$ cells gate – gating out macrophages. **F.** $CD11b^{-}$ cells include mast cells and basophils, and CD11b cells include neutrophils and eosinophils. **H.** Mast cells and basophils are further defined as FceR1 population and **G.** CD49d population. Mast cells are CD117 and basophils are $CD117^{-}$. **I.** Neutrophils and eosinophils are defined as CD15 **J.** Neutrophils are further defined as $CD49d^{-}$ and eosinophils are defined as $CD49d^{-}$ Percentages of all populations are average percent of total live leukocytes.

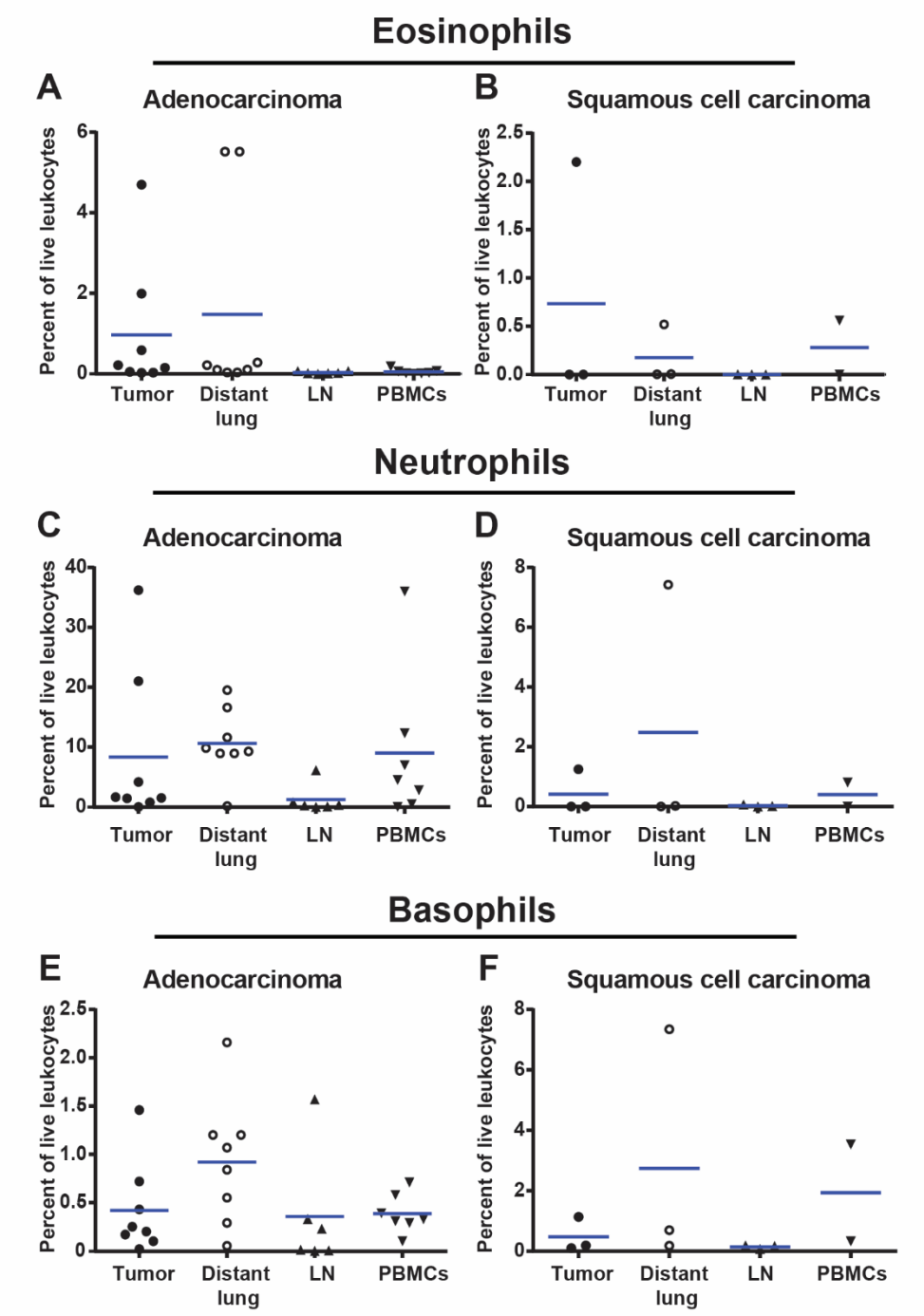

Figure 57. Characterization of eosinophils, neutrophils and basophils in different tissues of NSCLC patients. Comparison of eosinophils in different tissues of patients diagnosed with **A.** adenocarcinoma and **B.** squamous cell carcinoma. Comparison of neutrophils in different tissues of patients diagnosed with **C.** adenocarcinoma and **D.** squamous cell carcinoma. Comparison of basophils in different tissues of patients diagnosed with in **E.** in adenocarcinoma and **F.** squamous cell carcinoma. Kruskal-Wallis test and Dunn's multiple comparison were used to detect differences between means. Each symbol represents data collected from one patient, as a percentage of live leukocyte population, and the mean is represented by the blue line. Abbreviation meaning: LN = lymph node and PBMCs = peripheral blood mononuclear cells.

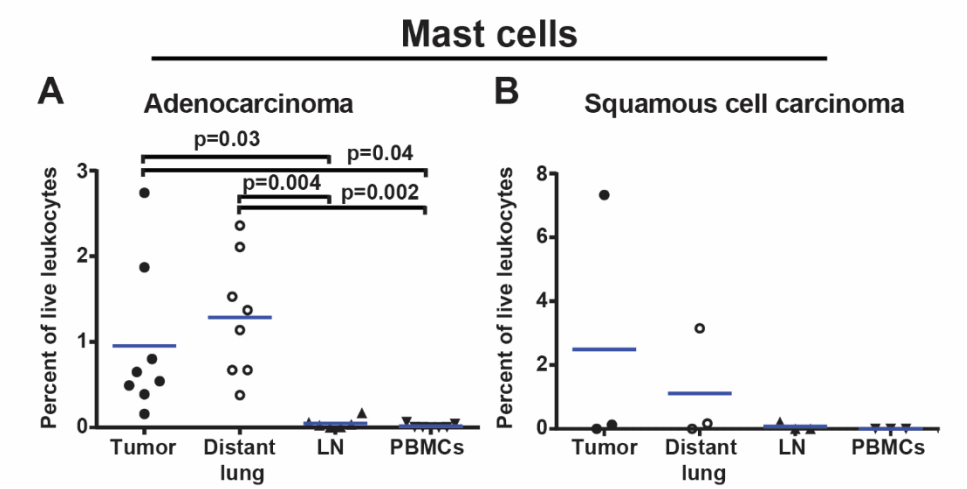

Figure 58. Characterization of eosinophils, neutrophils and basophils in different tissues of NSCLC patients. Comparison of mast cells in different tissues of patients diagnosed with **A.** adenocarcinoma and **B.** squamous cell carcinoma, Kruskal-Wallis test and Dunn's multiple comparison were used to detect differences between means. Each symbol represents data collected from one patient, as a percentage of live leukocyte population and the mean is represented by the blue line. Abbreviation meaning: LN = lymph node and PBMCs = peripheral blood mononuclear cells.

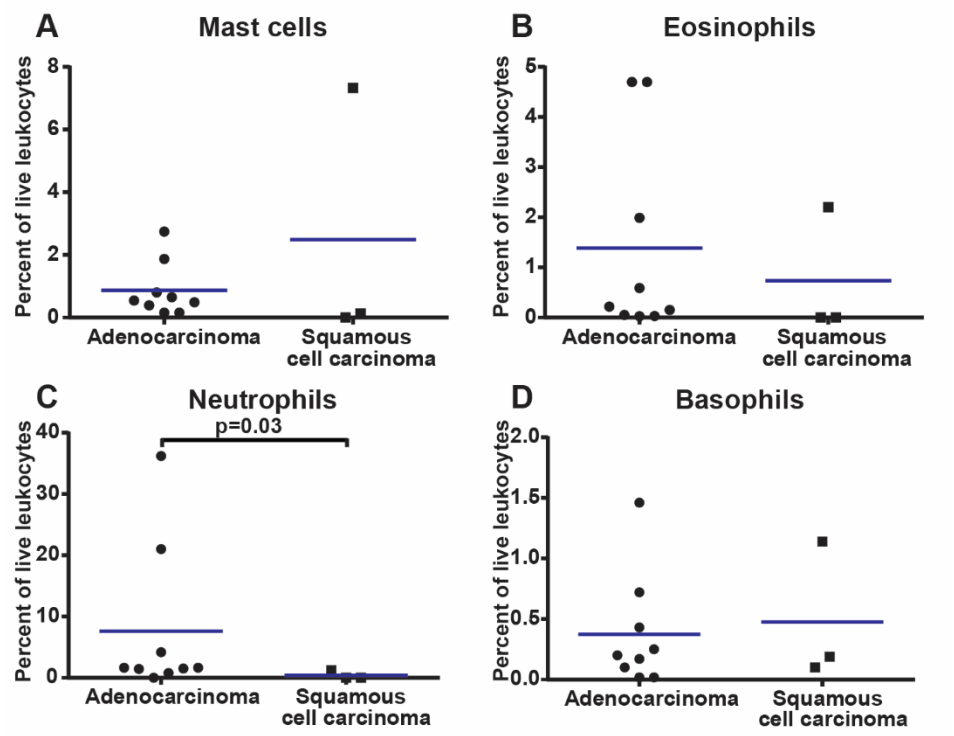

Figure 59. Characterization of granulocytes in different types of tumor. A. Comparison of **A.** mast cells, **B.** eosinophils, **C.** neutrophils, and **D.** basophils in adenocarcinoma and squamous cell carcinoma. Mann-Whitney test was used to detect differences between means. Each symbol represents data collected from one patient, as a percentage of live leukocyte population and the mean is represented by the blue line.

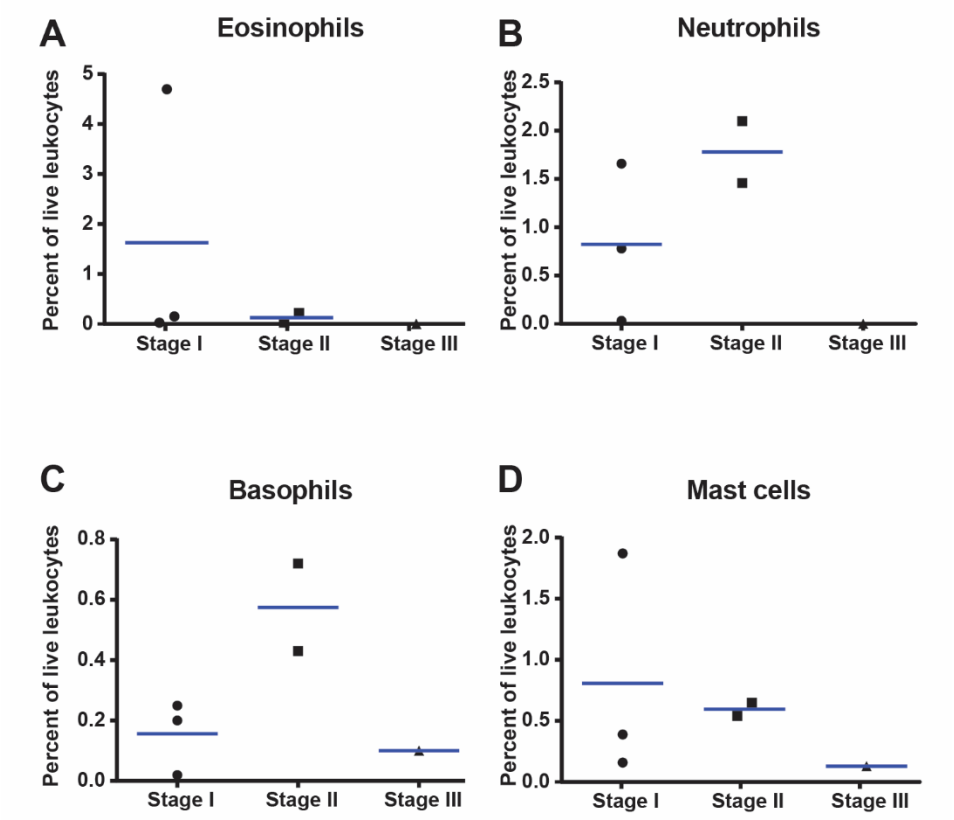

Figure 60. Characterization of granulocytes in different tumor stages. Comparison of **A.** eosinophils **B.** neutrophils **C.** basophils and **D.** mast cells in tumor tissue in stages I II and III of disease. Kruskal-Wallis test and Dunn's multiple comparison were used to detect differences between means. Each symbol represents data collected from one patient, as a percentage of live leukocyte population and the mean is represented by the blue.

5.2.6 Analysis of PD-1 expression on T cells

We analyzed expression of PD-1 co-inhibitory receptor on T cells in NSCLC patients using flow cytometry. To define T cells populations we used gating strategy for T cells (Figure 9-12). Each of the T cell populations ($CD4^+$, $CD8^+$, $CD4^-CD8^-$, and their naive and memory subtypes) was examined for PD-1 expression. The PD-1 expressing cells do not appear as a separate population on the graph, instead they show upregulation of PD-1. Therefore we used overlapping histograms of anti-PD-1 antibody and isotype control to visualize PD-1 expression (Figure 61). The isotype control defined the threshold for gating of PD-1 positive cells.

Percentages of PD-1 expressing T cells, obtained from the histograms, were used for statistical analysis. The analysis of PD-1 expression in $CD4^+$, $CD8^+$ and $CD4^-CD8^-$ tumor infiltrating T cells, and their memory and naive subsets, showed that memory subtypes have higher expression of PD-1 than naive subsets (Figure 62). Moreover we noticed high degree of individual differences between the patients. The PD-1 expression on tumor infiltrating T cells varies from no expression to 87.9 % (Figures 62).

Analysis of PD-1 expression on T cells in different tissues showed general higher expression of PD-1 in tumor tissue, than in PBMCs (Figures 63 and 64). However, there was no statistically significant difference between PD-1 expression on T cells in tumor and T cells in the distant lung.

Analysis of PD-1 expression on T cells in different tumor stages was only possible for stage I and stage II of the disease. This analysis showed no significant difference between the T cell populations (Figure 65 A, B, C). Comparison of PD-1 expression in T cells obtained from patients with different smoking histories was only possible for smoker and previous smokers, since only one of the patients was a non-smoker. Comparison of these two groups showed no significant difference in any of the T cell populations.

Comparison of PD-1 expression in T cells in adenocarcinoma and squamous cell carcinoma is presented in figure 65. The only significant difference observed in this analysis was higher expression of PD-1 in memory $CD8^+$ T cells in squamous cell carcinoma compared to adenocarcinoma.

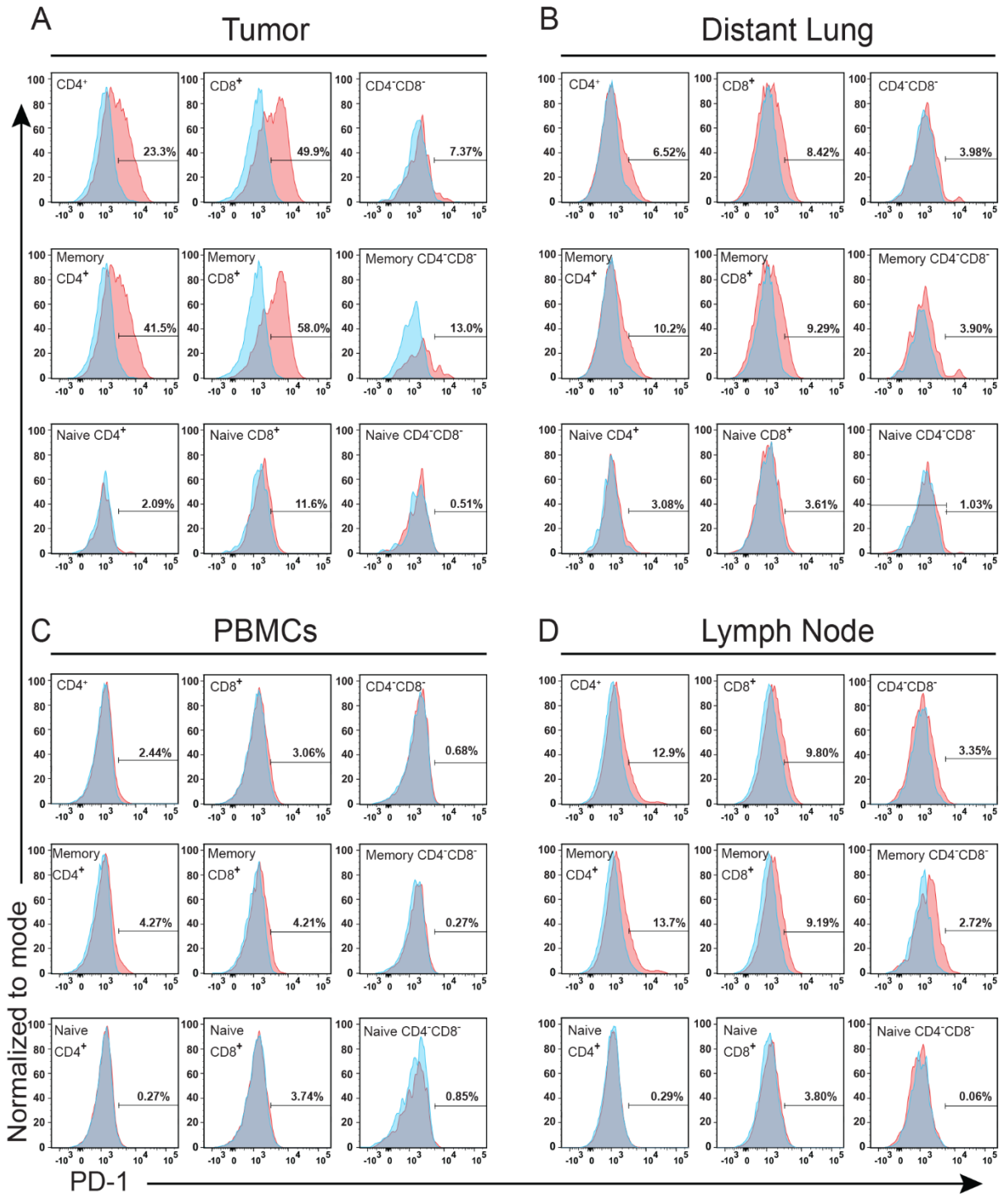

Figure 61. Example of gating strategy for PD-1 expression in tumor, distant lung, PBMCs, and lymph node in one patient. All histograms were obtained using the gating strategy for T cell. Each type of T cells populations, $CD4^+$,$CD8^+$ and $CD4^-CD8^-$, and their naive and memory subpopulations, were examined for PD-1 expression. Isotype control is shown in blue and PD-1 expression is shown in red.

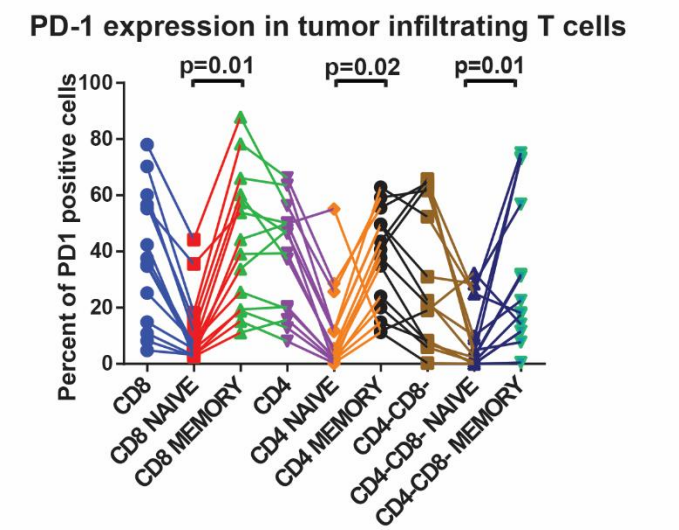

Figure 62. PD-1 expression in populations of tumor infiltrating T cells. Comparison of PD-1 expression in $CD8^+$, naive $CD8^+$, memory $CD8^+$, $CD4^+$, naive $CD4^+$, memory $CD4^+$, $CD8^+$, naive $CD8^+$, memory $CD8^+$, $CD4^-$ $CD8^-$, naive $CD4^-$ $CD8^-$, and memory $CD4^-$ $CD8^-$ cells. Kruskal-Wallis test and Dunn's multiple comparison were used to detect differences between means. Each symbol represents data collected from one patient and data from different tissues of the same patient are connected with the line.

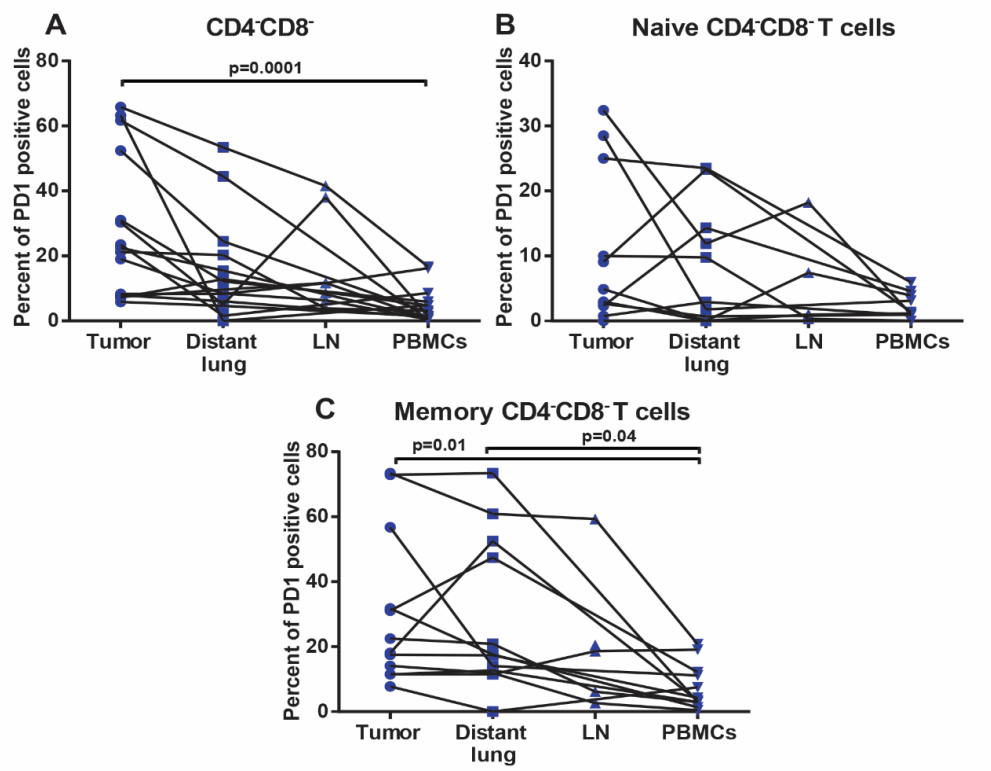

Figure 63. PD-1 expression in populations of tumor infiltrating $CD4^-$ $CD8^-$ T cells. Comparison of PD-1 expression in **A.** $CD4^-CD8^-$ T cells, **B.** naive population of $CD4^-CD8^-$ T cells, and **C.** memory population of $CD4^-CD8^-$ T cells. Kruskal-Wallis test and Dunn's multiple comparison were used to detect differences between means. Each symbol represents data collected from one patient, and data from different tissues of the same patient are connected with the line.

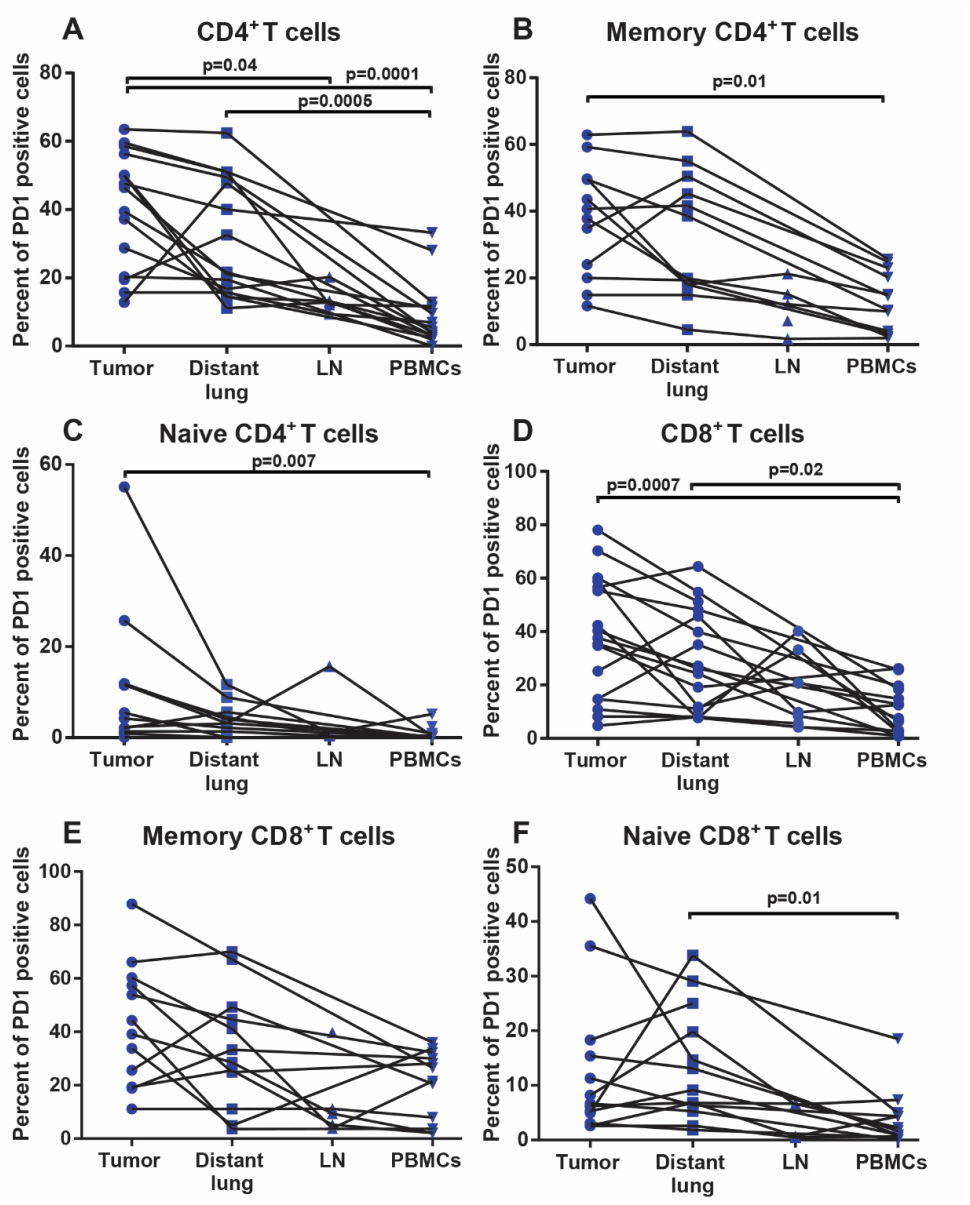

Figure 64. PD-1 expression in CD4⁺ and CD8⁺ T cell population in different tissues. Comparison of PD-1 expression in **A.** CD4⁺ T cells and **B.** memory and **C.** naive subtypes, **D.** CD8⁺ T cells and their **E.** memory and **F.** naive subsets. Kruskal-Wallis test and Dunn's multiple comparison were used to detect differences between means. Each symbol represents data collected from one patient and data from different tissues of the same patient are connected with the line.

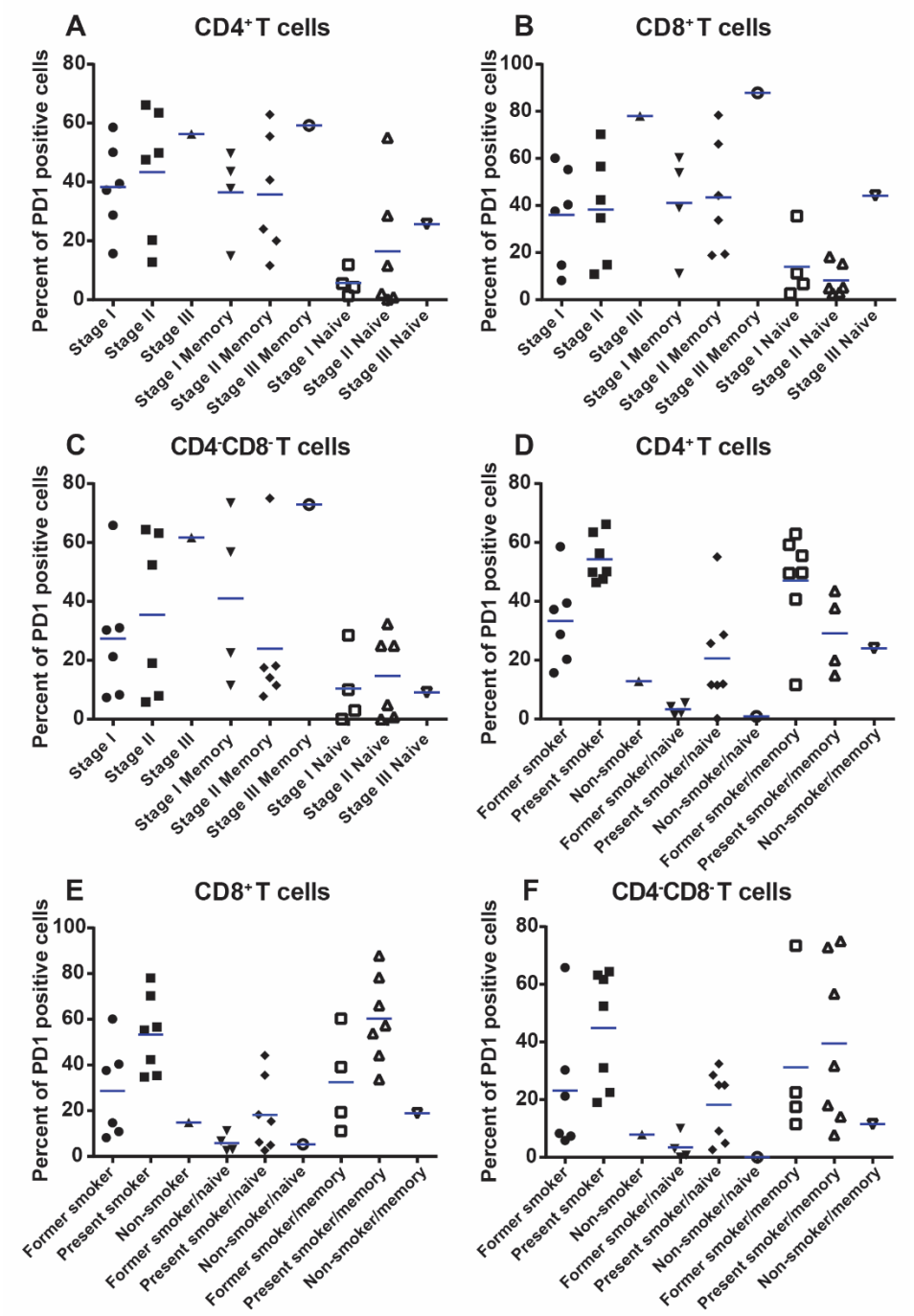

Figure 65. Comparison of PD-1 expression in T cell populations in different stages of the disease and in patients with different smoking histories. Comparison of PD-1 expression **A.** $CD4^+$ T cells and their naive and memory subtypes in tumor tissue in stage I and stage II of the disease **B.** $CD8^+$ T cells and their naive and memory subtypes in tumor tissue in stage I and stage II of the disease **C.** $CD4^-CD8^-$ T cells and their naive and memory subtypes in tumor tissue in stage I and stage II of the disease. **D.** $CD4^+$ T cells and their naive and memory subtypes in patients with different smoking histories **E.** $CD8^+$ T cells and their naive and memory subtypes in patients with different smoking histories **F.** $CD4^-CD8^-$ T cells and their naive and memory subtypes in patients with different smoking histories. Kruskal-Wallis test and Dunn's multiple comparison were used to detect differences between means. Each symbol represents data collected from one patient and data from different tissues of the same patient are connected with the line. Patients with stage III of the disease and patients that were qualified as non-smokers were not included in statistical anluysis due to the small number of samples.

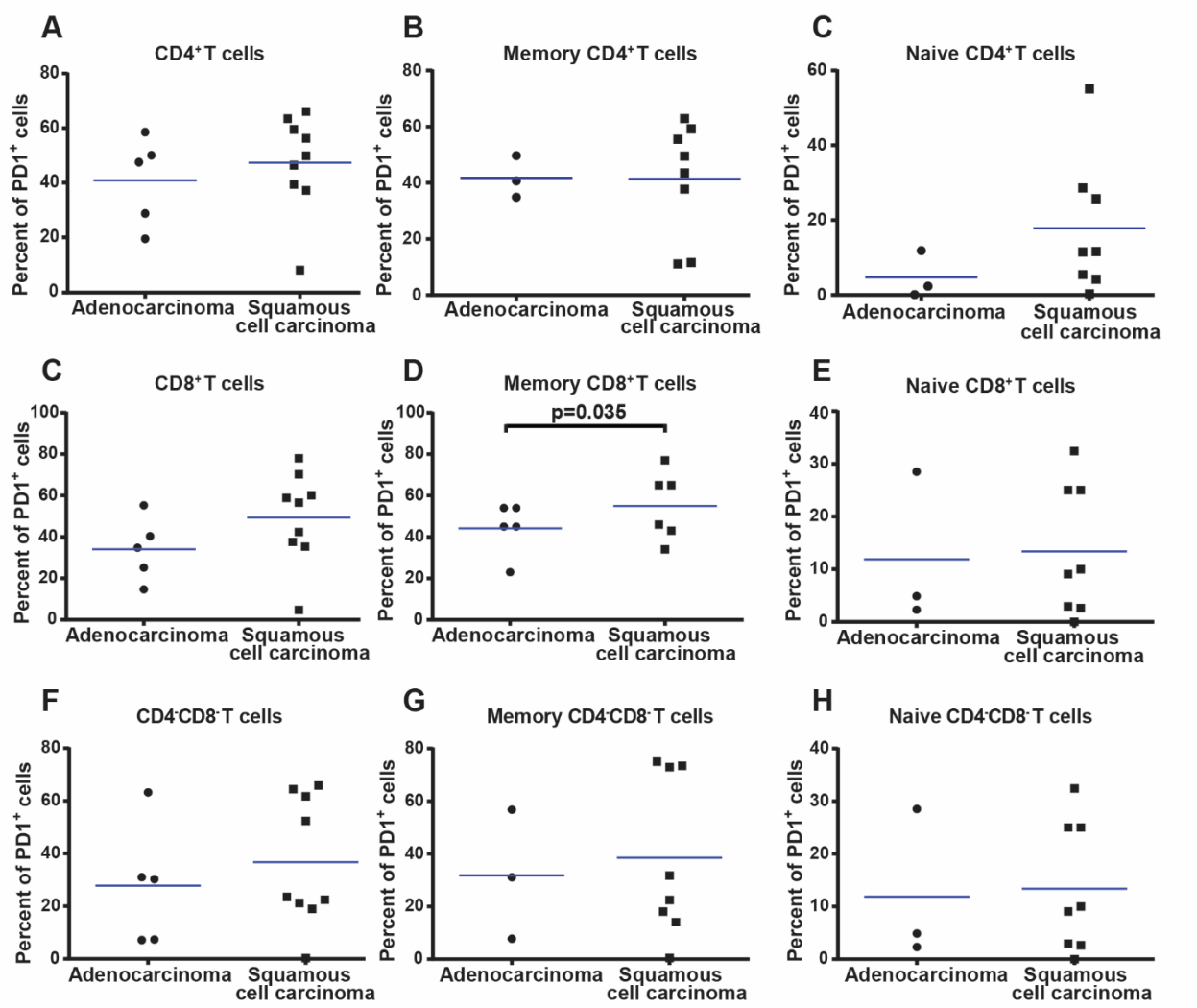

Figure 66. Comparison of PD-1 expression in T cell populations form adenocarcinoma and squamous cell carcinoma. Kruskal-Wallis comparison of PD-1 expression in **A.** $CD4^+$ T cells **B.** memory $CD4^+$ T cells, **C.** naive $CD4^+$ T cells, **D.** $CD8^+$ T cells, **E.** memory $CD8^+$ T cells, **F.** naive $CD8^+$ T cells, **G.** $CD4^-CD8^-$ T cells, **H.** memory $CD4^-CD8^-$ T cells, **I.** naive $CD4^-CD8^-$ T cells. Mann-Whitney test was used to detect differences between means. Each symbol represents data collected from one patient, as a percentage of live leukocyte population and the mean is represented by the blue line.

5.2.7 Summary of main findings

Using flow cytometry approach we have identified 25 population (types and subtypes) of immune cells in NSCLC (Table 14). Tumor infiltrating leukocytes were characterized as $CD45^{+}PI^{-}$ and showed higher percentages in the adenocarcinoma compared to the distant lung (Figure 6 A). From the leukocyte population in NSCLC we identified $CD3^{+}$ T cells, and divided them in $CD4^{+}$ T cells, $CD8^{+}$ T cells, double negative ($CD4^{-}CD8^{-}$) T cells. $CD4^{+}$, $CD8^{+}$, and $CD4^{-}CD8^{-}$ populations were further separated into the naive ($CD45RA^{+}CD45RO^{-}$) and the memory ($CD45RA^{-}CD45RO^{+}$) subsets (Figure 9). From the $CD3^{+}$ T cell population we identified $CD56^{+}$ NKT cells (Figures 43).

Further analysis of leukocytes in NSCLC revealed presence of $CD19^{+}$ B cells. B cells were present in adenocarcinoma ($p=0.0001$) and in squamous cell carcinoma ($p=0.006$) in higher degree than in distant lung tissue (Figure 26). In the $CD19^{+}$ B cell population five subsets were identified: naive, germinal center, non-conventional memory, memory and plasma cells (Figure 22). The memory B cell showed higher infiltration in adenocarcinoma compared to distant lung tissue ($p=0.04$; Figure 28).

Tumor infiltrating APCs defined in this project (after exclusion of B cells) were macrophages, pDC, $CD1c^{+}$ mDCs and $CD141^{+}$ mDCs. No significant difference was observed between tumor and distant lung tissues for any of the APC populations. Contrary to the APCs, the $CD56^{+}$ NK cells fund in the NSCLC showed differences between the tumor and the distant lung. We observed higher percentages of NK cells in

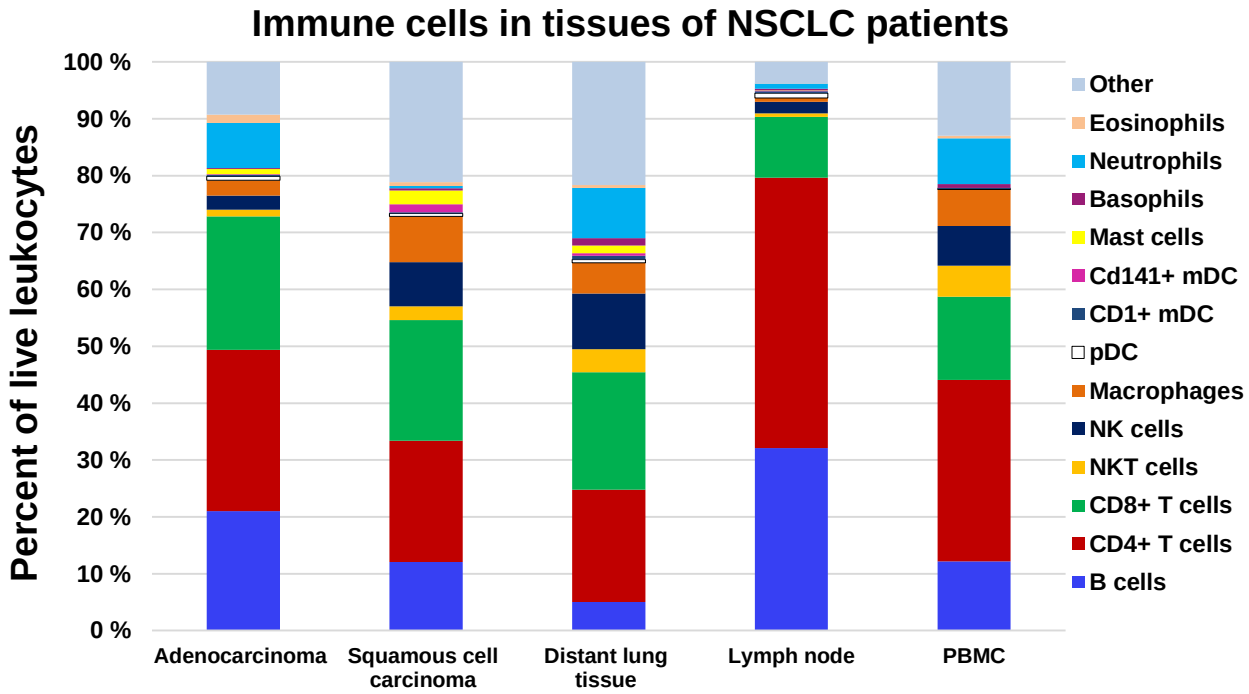

Figure 67. Immune cells in different tissues of NSCLC. The graph represents immune cell populations in adenocarcinoma, squamous cell carcinoma, distant lung, lymph node and PBMCs. All percentages in the graph represent a mean value calculated from all data collected for respective values.

distant lung than in adenocarcinoma (p= 0.013; Figure 49 A). This phenomenon seem to be mainly due to the decrease of both $CD16^+$ subset (p=0.01; Figure 49 C), while $CD16^-$ NK cells did not show significant difference between the tumor and the distant lung.

In the NSCLC we identified neutrophils, eosinophils, mast cells and basophils. The granulocyte populations showed no difference in infiltration between the tumor and the distant lung (Figures 57, 58).

We used data gathered from flow cytometry to analyze effect of clinicopathological parameters on tumor infiltrating immune cells. Three parameters were chosen for this analysis: histological type of tumor, stage of tumor and smoking history of the patient. The histological type of tumor had influence on the neutrophils infiltration in tumor, and the PD-1^+ $CD8^+$ T cells. Neutrophils showed higher infiltration in adenocarcinoma compared to squamous cell carcinoma (p= 0.03; Figure 59). Though the data set for neutrophils in squamous cell carcinoma is small and further analysis is needed to establish more reliable p values. The PD-1 expressing $CD8^+$ T cells were more prominent in squamous cell carcinoma than in adenocarcinoma (p=0.035; Figure 66), indicating that immune response to squamous cell carcinoma may be dampen down compared to adenocarcinoma. The tumor stage showed no influence on infiltration of immune cells, while the smoking history had influence on $CD1c^+$ and $CD141^+$ mDCs. Both types of dendritic cells showed to be increased in tumor tissues of former smokers, compared to the present smokers, indicating that cigarette smoke reduces presence of mDCs in the tumor tissue.

Table 14. Immune cells in NSCLC identified by Flow cytometry

Cell population	Molecular markers
T cells	$CD45^+PI^-CD3^+CD19^-$
$CD4^+$T cells	$CD45^+PI^-CD3^+CD19^-CD8^-CD4^+$
$CD4^+$ Naive cells	$CD45^+PI^-CD3^+CD19^-CD8^-CD4^+CD45RA^+CD45RO^-$
Memory $CD4^+$ T cells	$CD45^+PI^-CD3^+CD19^-CD8^-CD4^+CD45RA^-CD45RO^+$
$CD8^+$ T cell	$CD45^+PI^-CD3^+CD19^-CD8^+CD4^-$
$CD8^+$ Naive T cell	$CD45^+PI^-CD3^+CD19^-CD8^+CD4^-CD45RA^+CD45RO^-$
Memory $CD8^+$ T cell	$CD45^+PI^-CD3^+CD19^-CD8^-CD4^+CD45RA^-CD45RO^+$
B cells	$CD45^+PI^-CD3^-CD14^-CD19^+$
Naive B cells	$CD45^+PI^-CD3^-CD19^+CD14^-IgM^+IgD^+CD38^{+/-}CD27^-$
Non-conventional memory B cell	$CD45^+PI^-CD3^-CD19^+CD14^-IgM^+IgD^+CD38^{+/-}CD27^+$
Memory B cells	$CD45^+PI^-CD3^-CD19^+CD14^-IgM^-IgD^-CD38^{+/-}CD27^+$
Plasma cells	$CD45^+PI^-CD3^-CD19^+CD14^-IgM^-IgD^-CD38^{++}CD27^+$
Germinal center cells	$CD45^+PI^-CD3^-CD19^+CD14^-IgM^-IgD^-CD38^+CD27^+$
Macrophages/Monocytes	$CD45^+PI^-CD19^-CD14^+HLA\text{-}DR^+$
pDCs	$CD45^+PI^-CD19^-CD14^+HLA\text{-}DR^+CD11c^-CD123^+$
$CD1c^+$ DCs	$CD45^+PI^-CD19^-CD14^-CD11c^+CD1c^+CD141^-$
CD141 DCs	$CD45^+PI^-CD19^-CD14^-CD11c^+CD1c^-CD141^+$
NKT cells	$CD45^+PI^-CD19^-CD14^-CD3^+CD56^+$
NK cells	$CD45^+PI^-CD19^-CD14^-CD3^-CD56^+$
$CD16^+$ NK cells	$CD45^+PI^-CD19^-CD14^-CD3^-CD56^+CD16^+$
$CD16^-$ NK cells	$CD45^+PI^-CD19^-CD14^-CD3^-CD56^+CD16^-$
Neutrophils	$CD45^+PI^-CD19^-CD3^-C14^-CD11b^+CD15^+CD49d^+$
Basophils	$CD45^+PI^-CD19^-CD3^-C14^-CD11b^-Fc\varepsilon R1\alpha^+CD117^-CD49d^+$
Eosinophils	$CD45^+PI^-CD19^-CD3^-C14^-CD11b^+CD15^+CD49d^-$
Mast cells	$CD45^+PI^-CD19^-CD3^-C14^-CD11b^-Fc\varepsilon R1\alpha^+CD117^-CD49d^+$

6 Discussion

6.1 Tumor infiltrating immune cells

The main goal of this project was to establish flow cytometry protocols for comprehensive analysis of immune cell in NSCLC. Flow cytometry has many advantages as a method to identify and study immune cells. It allows definition of cells based on the size and granularity of the cell, exclusion of dead cells and multicolour analysis of the cells. The multicolour analysis allows accurate definition of immune cell subsets. In this study we used 10 colour flow cytometry to analyse immune cells in NSCLC. This method also has its drawbacks and in this study the main drawback was the need for tissue digestion. This is evident in quantification of $CD45^+PI^-$ leukocytes in the population of single cells, where percentages of live leukocytes ($CD45^+PI^-$) in tumor show great variation between the patients (Figure 6). When results from flow cytometry were compared with results from, semi-quantitative visual analysis of immunostained slide, we noticed that leukocyte percentages in tumor do grossly correlate. However, results from flow cytometry indicate higher percent of tumor infiltrating leukocytes than results from immunohistochemistry. In our opinion this phenomena could be due to the process of cell isolation in flow cytometry, when some of the non-immune cells could be lost in filtration steps. Therefore further detailed quantitative analysis of tumor tissue slides stained with CD45 antibody is recommended to strengthen our current findings. One such study of $CD45^+$ leukocytes in NSCLC, done by Ganesan *et al,* is consistent with our findings from flow cytometry [92]. They report increase of $CD45^+$ cells in six adenocarcinoma tumors compared to lung tissue. From both our study and the study of Ganesan *et al* we can conclude that the tumor microenvironment of NSCLC recruits immune cells [92].

Using flow cytometry Ganesan *et al* further reports that NSCLC is predominantly infiltrated by $CD4^+$ and $CD8^+$ T cells [92]. In our study we reported that about 50% of all leukocytes are $CD3^+$ T cells (Figure 67). In the $CD3^+$ T cell population about 50% of the cells were $CD4^+$ and about 40% of cells were $CD8^+$ (Figure 19). In this our study correlates with findings from Ganesan *et al* [92]. However they further report higher percentages of $CD4^+$ T cells in tumor compared to distant lung, and these findings contradicts our findings. This could be the result of small number of patients included in Ganesan *et al* study (n=6).

In our study we further investigated the populations of $CD4^+$, $CD8^+$ and $CD4^-CD8^-$ T cells for the $CD45RA^+CD45RO^-$ naive subset and $CD45RA^-CD45RO^+$ memory subsets. In the tumor tissue we noticed general higher percentages of memory cells than there was naive cells (Figure 19) for both $CD4^+$ and $CD8^+$ T cells. These results are expected as the T cells in tumor are expected to encounter anti-tumor antigens.

Analysis of naive $CD4^+$ and $CD8^+$ T cells between the different tissues revealed general higher percentages in PBMCs than in tumor. This was expected since PBMCs

contain more naive circulation cells. In the analysis of memory T cells the only interesting difference was the increase of $CD8^+$ T cells in adenocarcinoma compared to lymph node (Figure 15 A). This point to increase of antigen-experienced $CD8^+$ T cells in tumor tissue.

The lack of significant difference in antigen-experienced $CD8^+$ T cells between the tumor tissue and the distant lung could be explained by the dual personality of $CD8^+$ memory T cells. Literature reports show presence of tissue resident $CD8^+$ memory T cells which can revert to expression of CD45RA [93,94]. These cells could skew the memory/naive ratio in our analysis. However, these cells, unlike the naive $CD45RA^+CD8^+$ T cells, express very low levels of CCR7 [94]. This chemokine receptor controls homing of naive cells to secondary lymphoid organs, and is a common marker for naive T cells. Addition of anti-CCR7 antibody to our T cell mix could help to solve the problem of dual personality of $CD8^+$ T cells. One additional benefit of this antibody is that it would allow discrimination between central memory and central effector cells.

In their study of leukocytes in NSCLC Ganesan *et al* found increased percentages of B cells in adenocarcinoma compared with lung tissue [92]. Our analysis of $CD19^+$ B cells shows higher infiltration of these cells in adenocarcinoma, confirming their findings. Moreover we found similar results in squamous cell carcinoma. We took the analysis even further and defined B cell subsets in NSCLC. From the B cell subsets we observed higher increase of memory B cells in the adenocarcinoma compared to the distant lung tissue (Figure 28 C). This findings correlate with previous studies of B cell subsets that report increase of memory cells [49]. However, these studies also report increase of plasma cells in the tumor. Our findings do not report increased plasma cell infiltration in the tumor, but we can see a trend towards the increase (Figure 28 E, F). One of the reasons for the difference between our findings and previous reports could be a small sample size in our study, or high individual differences between the patients.

Our analysis of $CD19^+$ B cells shows high variation in the percentages in tumors of different patients. This means that high number of samples is needed for good statistical analysis. This variation could be caused by individual differences between the patients, or by the sampling effect. As indicated in previous reports, tumor infiltrating B cells are mainly found in tertiary lymphoid structures (TLS) [49, 95]. The TLS are very heterogenic, have different sizes and they are not visible to the naked eye. This makes it hard for us to know if the sampled tumor tissue contains TLS. The presence of TLS will influence the percentages of B cells obtained in the analysis. To minimize this mistake we have standardized the sampling procedure for tumor (see 4.2 Tissue sampling). However, additional analysis of tumor samples could be beneficial to establish whether the variation in B cell percentages are due to the sampling effect or individual differences between patients. Sampling of different parts of tumor would allow comparison of B cell percentages from different locations in the tumor.

In the gating strategy for B cells we found a population that is $CD45^+PI^-CD19^+IgM^+IgD^-$, which we did not define further. The study by Martin *et al* describes a population of memory B cells that has high expression of IgM and low expression of IgD

[96]. They hypothesize that proportion of these cells can be memory B cells. Theoretically our IgM^+IgD^- population could contain these IgM^+IgD^- memory B cells reported by Martin *et al*. Further investigation is required to closer define IgM^+IgD^- population in our samples.

In our study, analysis of macrophages in different tissues showed no differences between the tumor and the distant lung, and these findings correlate with results from Ganesan *et al* [92]. However looking into the flow cytometry analysis of the macrophages from tumor and distant lung, and monocytes from PBMCs, we observed different expression of HLA-DR in these three populations. Macrophages from tumor tissue have the highest expression of HLA-DR. Macrophages from distant lung tissue show populations with somewhat lower expression of HLA-DR, and monocytes from PBMCs show significantly lower expression of HLA-DR. This indicates that macrophages in tumor tissue have a more activated phenotype than those in distant lung or monocytes from PBMCs. To confirm this we need further investigation of HLA-DR expression.

When analysing DCs in NSCLC we observed three populations: $CD1c^+$ mDCs, $CD141^+$ mDC and pDCs. We also observed population of $CD11c^+HLA\text{-}DR^+CD14^-CD1c^-CD141^-$ cells that we do not define as DCs. Even though it was indicated through previous studies that this double negative population can behave as DCs, we need to further examine this population and use markers that are more specific for DCs (like BDCA-3) to define these cells as DCs [97]. Our analysis of mDCs populations and pDCs showed no significant difference between the tumor and the distant lung.

The third population of lymphocytes analysed in our study were NK cells. We identified two subsets of NK cells based on CD16 expression – cytotoxic $CD16^+$ NK cells and cytokine producing $CD16^-$ NK cells. When analysing $CD56^+$ NK cells in different tissues we noticed decrease in adenocarcinoma compared to the distant lung. We further looked into subsets of NK cells as a percent of $CD45^+$ leukocytes and found lower percentages of $CD16^+$ NK cells in adenocarcinoma compared to distant lung tissue. This indicates decreased NK-cell cytotoxicity in adenocarcinoma.

When characterizing granulocytes we defined eosinophil, neutrophils, basophils and mast cells. The granulocyte populations made a small portion of leukocytes in tumor, and statistically did not show any significant difference from populations in distant lung. Our findings on granulocyte populations correlate previous reports [92]. Our study of granulocytes only evaluates presence of this population in tumor and not the activation status. A good example of that are the neutrophils, which were only evaluated based on CD15 and CD11b surface markers. This gives insight into presence of neutrophils in NSCLC, but it does not give any information on activation status of neutrophils. Eruslanov *et al* study have shown that neutrophils in lung cancer can stimulate activation of T cells by production of proinflammatory cytokines [78]. In this study they show that activation markers CD62L and CD54 are triggered by tumor factors. Addition of antibodies against these markers in our granulocyte mix would allow us to examine activation status of neutrophils and examine not only presence but also function of neutrophils in NSCLC.

6.2 PD-1 expression

Our main reason for looking into the PD-1 expression on T cells is to investigate if there is difference in PD-1 expression, by tumor infiltrating T cells, between tumor and distant lung and if there are individual differences between the patients. This analysis could help explain why patients react differently to anti-PD-1 treatment. We found that memory cells have higher expression of PD-1 than naive cells, which was expected since PD-1 is upregulated after activation of T cells. We also notice high degree of individual differences in PD-1 expression. Previous studies of NSCLC treated with anti-PD-1 antibodies show that PD-1 expression does not correlate with responsiveness to therapy, but that expression of PD-L1 in tumor correlates with the responsiveness to therapy with anti-PD-1 [91]. Other studies on PD-L1 expression in tumors suggest that tumors might upregulate PD-L1 as a response to presence of $PD\text{-}1^+$ TILs [98]. This leads to the hypothesis that individual differences in expression of PD-1 on T cells can be used to predict which patient will benefit from anti-PD-1 treatment. However further investigation of the PD-1/PD-L1 pathway is necessary.

6.3 Clinicopathological parameters

One of the aims of this project was to study correlation of different clinicopathological parameters and tumor infiltrating immune cells. Here we reported results from comparison of tumor infiltrating cells in respect to the histological type of tumor, stage of tumor and smoking history of the patient.

The analysis of different histological types of tumor revealed great difference between percentages of $CD45^+$ leukocytes in adenocarcinoma and carcinoid carcinoma. Analysis of granulocytes revealed increase of neutrophils in adenocarcinoma compared to squamous cell carcinoma and analysis of $PD\text{-}1^+CD8^+$ memory T cells revealed increase in squamous cell carcinoma than in adenocarcinoma. This indicates that histological subtype has influence on composition of immune cells. However many of our data sets are small and we need to collect more data before we can draw conclusions.

The stage of the tumor is important parameter that will determine cause of treatment for the patient and give a prediction of prognosis of the disease. Immune cells have been reported to be a good prognostic factor as well [80]. Since the future perspective of this study is to see if immune cells can be used as prognostic factor, we have divided the patients according to stage of the tumor and analysed infiltration of immune cells in the groups. Our conclusion is that immune cell infiltration is not influenced by tumor stage, but many of our data sets are small, and further analysis is needed.

Smoking is a number one cause of lung cancer because of the carcinogens contained in the cigarette smoke. Previous studies show that nicotine has immunosuppressive role [99]. In this study we divided patients in to three groups, non-smokers, former smokers and present smokers, to investigate if smoking has effect on immune response to tumor. Our analysis of DCs showed that former smokers had higher levels of $CD1c^+$ mDCs and $CD141^+$ mDCs compared to the smokers. This suggests that smoke reduces presence of the mDCs in the tumor tissue, which can be harmful for the antitumor immune response.

6.4 Future perspectives

The aim of this master thesis was to establish staining protocols for flow cytometry and to characterize immune cells in NSCLC. The data acquired in the work presented in this thesis can further be used to correlate survival of patients with composition of immune cells in NSCLC. Many of the immune cell populations in NSCLC show high variations between the patients (like $CD45^+PI^-$ leukocytes, $CD3^+$, $CD4^+$, $CD8^+$ T cells, and $CD19^+$ B cells). This observation may be used to separate patients into two populations: one with low and one with high infiltrations of different immune cell populations. These two population may be used to investigate association of immune cell infiltrate with patient survival length. For this analysis, the mean value can be used as a cut-off point and Kaplan-Meier survival curves can be used to look for correlation with survival.

The flow cytometry analysis of macrophages in tumor and distant lung, and monocytes in PBMCs revealed different expression of HLA-DR between these tissues. As we discussed over, this is due to the fact that the more macrophages are activated the more HLA-DR they express. We also noticed a difference in HLA-DR expression between the tumor and the distant lung. This can be used to further investigate activation levels in these two tissues. Mean florescence intensity (MFI) can be used to measure expression levels of HLA-DR on macrophages and to look into abundance of HLA-DR on macrophages in tumor and distant lung.

6.5 Methodological considerations

Flow cytometry is a very powerful and useful method in immunology, but it has its limitations. The first major limitation of flow is the requirement to analyse cells in suspension, making information on tissue architecture unavailable. This eliminates the possibility to see if immune cells infiltrate tumor stroma or tumor islets. The need for cell suspension in flow analysis also leads to another problem. As we observed in the analysis of $CD45^+$ leukocytes some of the non-immune cells might be lost during the isolation from tissue resulting in false higher percentages of leukocytes in single cell population. Both

of these problems could, to a certain extent, be eliminated if flow analysis is coupled with immunohistochemistry stainings of tumor tissue.

The second limitation of this method is that obtained results strongly depend on the gating strategy. The way gates are set during the analysis will have huge influences on number of events included in the analysis. To minimize this effect we used the same gating strategy for all tissues in all patients. Threshold for the gates was set based on matched antibody isotype control, and kept as constant as possible through experiments.

When looking into experimental design we need to consider two limitations in our protocols for cell isolation. One of the problems we encounter during cell isolation is that blood may contaminate the tissue. Both tumor and distant lung tissues contain small capillaries filled with blood that can contaminate the samples. To minimize the contamination, we carefully washed the samples in the transport media.

Another limitation we encountered was isolation of PBMCs with density gradient media (Lymphoprep). This density gradient should remove all granulocytes from the blood after centrifugation. However, we notice that in some patient granulocyte populations are not removed from PBMCs. This will affect the total percent of leukocytes and more importantly it will affect percentages of other immune cells in leukocyte population.

7 References

1. *Lobectomy*. 2015 [cited 2015 01.06].
2. Bio-protocol. *Isolation and Characterisation of Dendritic Cells from Peripheral Blood*.
3. Vasaturo, A., et al., *Clinical implications of co-inhibitory molecule expression in the tumor microenvironment for DC vaccination: a game of stop and go.* Frontiers in Immunology, 2013. **4**.
4. Cancer, I.A.f.R.o. *"GLOBOCAN 2012: Estimated Cancer Incidence, Mortality and Prevalence Worldwide in 2012," WHO, 2012.* 2012 [cited 2015 15.07].
5. US, N.c.i. *SEER Stat Fact Sheets: Lung and Bronchus Cancer*. [cited 2015 15.07.].
6. Wong, D.W., et al., *The EML4-ALK fusion gene is involved in various histologic types of lung cancers from nonsmokers with wild-type EGFR and KRAS.* Cancer, 2009. **115**(8): p. 1723-33.
7. Jadus, M.R., et al., *Lung Cancer: A Classic Example of Tumor Escape and Progression While Providing Opportunities for Immunological Intervention.* Clinical and Developmental Immunology, 2012. **2012**: p. 160724.
8. Elias, A.D., *Small cell lung cancer : State-of-the-art therapy in 1996.* Chest, 1997. **112**(4_Supplement): p. 251S-258S.
9. Govindan, R., et al., *Changing epidemiology of small-cell lung cancer in the United States over the last 30 years: analysis of the surveillance, epidemiologic, and end results database.* J Clin Oncol, 2006. **24**(28): p. 4539-44.
10. Chen, Z., et al., *Non-small-cell lung cancers: a heterogeneous set of diseases.* Nat Rev Cancer, 2014. **14**(8): p. 535-546.
11. Wynder, E.L. and J.E. Muscat, *The changing epidemiology of smoking and lung cancer histology.* Environ Health Perspect, 1995. **103 Suppl 8**: p. 143-8.
12. Stellman, S.D., et al., *Risk of squamous cell carcinoma and adenocarcinoma of the lung in relation to lifetime filter cigarette smoking.* Cancer, 1997. **80**(3): p. 382-8.
13. Stellman, S.D., et al., *Impact of filter cigarette smoking on lung cancer histology.* Prev Med, 1997. **26**(4): p. 451-6.
14. Mirsadraee, S., et al., *The 7th lung cancer TNM classification and staging system: Review of the changes and implications.* World Journal of Radiology, 2012. **4**(4): p. 128-134.
15. Krsmo, H.A., *Immune cell composition in human non-small cell lung cancer*, in *Department of Molecular Bioscience* 2014, UIO.
16. Goldstraw, P., et al., *The IASLC Lung Cancer Staging Project: proposals for the revision of the TNM stage groupings in the forthcoming (seventh) edition of the TNM Classification of malignant tumours.* J Thorac Oncol, 2007. **2**(8): p. 706-14.
17. Nicot, C., *Tumor Suppressor Inactivation in the Pathogenesis of Adult T-Cell Leukemia.* J Oncol, 2015. **2015**: p. 183590.
18. Corthay, A., *Does the immune system naturally protect against cancer?* Front Immunol, 2014. **5**: p. 197.
19. Shankaran, V., et al., *IFNgamma and lymphocytes prevent primary tumour development and shape tumour immunogenicity.* Nature, 2001. **410**(6832): p. 1107-11.
20. Smyth, M.J., et al., *Perforin-mediated cytotoxicity is critical for surveillance of spontaneous lymphoma.* J Exp Med, 2000. **192**(5): p. 755-60.
21. van den Broek, M.E., et al., *Decreased tumor surveillance in perforin-deficient mice.* J Exp Med, 1996. **184**(5): p. 1781-90.
22. Street, S.E., E. Cretney, and M.J. Smyth, *Perforin and interferon-gamma activities independently control tumor initiation, growth, and metastasis.* Blood, 2001. **97**(1): p. 192-7.
23. Schreiber, R.D., L.J. Old, and M.J. Smyth, *Cancer immunoediting: integrating immunity's roles in cancer suppression and promotion.* Science, 2011. **331**(6024): p. 1565-70.
24. Dunn, G.P., L.J. Old, and R.D. Schreiber, *The three Es of cancer immunoediting.* Annu Rev Immunol, 2004. **22**: p. 329-60.
25. Otranto, M., et al., *The role of the myofibroblast in tumor stroma remodeling.* Cell Adh Migr, 2012. **6**(3): p. 203-19.
26. Orimo, A., et al., *Stromal Fibroblasts Present in Invasive Human Breast Carcinomas Promote Tumor Growth and Angiogenesis through Elevated SDF-1/CXCL12 Secretion.* Cell. **121**(3): p. 335-348.
27. Cooke, Vesselina G., et al., *Pericyte Depletion Results in Hypoxia-Associated Epithelial-to-Mesenchymal Transition and Metastasis Mediated by Met Signaling Pathway.* Cancer Cell. **21**(1): p. 66-81.
28. Yonenaga, Y., et al., *Absence of Smooth Muscle Actin-Positive Pericyte Coverage of Tumor Vessels Correlates with Hematogenous Metastasis and Prognosis of Colorectal Cancer Patients.* Oncology, 2005. **69**(2): p. 159-166.
29. Nieman, K.M., et al., *Adipocytes promote ovarian cancer metastasis and provide energy for rapid tumor growth.* Nat Med, 2011. **17**(11): p. 1498-1503.

30. Call, M.E., et al., *The Organizing Principle in the Formation of the T Cell Receptor-CD3 Complex.* Cell, 2002. **111**(7): p. 967-979.
31. *Identification of amino acids at the junction of exons 3 and 7 that are used for the generation of glycosylation-related human CD45RO and CD45RO-like antigen specificities.* The Journal of Experimental Medicine, 1994. **179**(3): p. 1035-1040.
32. Vitetta, E.S., et al., *Memory B and T cells.* Annu Rev Immunol, 1991. **9**: p. 193-217.
33. Lanzavecchia, A. and F. Sallusto, *Dynamics of T lymphocyte responses: intermediates, effectors, and memory cells.* Science, 2000. **290**(5489): p. 92-7.
34. Podojil, J.R. and S.D. Miller, *Molecular Mechanisms of T cell Receptor and Costimulatory Molecule Ligation/Blockade in Autoimmune Disease Therapy.* Immunological reviews, 2009. **229**(1): p. 337-355.
35. Grewal, I.S. and R.A. Flavell, *The role of CD40 ligand in costimulation and T-cell activation.* Immunol Rev, 1996. **153**: p. 85-106.
36. Keene, J.A. and J. Forman, *Helper activity is required for the in vivo generation of cytotoxic T lymphocytes.* J Exp Med, 1982. **155**(3): p. 768-82.
37. Mitchison, N.A., *The carrier effect in the secondary response to hapten-protein conjugates. II. Cellular cooperation.* European Journal of Immunology, 1971. **1**(1): p. 18-27.
38. Shresta, S., et al., *How do cytotoxic lymphocytes kill their targets?* Curr Opin Immunol, 1998. **10**(5): p. 581-7.
39. Goping, I.S., et al., *Granzyme B-Induced Apoptosis Requires Both Direct Caspase Activation and Relief of Caspase Inhibition.* Immunity, 2003. **18**(3): p. 355-365.
40. Nagata, S. and P. Golstein, *The Fas death factor.* Science, 1995. **267**(5203): p. 1449-56.
41. Schoenberger, S.P., et al., *T-cell help for cytotoxic T lymphocytes is mediated by CD40-CD40L interactions.* Nature, 1998. **393**(6684): p. 480-3.
42. Hung, K., et al., *The central role of CD4(+) T cells in the antitumor immune response.* J Exp Med, 1998. **188**(12): p. 2357-68.
43. Mumberg, D., et al., *CD4(+) T cells eliminate MHC class II-negative cancer cells in vivo by indirect effects of IFN-gamma.* Proc Natl Acad Sci U S A, 1999. **96**(15): p. 8633-8.
44. Corthay, A., et al., *Primary antitumor immune response mediated by CD4+ T cells.* Immunity, 2005. **22**(3): p. 371-83.
45. Kapsenberg, M.L., et al., *The paradigm of type 1 and type 2 antigen-presenting cells. Implications for atopic allergy.* Clin Exp Allergy, 1999. **29 Suppl 2**: p. 33-6.
46. Legrand, F., et al., *Human eosinophils exert TNF-alpha and granzyme A-mediated tumoricidal activity toward colon carcinoma cells.* J Immunol, 2010. **185**(12): p. 7443-51.
47. Lan, Q., et al., *Cytokine polymorphisms in the Th1/Th2 pathway and susceptibility to non-Hodgkin lymphoma*. Vol. 107. 2006. 4101-4108.
48. Nelson, B.H., *CD20+ B Cells: The Other Tumor-Infiltrating Lymphocytes.* The Journal of Immunology, 2010. **185**(9): p. 4977-4982.
49. Germain, C., et al., *Presence of B Cells in Tertiary Lymphoid Structures Is Associated with a Protective Immunity in Patients with Lung Cancer.* American Journal of Respiratory and Critical Care Medicine, 2014. **189**(7): p. 832-844.
50. Li, Q., et al., *In vivo sensitized and in vitro activated B cells mediate tumor regression in cancer adoptive immunotherapy.* J Immunol, 2009. **183**(5): p. 3195-203.
51. Imahayashi, S., et al., *Tumor-infiltrating B-cell-derived IgG recognizes tumor components in human lung cancer.* Cancer Invest, 2000. **18**(6): p. 530-6.
52. Drayton, D.L., et al., *Lymphoid organ development: from ontogeny to neogenesis.* Nat Immunol, 2006. **7**(4): p. 344-53.
53. Carragher, D.M., J. Rangel-Moreno, and T.D. Randall, *Ectopic lymphoid tissues and local immunity.* Seminars in Immunology, 2008. **20**(1): p. 26-42.
54. Schreiber, R.D., et al., *Macrophage-activating factor produced by a T cell hybridoma: physiochemical and biosynthetic resemblance to gamma-interferon.* J Immunol, 1983. **131**(2): p. 826-32.
55. Wang, H.W. and J.A. Joyce, *Alternative activation of tumor-associated macrophages by IL-4: priming for protumoral functions.* Cell Cycle, 2010. **9**(24): p. 4824-35.
56. Martinez-Nunez, R.T., F. Louafi, and T. Sanchez-Elsner, *The interleukin 13 (IL-13) pathway in human macrophages is modulated by microRNA-155 via direct targeting of interleukin 13 receptor alpha1 (IL13Ralpha1).* J Biol Chem, 2011. **286**(3): p. 1786-94.
57. Mantovani, A., et al., *The chemokine system in diverse forms of macrophage activation and polarization.* Trends Immunol, 2004. **25**(12): p. 677-86.
58. Zhang, Q.W., et al., *Prognostic significance of tumor-associated macrophages in solid tumor: a meta-analysis of the literature.* PLoS One, 2012. **7**(12): p. e50946.
59. Porcheray, F., et al., *Macrophage activation switching: an asset for the resolution of inflammation.* Clinical and Experimental Immunology, 2005. **142**(3): p. 481-489.
60. Jongbloed, S.L., et al., *Human CD141+ (BDCA-3)+ dendritic cells (DCs) represent a unique myeloid DC subset that cross-presents necrotic cell antigens.* J Exp Med, 2010. **207**(6): p. 1247-60.

61. Collin, M., N. McGovern, and M. Haniffa, *Human dendritic cell subsets.* Immunology, 2013. **140**(1): p. 22-30.
62. Piccioli, D., et al., *Functional specialization of human circulating CD16 and CD1c myeloid dendritic-cell subsets.* Blood, 2007. **109**(12): p. 5371-9.
63. Schnurr, M., et al., *Tumor antigen processing and presentation depend critically on dendritic cell type and the mode of antigen delivery.* Blood, 2005. **105**(6): p. 2465-72.
64. Teicher, B.A. and S.P. Fricker, *CXCL12 (SDF-1)/CXCR4 Pathway in Cancer.* Clinical Cancer Research, 2010. **16**(11): p. 2927-2931.
65. Liang, S., et al., *IFNalpha regulates NK cell cytotoxicity through STAT1 pathway.* Cytokine, 2003. **23**(6): p. 190-9.
66. Marrack, P., J. Kappler, and T. Mitchell, *Type I interferons keep activated T cells alive.* J Exp Med, 1999. **189**(3): p. 521-30.
67. von Marschall, Z., et al., *Effects of interferon alpha on vascular endothelial growth factor gene transcription and tumor angiogenesis.* J Natl Cancer Inst, 2003. **95**(6): p. 437-48.
68. Hartmann, E., et al., *Identification and functional analysis of tumor-infiltrating plasmacytoid dendritic cells in head and neck cancer.* Cancer Res, 2003. **63**(19): p. 6478-87.
69. Labidi-Galy, S.I., et al., *Plasmacytoid dendritic cells infiltrating ovarian cancer are associated with poor prognosis.* Oncoimmunology, 2012. **1**(3): p. 380-382.
70. Treilleux, I., et al., *Dendritic cell infiltration and prognosis of early stage breast cancer.* Clin Cancer Res, 2004. **10**(22): p. 7466-74.
71. Waugh, D.J. and C. Wilson, *The interleukin-8 pathway in cancer.* Clin Cancer Res, 2008. **14**(21): p. 6735-41.
72. Vivier, E., et al., *Functions of natural killer cells.* Nat Immunol, 2008. **9**(5): p. 503-10.
73. Cooper, M.A., T.A. Fehniger, and M.A. Caligiuri, *The biology of human natural killer-cell subsets.* Trends Immunol, 2001. **22**(11): p. 633-40.
74. Ljunggren, H.G. and K. Karre, *Host resistance directed selectively against H-2-deficient lymphoma variants. Analysis of the mechanism.* J Exp Med, 1985. **162**(6): p. 1745-59.
75. Paolino, M., et al., *The E3 ligase Cbl-b and TAM receptors regulate cancer metastasis via natural killer cells.* Nature, 2014. **507**(7493): p. 508-512.
76. Stocks, S.C. and M.A. Kerr, *Stimulation of neutrophil adhesion by antibodies recognizing CD15 (Le(X)) and CD15-expressing carcinoembryonic antigen-related glycoprotein NCA-160.* Biochemical Journal, 1992. **288**(Pt 1): p. 23-27.
77. Wislez, M., et al., *Hepatocyte growth factor production by neutrophils infiltrating bronchioloalveolar subtype pulmonary adenocarcinoma: role in tumor progression and death.* Cancer Res, 2003. **63**(6): p. 1405-12.
78. Eruslanov, E.B., et al., *Tumor-associated neutrophils stimulate T cell responses in early-stage human lung cancer.* J Clin Invest, 2014. **124**(12): p. 5466-80.
79. Heneberg, P., *Mast cells and basophils: trojan horses of conventional lin- stem/progenitor cell isolates.* Curr Pharm Des, 2011. **17**(34): p. 3753-71.
80. Welsh, T.J., et al., *Macrophage and mast-cell invasion of tumor cell islets confers a marked survival advantage in non-small-cell lung cancer.* J Clin Oncol, 2005. **23**(35): p. 8959-67.
81. Zhang, B., et al., *M2-Polarized tumor-associated macrophages are associated with poor prognoses resulting from accelerated lymphangiogenesis in lung adenocarcinoma.* Clinics, 2011. **66**(11): p. 1879-1886.
82. Ohri, C.M., et al., *Macrophages within NSCLC tumour islets are predominantly of a cytotoxic M1 phenotype associated with extended survival.* Eur Respir J, 2009. **33**(1): p. 118-26.
83. Al-Shibli, K., et al., *The prognostic value of intraepithelial and stromal innate immune system cells in non-small cell lung carcinoma.* Histopathology, 2009. **55**(3): p. 301-12.
84. Wakabayashi, O., et al., *CD4+ T cells in cancer stroma, not CD8+ T cells in cancer cell nests, are associated with favorable prognosis in human non-small cell lung cancers.* Cancer Sci, 2003. **94**(11): p. 1003-9.
85. Al-Shibli, K.I., et al., *Prognostic effect of epithelial and stromal lymphocyte infiltration in non-small cell lung cancer.* Clin Cancer Res, 2008. **14**(16): p. 5220-7.
86. Arriagada, R., et al., *Cisplatin-based adjuvant chemotherapy in patients with completely resected non-small-cell lung cancer.* N Engl J Med, 2004. **350**(4): p. 351-60.
87. Forde, P.M., et al., *What lies within: novel strategies in immunotherapy for non-small cell lung cancer.* Oncologist, 2013. **18**(11): p. 1203-13.
88. Ji, M., et al., *PD-1/PD-L1 pathway in non-small-cell lung cancer and its relation with EGFR mutation.* Journal of Translational Medicine, 2015. **13**: p. 5.
89. Dong, H., et al., *Tumor-associated B7-H1 promotes T-cell apoptosis: a potential mechanism of immune evasion.* Nat Med, 2002. **8**(8): p. 793-800.
90. Tykodi, S.S., *PD-1 as an emerging therapeutic target in renal cell carcinoma: current evidence.* OncoTargets and therapy, 2014. **7**: p. 1349-1359.
91. Topalian, S.L., et al., *Safety, Activity, and Immune Correlates of Anti–PD-1 Antibody in Cancer.* The New England journal of medicine, 2012. **366**(26): p. 2443-2454.
92. Ganesan, A.P., et al., *Tumor-infiltrating regulatory T cells inhibit endogenous cytotoxic T cell responses to lung adenocarcinoma.* J Immunol, 2013. **191**(4): p. 2009-17.

93. Carrasco, J., et al., *CD45RA on human CD8 T cells is sensitive to the time elapsed since the last antigenic stimulation.* Blood, 2006. **108**(9): p. 2897-905.
94. Faint, J.M., et al., *Memory T Cells Constitute a Subset of the Human CD8+CD45RA+ Pool with Distinct Phenotypic and Migratory Characteristics.* The Journal of Immunology, 2001. **167**(1): p. 212-220.
95. Dieu-Nosjean, M.C., et al., *Long-term survival for patients with non-small-cell lung cancer with intratumoral lymphoid structures.* J Clin Oncol, 2008. **26**(27): p. 4410-7.
96. Martin, V., et al., *Age-related aspects of human IgM B cell heterogeneity.* Ann N Y Acad Sci, 2015.
97. Dzionek, A., et al., *BDCA-2, BDCA-3, and BDCA-4: three markers for distinct subsets of dendritic cells in human peripheral blood.* J Immunol, 2000. **165**(11): p. 6037-46.
98. Taube, J.M., et al., *Colocalization of inflammatory response with B7-h1 expression in human melanocytic lesions supports an adaptive resistance mechanism of immune escape.* Sci Transl Med, 2012. **4**(127): p. 127ra37.
99. Nouri-Shirazi, M. and E. Guinet, *Evidence for the immunosuppressive role of nicotine on human dendritic cell functions.* Immunology, 2003. **109**(3): p. 365-373.

Norwegian University
of Life Sciences

Postboks 5003
NO-1432 Ås, Norway
+47 67 23 00 00
www.nmbu.no